Master Thesis
Wind Induced Vibrations of frUHSC Bridge Decks

Graduation Project

September 2012

Ing. E. Bosman
4029364

Delft University of Technology

Delft University of Technology
Faculty of Civil Engineering and Geosciences
Structural Engineering
Concrete structures

Thesis Committee

Prof. dr. ir. J.C. Walraven	TUDelft
Dr. ir. C. van der Veen	TUDelft
Dr. ir. P.C.J. Hoogenboom	TUDelft
Prof. dr. ir. C. Geurts	TNO/TUe
Ing. P.A.M. Taken	Engineering office F.Wiggers B.V.
Ing. M. Wiggers	Engineering office F.Wiggers B.V.

Student
Ing. E. Bosman

Contents

Preface

This report is my Master Thesis for the conclusion of my master Structural Engineering of the study Civil Engineering & Geosciences at Delft University of Technology. Using this opportunity, I would like to thank the people who supported me during my study.

My thanks goes to the graduation committee, who gave me their support and used their expertise to help me successful complete the study. I would like to thank Prof. dr. ir. J.C. Walraven for his great expertise of concrete structures. And Dr. ir. C. van der Veen for his positive approach and major knowledge of bridges. I also would like to thank Dr. ir. P.C.J. Hoogenboom, who always made time for consultancy and gave me excellent advice. I am also very grateful for the guidance of Prof. dr. ir. C. Geurts and his great expertise in the field of wind loading and his critical view of the report. I want to thank the people of the Engineering Office F. Wiggers b.v., and especially Ing. P.A.M. Taken and Ing. M. Wiggers for their counsel during the project.

Finally, I am very grateful for the constant support and encouragements of my family.

ESLI BOSMAN

Ellecom, The Netherlands
September 2012

Summary

Owing to the development of frUHSC, more slender structures can be developed. Problems that were never governing for concrete structures can now become more important for design. In this research the buffeting performance of a frUHSC bridge is investigated and compared with the performance of a NSC bridge. A traditional cable stayed bridge is designed for the concrete classes C35/45 and C170/200. By using frUHSC not only the bridge deck can be made more slender but material can also be saved in the stays and the substructure as well. The goal of the project is to investigate whether or not the frUHSC bridge is more susceptible for vertical vibrations due to wind buffeting in comparison with a NSC bridge design.

The preliminary survey is a literature study to mathematically modeling of the wind and the behavior around structures. The wind velocity in a certain direction can be approached mathematically by dividing the wind speed in a mean wind velocity and a fluctuating part. The fluctuating part can be modeled for a certain time period with a stationary Gaussian process. The buffeting behavior of a bridge is caused due to the varying wind speed. The buffeting performance can be described on the basis of the wind spectra and the transfer functions.

The bridge design is based on a traditional cable stayed bridge and for both design calculations the same starting points are used. From the design calculations it seems that the cross sectional area of the bridge deck can be reduced with 50% by applying frUHSC. The weight that can be saved at the bridge deck, has also consequence for the amount of strands in the stay cables.

The main span of the bridge can be modeled as a Euler-Bernoulli beam on an elastic foundation with at both ends a rotational spring. For this model the natural frequencies can be determined. The fundamental frequency can be verified with the Rayleigh-Ritz method, which makes use of the energy stored in the system. Also the reference projects of bridges have fundamental frequencies that coincides with the values found for the model. The damping ratios are based on the material damping of the concrete and the aerodynamic damping. Based on the values of the models and the properties of the bridge designs the transfer functions can be determined. The response of the system is composed with the transfer functions and the force spectra. A parameter study is performed in order to determine the susceptibility for the different parameters. Especially the stiffness of the cable stays have large influence on the response.

By means of a FE-model of the bridges a second analysis is performed. This FE-model is designed in Matlab with two dimensional two nodes Euler-Bernoulli beam elements. With this model an analysis of the response is made in Matlab. The results for the fundamental frequencies are confirming with the fundamental frequencies found with the first model. The resonance peaks at the natural frequencies have little influence on response of the structure. Most of the response is determined by lower frequencies, because the force spectrum is has the highest values in this area.

The vertical vibrations of the bridge do not cause unsafe structural behavior of the bridge. Fatigue problems of the reinforcement bars due to the vibrations caused by the wind do not occur for both bridge designs. Based on Irwin's curve the traffic can experience discomfort in storm conditions on the frUHSC bridge because of the accelerations that can occur. In order to reduce the accelerations of the bridge, a Tuned Mass Damper can be applied.

List of Symbols

a_k	Amplitude of the wind velocity for the frequency ω_k	$[m/s]$
c	Damping	$[kg/s]$
c_{eff}	Effective damping	$[kg/s]$
c_α	Rotational damping	$[kgm^2/srad]$
E_{cm}	Mean value Young's modulus concrete	$[N/m^2]$
f	Frequency	$[Hz]$
f_{cd}	Design value concrete compressive strength	$[N/m^2]$
f_{ck}	Characteristic value concrete compressive strength	$[N/m^2]$
f_{cm}	Average concrete compressive strength	$[N/m^2]$
f_{ctm}	Mean value tensile strength concrete	$[N/m^2]$
h_0	Reference height	$[m]$
k_d	Modulus of subgrade	$[N/m^2]$
k_r	Rotational spring stiffness	$[Nm/rad]$
k_s	Spring stiffness	$[N/m]$
k_α	Rotational spring stiffness	$[Nm/rad]$
l_{ref}	Reference length	$[m]$
m	Mass	$[kg]$
q	Dynamic pressure	$[N/m^2]$
u^*	Shear velocity	$[m/s]$
u_i	Normal mode	$[-]$
z_0	Roughness of the terrain	$[m]$
z	Displacement in vertical direction	$[m]$
$\dot{z}$	Velocity in vertical direction	$[m/s]$
$\ddot{z}$	Acceleration in vertical direction	$[m/s^2]$
A_c	Cross sectional area	$[m^2]$
A_{ref}	Reference area	$[m^2]$
B	Width of the structure	$[m]$
$\boldsymbol{C}$	Damping matrix	$[kg/s]$
C_D	Drag coefficient	$[-]$
C_L	Lift coefficient	$[-]$
C_M	Aerodynamic moment coefficient	$[-]$
$Coh_{v_1v_2}$	Coherence between v_1 and v_2	$[-]$
C_y	Factor for coherence in the z-direction	$[-]$
C_z	Factor for coherence in the z-direction	$[-]$
D	Drag force	$[N]$
$\boldsymbol{E}$	Eigen matrix	$[-]$
$\boldsymbol{F}$	Force vector	$[N]$
G	Shear modulus	$[N/m^2]$
$H(\omega)$	Transfer function	$[m/N]$
I	Turbulence intensity	$[-]$
I_{zz}	Moment of Inertia	$[m^4]$
J	Mass moment of Inertia	$[kgm^2/rad]$
J_t	Torque constant	$[m^4]$
$\boldsymbol{K}$	Stiffness matrix	$[N/m]$
L	Lift force	$[N]$
L	Length of the structure	$[m]$

L_u	Turbulence length	$[m]$
$\boldsymbol{M}$	Mass matrix	$[kg]$
Re	Reynolds number	$[-]$
S_{FF}	Force spectrum	$[N^2 s/rad]$
S_{uu}	Response spectrum	$[m^2 s/rad]$
S_{vv}	Spectrum for the wind velocity	$[m^2/srad]$
$T(w)$	Kinetic energy	$[J]$
U	Velocity of flow in x-direction	$[m/s]$
U_g	Geostrophic wind velocity in x-direction	$[m/s]$
U_m	Mean wind velocity	$[m/s]$
$U(t)$	Wind velocity varying in time	$[m/s]$
$U(w)$	Potential energy	$[J]$
V	Velocity of flow in x-direction	$[m/s]$
V_g	Geostrophic wind velocity in y-direction	$[m/s]$
W	Velocity of flow in x-direction	$[m/s]$
W_c	Section modulus	$[m^3]$

α	Exponent for power law	$[-]$
β	Characteristic length	$[m^{-1}]$
γ	Mass ratio	$[-]$
δ	Thickness of the Boundary layer	$[m]$
ζ	Damping ratio	$[-]$
κ	Von Karman constant	$[-]$
ρ	Density of air	$[kg/m^3]$
ρ_c	Density of concrete	$[kg/m^3]$
σ_v	Standard deviation for the wind velocity	$[m/s]$
τ_u	Shear stress in x-direction	$[N/m^2]$
τ_v	Shear stress in y-direction	$[N/m^2]$
χ	Aerodynamic admittance	$[-]$
ω_k	Frequency	$[rad/s]$
ω_n	Natural frequency	$[rad/s]$
φ_k	Random variable	$[rad]$
μ	Mean value	$[-]$
Γ	Gamma function	$[-]$
$\Delta\omega$	Frequency step	$[rad/s]$

1. Introduction

Material consumption keeps increasing due to the growing world population, therefore, durable and sustainable materials become more and more important as well as saving raw materials. Over the past decades concrete has developed considerably. As a result, higher concrete classes can be reached. One of the latest developments is the adding of steel fibres to the concrete mixture. These fibre reinforced Ultra High Strength Concrete (frUHSC) classes can reach strengths up to 800N/mm^2. The higher costs of the material can be compensated with the material savings due to more slender structures. This does not only affect the required concrete cross section but influence the required supporting elements as well due to a lower self-weight of the structure. Dependent of the type of structure and where the frUHSC is applied, it is possible that raw material can be saved. However for these more slender structures, it is thinkable that the dynamic behavior of the structure becomes more important. It is possible that problems that did not occur for concrete bridge decks in the past, should now be checked in the design.

For bridge building the use of frUHSC can have a great impact on the design and dimensions. In the Netherlands the longest bridges have a length of around 300 meters and most of these bridges are cable stayed bridges. The increasing strength properties of concrete can have an important influence on the design of a cable stayed bridge. Because the design of the deck is mostly dependent of the moment capacity of the cross section under the large horizontal compressive force from the stays. For this objective the frUHSC is very suitable. As a result of the reduced cross section of the deck, a reduction of the cross sections of the other parts of the superstructure and substructure can be made as well. Another aspect of using frUHSC is that the damping ratio may be influenced as well.

The wind flow can cause loads on the structure which can give a dynamic response of the bridge. For bridges different mechanisms can occur due to the wind flow. In preliminary survey the different mechanisms are explained. One of the mechanisms is caused by the varying wind speed. This force driven mechanism is called buffeting.

In this thesis the vertical buffeting performance of a typical cable stayed bridge design of Normal Strength Concrete (NSC) is tested and compared with the performance of a frUHSC bridge design. In order to give a decent comparison between the two concrete classes the same design principles and main dimensions are used. The values for the cross sections of both bridges are calculated with some design calculations. This study will focus on the difference in dynamic displacements and accelerations of the midspan of both bridge designs. The analysis will be done based on an analytical model and a two dimensional numerical model (FE-model). For the comparison between the bridge designs the relative displacements and accelerations are of most importance. Whether or not the displacements and accelerations are acceptable based on comfort and safety will also be tested.

2. Preliminary Survey

This preliminary survey is part of the master thesis and is a literature study to the modeling of wind and the effects of wind on structures. In this survey it is explained how the wind is modeled for engineering purposes. The preliminary survey is divided into different parts. First it is explained how the wind flow is described mathematically and the behavior of the wind flow around structures is defined. In order to understand the wind flow and the behavior around structures, it is necessary to explain the theory of wind engineering. The aeroelastic effects of structures are explained in APPENDIX 0. Basically in these first chapters an explanation is given from the wind velocity to the effect of wind on structures. The process description for the approach of the project is described in chapter 2.5. This is done to give insight in the strategy of the project and it contains the flowchart for successful completion of the project. The goal of the preliminary survey is to understand the system concept of wind modeling and effects that wind can have on a structure. It also provides an approach for the development of the project.

2.1 List of Definitions

In advance a short explanation of some of the definitions is given. This is done to increase the surveyability of the onward chapters. The most important terms of the preliminary survey are defined. The definitions of the terms are based on literature.

Aerodynamic Admittance
The aerodynamic admittance function is an adjustment for the dynamic pressure coefficient for the actual body in a wind flow. The aerodynamic admittance function gives the effectiveness of a frequency when the turbulent wind velocity is transformed to an aerodynamic force.

Buffeting
Buffeting is a force driven mechanism that occurs due to the fluctuating wind velocity. It is assumed that the motion of the structure does not influence the magnitude of the forces acting on the structure. Due to the varying wind speed, an alternating pressure acts on the structure. When the frequency of the loading has a value close to the eigenvalue of the structure, resonance can occur. By Simiu and Scanlan the following description of buffeting is given (Simiu, et al., 1996):
"*Buffeting is defined as the unsteady loading of a structure by velocity fluctuations*." (p.257).

Coherence
The coherence is used to describe the mutual relation between two series. Coherence is a function to describe the frequency-dependent correlation between two points. Holmes stated the coherence as following (Holmes, 2003).
"The coherence is a normalized magnitude of the cross spectrum, approximately equivalent to a frequency-dependent correlation coefficient." (p. 59).
For the wind velocity or wind pressure the coherence is used to determine the relation between two different points.

Correlation	For wind velocities or wind pressures Holmes gives the following description for correlation (Holmes, 2003)**:** *“In the present context, it relates the fluctuating wind velocities at two points in space, or wind pressures at two points on a building”*(p.57).
Cross-spectrum	In the context of wind velocities, the following description for a cross-spectrum is given by Dyrbye and Hansen (Dyrbye, et al., 1997): *“The normalized cross-spectrum describes the statistical dependence between turbulence components at two points at a given frequency …”*(p.44)
Divergence	Divergence is an interactive mechanism that can occur for flat shaped cross sections in a flow. A description of this phenomenon is given by Simiu and Scanlan in *Wind Effects on Structures* (Simiu, et al., 1996). *“Under the effect of wind, the structure will be subjected to, and will act to resist, a drag force, a lift force, and a twisting moment. As the wind velocity increases, the twisting moment in particular increases also. This in turn twists the structure further, but this condition may also, by increasing the effective angle of attack of the wind relative to the structure, further increase the twisting moment, which then demands additional reactive moment from the structure. Finally, a velocity is reached at which the magnitude of the wind induced moment, together with the tendency for twist demand additional structural reaction, creates an unstable condition and the structure twists to destruction.”* (p. 243).
Flutter	Flutter is an interactive phenomenon between the forces (drag, lift and moment) and the motion of the structure. In 1988 Smith gave the following description of classical flutter (Smith, 1988): *“Classical flutter is an unstable coupled motion in any two degrees of freedom, such as combined bending and torsion. It is similar to galloping in that the aerodynamic forces depend on the motion. It differs in that there would be positive damping in either of the motions acting independently, but aerodynamic cross-coupling results in one of the motions giving rise to fluctuating forces affecting the other.”* (p.229).
Galloping	Galloping is a vertical motion of a structure in a flow and is caused by an interaction between the forces acting on the structure and the vertical velocity of the structure. In *Vibrations of Structures* by Smith the following description is given (Smith, 1988): *“Galloping is an unstable phenomenon which arises from the aerodynamic forces generated on certain cross-sectional shapes as they displace transverse to the wind.”*(p.228) Due to the interaction of the forces acting on the structure and the velocity of the structure, negative effective damping can occur and this can lead to an unstable system. Dyrbye and Hansen mention galloping as (Dyrbye, et al., 1997): *“Galloping refers to structural vibrations in a direction almost perpendicular to the wind direction, if these vibrations are mainly due to negative aerodynamic damping.”* (p. 173).

Logarithmic law Function to describe the mean wind velocity over the height. Where the function is dependent on the roughness of the terrain, the shear velocity and the Von Karman constant.

Power law Function to describe the mean wind velocity over the height. The parameters in this function are the exponent and the reference height.

Reynolds number The Reynolds number is a measure of ratio of inertia forces to viscous forces in a flow.

Turbulence intensity The turbulence intensity is the ratio between the standard deviation and the mean wind velocity.

Vortex induced Vibrations Vortex induced vibrations are caused by Von Karman vortexes which are formed at the rear side of the structure. These vortexes causes pressure deviations and this can cause an oscillating motion of the structure. The formation of the vortexes in dependent on the motion of the structure. This makes the vortex induced vibrations interactive with the motion of the structure. The definition of vortex shedding is described by Smith (Smith, 1988):
"The asymmetric pressure distribution created by the vortices around the cross section results in an alternating transverse force as they shed. If the structure is flexible, oscillation will occur transverse to the wind and the conditions for resonance would exist if the vortex shedding frequency coincided with the natural frequency of the structure." (p.226).

2.2 Wind Engineering

This chapter of the preliminary survey is devoted to the approach of modeling the wind velocity. In this chapter a short description is given of the how the wind is generated in the atmosphere. In order to model the wind, a distinction should be made between the mean wind velocity and the fluctuating wind speed. Both parts are described in this chapter.

Wind is generated by pressure differences in the air around the earth. The temperature distribution in the atmosphere plays an important role in the motion of the air. Due to solar heating of the of the earth's atmosphere by the sun, differences in pressure occur. Other effects like, the rotation of the earth, humidity differences in the air and the earth's surface all determine in certain amounts the wind velocity. However the most important initial factor is the influence of the sun on the atmosphere. When the air is heated up it will expand. This will cause a certain flow to an area where the pressure is lower. Because the pressure in the original area will drop, a flow is generated. This is a continuous process, and changes in time because of all the effects involved.

For engineering purposes it is necessary to model the wind behavior. The motion of the atmosphere is not limited to one direction. The flow is three-dimensional and this makes it difficult to model the behavior of the wind. From the continuum mechanics the equations of mean motion of the atmosphere can be given. These equations of mean motion are built up from the equation of continuity and the equations of balance of momenta.

$$\rho\left(\frac{\partial \mathbf{v}}{\partial t} + \mathbf{v}\cdot\nabla\mathbf{v}\right) = -\nabla\mathbf{p} + \frac{\partial \tau}{\partial z} + \mathbf{f} \qquad \textbf{(2.2.1)}$$

Where the term at the left side of the equation is the Inertia per volume. The first two terms at the right side are divergences of stress and the last term are the body forces. When the equation is averaged with respect to time and the gravity forces are neglected, the equations for the mean motion along the axes x and y can be given as following:

$$\rho\left(U\frac{\partial U}{\partial x}+V\frac{\partial U}{\partial y}+W\frac{\partial U}{\partial z}\right)=-\frac{\partial p}{\partial x}+\frac{\partial \tau_u}{\partial z}+\rho f V \quad \textbf{(2.2.2)}$$

$$\rho\left(U\frac{\partial V}{\partial x}+V\frac{\partial V}{\partial y}+W\frac{\partial V}{\partial z}\right)=-\frac{\partial p}{\partial y}+\frac{\partial \tau_v}{\partial z}+\rho f U \quad \textbf{(2.2.3)}$$

Where ρ is the density of the air and U, V, W are respectively the velocities of the flow in the x, y and z-direction. In this equation is f the Coriolis parameter. A relation can be found for the pressure gradient and the Coriolis force. The shear stresses can be defined as a relation of the wind speed over the height. Eventually the relations can be substituted into the equations of mean motion. It is however not possible to find a solution for this problem.

Modeling the mean wind profile

In order to give a description for the wind profile, some different approaches are presented. Friction between the surface of the earth and the air flow causes retardation of the flow. The roughness of the surface determines the wind speed of the flow in the boundary layer. When the distance from the surface increases, the influence of the friction will become smaller. At a certain distance the surface has no influence on the wind speed anymore. There are functions designed to describe the wind profile. Two possible functions are the Power Law and the Logarithmic Law. The first mean wind profile that was developed in homogeneous terrain is the Power Law. The mean wind velocity is given by a reference wind velocity multiplied with the relative height to the power. The exponent is dependent of the roughness of the terrain.

$$U(z)=U(h_0)\left(\frac{z-d}{h_0}\right)^{\alpha} \quad \textbf{(2.2.4)}$$

The Power Law is still used in some building codes (National Building Code of Canada), but in most codes the Logarithmic Law regarded as the most representative function of the mean wind profile. The Logarithmic Law is based on the friction with the surface of the earth. The boundary layer is divided into two regions, a layer that is influences by the surface and an outer layer. The shear with the surface layer is mostly dependent of the roughness of the terrain, the density of the air and the velocity. Therefore it can be stated that the shear is a function of these parameters.

$$\tau = f(U\mathbf{i}+V\mathbf{j}, z, z_0, \rho) \quad \textbf{(2.2.5)}$$

Where U is the velocity in the x-direction and V is the velocity in the y-direction. The $\mathbf{i}$ and $\mathbf{j}$ are unit vectors. The roughness of the terrain is given by the value z_0. The function can be written down in a non-dimensional form.

$$\frac{U\mathbf{i}+V\mathbf{j}}{u^*}=f_1\left(\frac{z}{z_0}\right) \quad \textbf{(2.2.6)}$$

In this equation u^* is the shear velocity and is a function of the shear stress and the density of the air. At the transition from the surface layer to the outer layer the conditions must hold. It is assumed that the boundary layer has a thickness δ. In the outer layer the reduction of velocity should be equal to:

$$\frac{(U\mathbf{i}+V\mathbf{j})-\left(U_g\mathbf{i}+V_g\mathbf{j}\right)}{u^*}=f_2\left(\frac{z}{\delta}\right) \tag{2.2.7}$$

Where U_g and V_g are the velocities which are not influenced by the friction. Substituting this into equation 2.2.6, will give the following:

$$f_1\left[\left(\frac{z}{\delta}\right)\left(\frac{\delta}{z_0}\right)\right]=\frac{U_g\mathbf{i}+V_g\mathbf{j}}{u^*}+f_2\left(\frac{z}{\delta}\right) \tag{2.2.8}$$

It can be seen that the equations f_1 and f_2 should be logarithmic functions to satisfy the conditions.

$$f_1(\alpha)=\ln(\alpha^{1/\kappa})\mathbf{i} \tag{2.2.9}$$
$$f_2(\alpha)=\ln(\alpha^{1/\kappa})\mathbf{i}+\frac{B}{\kappa}\mathbf{j} \tag{2.2.10}$$

Where B is a constant. When this is substituted into equation 2.2.6, the mean velocity in the x-direction can be written as:

$$U(z)=\frac{u^*}{\kappa}\ln\left(\frac{z}{z_0}\right) \tag{2.2.11}$$

This is function is the mean velocity of the wind according to the Logarithmic Law. Where κ is the Von Karman constant.

In Figure 2.1 the two lines are plotted for certain parameters. The blue line represents the Logarithmic Law and the red line represents the Power Law. From the comparison it can be seen that both lines follow the same trend, especially in the middle part of the graph. At small and very large heights the graphs deviate from each other.

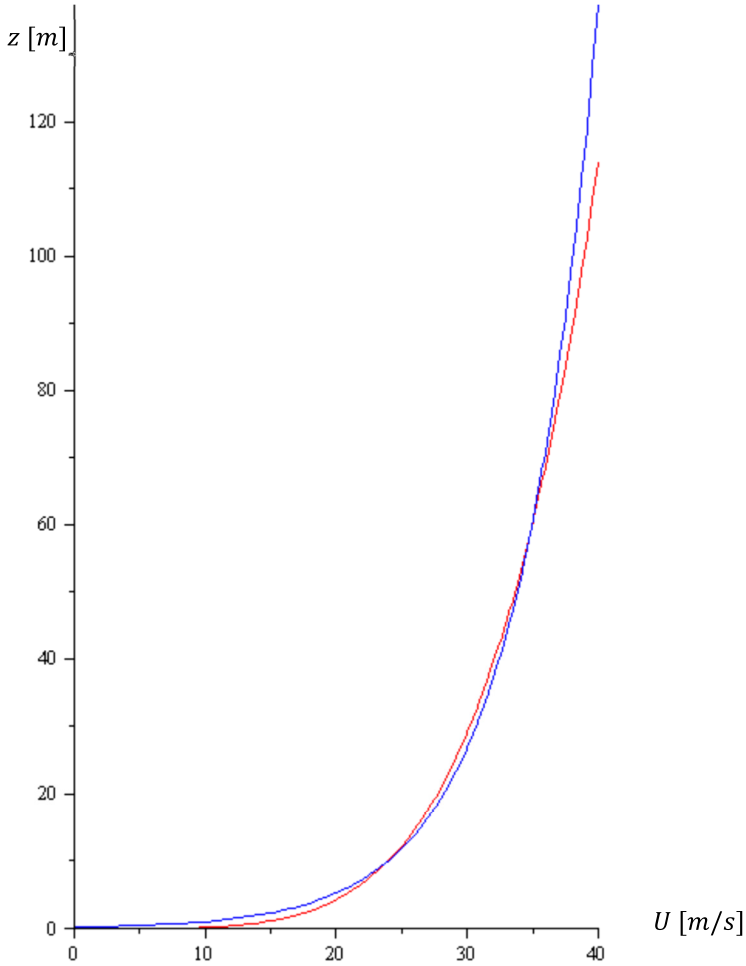

Figure 2.1 Comparison between the Logarithmic Law [blue line] and the Power Law [red line]
(Use is made of the following parameters; σ=6 m/s, z_0=0.2m, h_0=10m, U(10)=23.96 m/s)

From the equations 2.2.4 and 2.2.11 it can be seen that the height above the surface of the earth is the most important parameter for determining the mean wind velocity. The area around the structure plays an important role as well for determining the mean wind velocity. Different roughness terrain leads to different mean wind velocities. Hills and cliffs also affect the wind velocity.

Statistical distribution extreme average wind speeds

In order to model the wind velocity, a mean wind velocity is required. First a distinction should be made between the extreme and the momentary hourly averaged wind speed. For the design of structures it is important to use an extreme value for this mean wind speed. The extreme average wind speed can be obtained from recorded wind speed data. When the recorded data is divided into certain periods of time and the mean value of each of these periods is determined, the maximum mean value can be obtained. It is important to notice that the extreme average wind speed therefore increases when the period becomes smaller. The Eurocode uses a period of 10 minutes for the extreme average wind speed that occurred during one year. The extreme hourly-average wind speed over one year can be recorded by certain weather stations.

The return period can be expressed as the inverse of the probability of exceedence. For a return period of 100 years the probability of exceedence every year is 0.01. For the prediction of extreme wind speeds use can be made of the Extreme Value Type I distribution or the Extreme Value Type III distribution. The Extreme Value Type I distribution is also referred to as the Gumbel distribution.

The general formula for the probability density function can be given by:

$$F(x) = \frac{1}{\beta} e^{\frac{x-u}{\beta}} e^{-e^{\frac{x-u}{\beta}}} \tag{2.2.12}$$

Where β is the scale parameter and u is the location parameter. The mean and standard deviation can be obtained by:

$$\mu = u + 0.5772\beta \tag{2.2.13}$$

$$\sigma = \frac{\beta\pi}{\sqrt{6}} \tag{2.2.14}$$

The constant value 0.5772 is Euler's number. If u_1 is the parameter for one year, than the parameter for R years can be expressed as:

$$u_R = u_1 + \beta \ln(R) \tag{2.2.15}$$

The mean value for R years becomes.

$$\mu(R) = u_1 + \frac{\sqrt{6}}{\pi} \sigma(U_1)(\ln(R) + 0.5772) \tag{2.2.16}$$

The maximum hourly-averaged wind speed in R years has a Gumbel distribution as well with the same standard deviation. The only difference is that the mean has shifted over a distance $\beta \ln(R)$.

Another possibility is to make use of the Extreme Value Type III distribution, also known as the Reversed Weibull distribution. The general formula for the probability density function is:

$$F(x) = \frac{\gamma}{\alpha}\left(\frac{x-u}{\alpha}\right)^{\gamma-1} e^{-\left(\frac{x-u}{\alpha}\right)^{\gamma}} \tag{2.2.17}$$

Where γ is the shape parameter, α is the scale parameter and u is the location parameter. The mean and standard deviation can be given by:

$$\mu = \Gamma\left(\frac{\gamma+1}{\gamma}\right) \tag{2.2.18}$$

$$\sigma = \sqrt{\Gamma\left(\frac{\gamma+2}{\gamma}\right) - \left(\Gamma\left(\frac{\gamma+1}{\gamma}\right)\right)^2} \tag{2.2.19}$$

The mean value for R years becomes.

$$\mu(R) = u_1 + \frac{\sigma(U_1)}{\sqrt{\Gamma(1-2c) - \left(\Gamma(1-c)\right)^2}}\left(\Gamma(1-c) - \left[-\ln\left(1 - \frac{1}{R}\right)\right]^{-c}\right) \tag{2.2.20}$$

The parameter c has a negative value, and in most cases it is assumed to be -0.1. The Γ is the gamma function. It can be seen that the expression for the mean and the standard deviation for the Gumbel distribution is much simpler than for the reversed Weibull distribution.

The extreme of the hourly averaged wind speed over one year can be assumed to be equal to the maximum hourly average wind speed that occurs in the $N = 365x24 = 8760$ hours. This assumption is not entirely correct, because the weather situation does not change every hour. Basically it can be said that the weather situation changes on average every 6 hours. This would mean that N should be divided by 6. The number of independent weather situation is now reduced to $N = 1460$. A Gumbel distribution can be used to determine the maximum hourly wind speed in one year.

Modeling the fluctuating part in the wind speed

Not only the mean wind velocity is determined by the friction with the surface, turbulence is influenced as well. Most of the wind flows are not laminar but fluctuate in time and space, this is called turbulence. The turbulence is higher when the terrain is rougher. The turbulence is time-varying and can cause a dynamic response of structures. The intensity of the turbulence can be expressed as a dimensionless number. The turbulence intensity is the ratio between the standard deviation and the mean wind speed.

$$I(z) = \frac{\sigma_v(z)}{U(z)} \tag{2.2.21}$$

The standard deviation also varies with the height above the face of the earth. This variation can be described by a power function.

$$\sigma_v(z) = \sigma_v(h_0)\left(\frac{z-d}{h_0}\right)^{\beta} \tag{2.2.22}$$

However this function is only appropriate to use when the mean velocity is described with the Power Law. When the Logarithmic Law is used to describe the mean wind velocity, the turbulence intensity can be given by:

$$I(z) = \frac{\sigma_v}{\frac{u^*}{\kappa}\ln\left(\frac{z}{z_0}\right)} \tag{2.2.23}$$

In this equation the standard deviation is constant over the height and it is assumed that the shear velocity is directly related to the standard deviation based on (Simiu, et al., 1996).

$$\sigma_v{}^2 = 6u^{*2} \tag{2.2.24}$$

Because $\kappa\sqrt{6} \approx 1$, the turbulence intensity can be given as the following function:

$$I(z) = \frac{1}{\ln\left(\frac{z}{z_0}\right)} \tag{2.2.25}$$

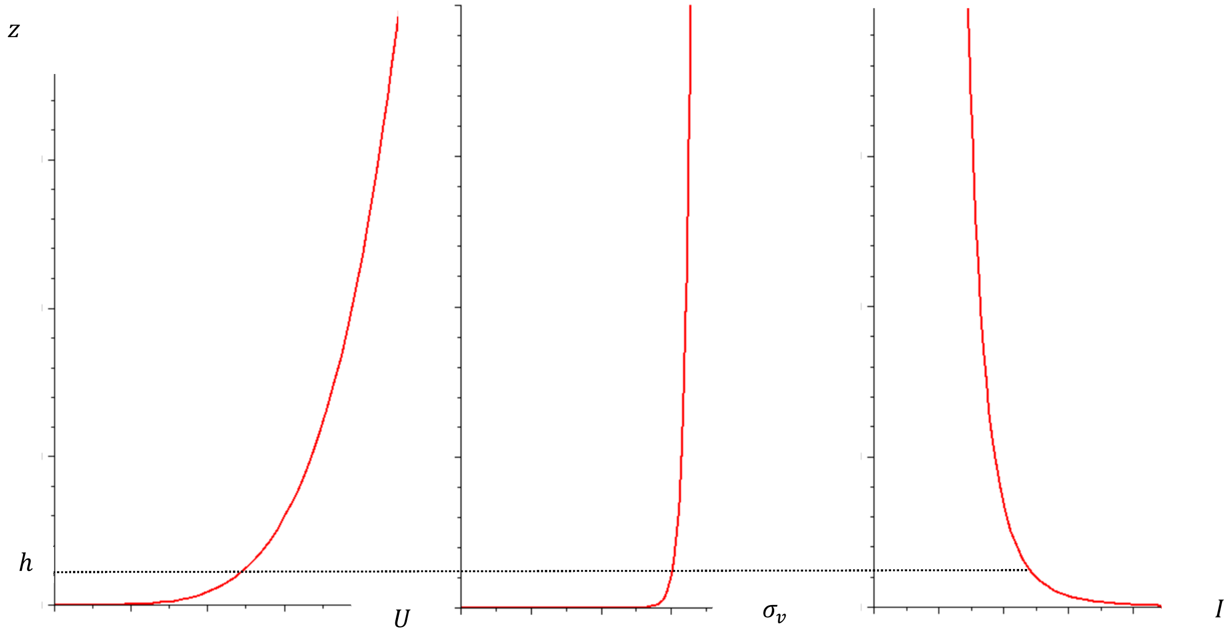

Figure 2.2 From left to right graph of the velocity, standard deviation, turbulence intensity

In order to describe the fluctuating wind velocity in a function, it is necessary to make use of a variance spectrum of the wind velocity. This spectrum represents the distribution across different frequencies. The most common known reduced spectra are the spectra of Davenport, Harris and Simiu. Figure 2.3 shows these three spectra. Spectra for the other two directions are available as well. For the spectrum of vertical turbulence the equation of Busch and Panofsky can be used.

Formula 2.2.26 gives the relation between the variance and the spectrum. In APPENDIX I a more detailed description is given.

$$\sigma^2 = \int_0^\infty S_{xx}(f)df \tag{2.2.26}$$

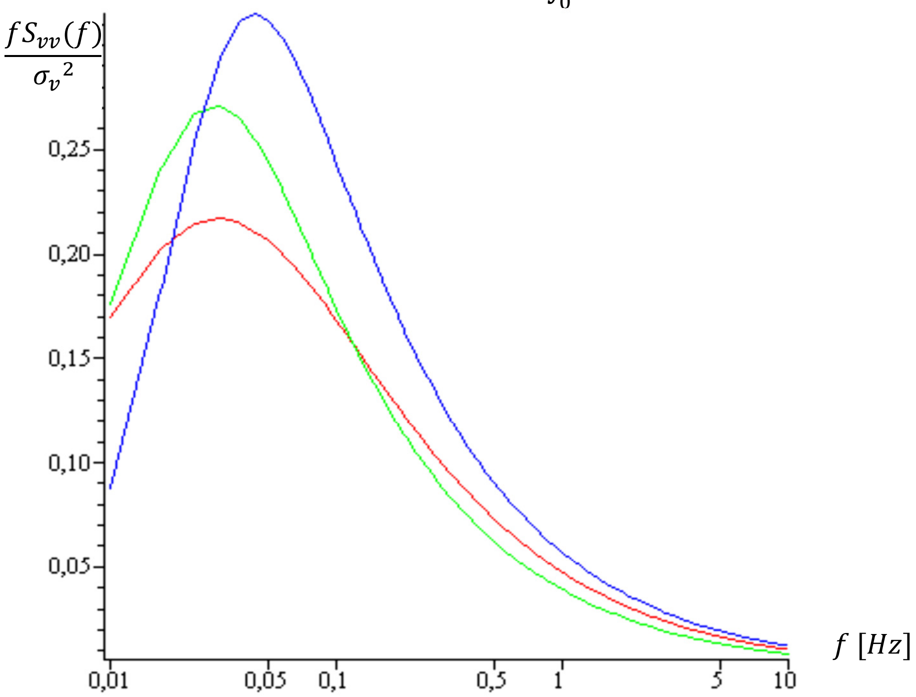

Figure 2.3 Different reduced spectra, blue line = Davenport, green line = Harris, red line = Simiu

It should be noted that the scale of figure 2.3 is for the horizontal axis logarithmic. So it can be seen that the reduced spectra show a similar shape that have the highest values varying between 0.01-0.1Hz.

The spectrum is used to model the variable part of the wind speed. This is done by what is known from the approach of a stationary Gaussian process. The variable part can be generated by dividing the spectrum into small parts with a width of $\Delta\omega$. The frequency and the spectrum are used for the amplitude and the frequency of the variable wind speed (see also APPENDIX I).

$$U(t) = \sum_{k=1}^{\infty} a_k \sin(\omega_k + \varphi_k) \tag{2.2.27}$$

The amplitude can be expressed as:

$$a_k = \sqrt{2S_{vv}(\omega_k)\Delta\omega} \tag{2.2.28}$$

In APPENDIX I it is explained that the standard deviation of a stationary Gaussian process is related to the variance spectrum, and therefore is the amplitude also related to the variance spectrum.
The turbulence is a random process and a random generator is used in φ_k. This parameter has a random value between 0 and 2π for every different k.

Coherence

The wind velocity is not only changing in time, it changes in space as well. When a structure is considered, the wind velocity at two certain points is not equal, but is related to each other. The coherence gives the physical relation between two spectra. With a cross spectrum the correlation between the two different points can be described. Two different extreme situations can be described. When the processes are completely coupled the variable part of the wind speed is only varying in time and not in location. Every point on the structure will experience an equal amount of turbulence. When the processes are independent of each other the fluctuating wind speed at different locations are uncorrelated. This means that the wind velocity at every different point on the structure is generated by a different process. A possible expression for the coherence function is given below:

$$Coh_{v_1 v_2}(f) = \exp\left(-f\,\frac{\sqrt{{C_z}^2(z_1 - z_2)^2 + {C_y}^2(y_1 - y_2)^2}}{U(10)}\right) \tag{2.2.29}$$

In the figures Figure 2.4,Figure 2.5 and Figure 2.6 the effect of correlated wind speeds is shown. The difference between these three figures is clearly to see. In the first figure there is only a shift in mean value for the wind speed at different heights. The turbulence is in this figure at both locations exactly the same. In the second figure the processes are related with a cross-spectrum. The turbulence is therefore not the same for both locations. But the trend of both lines is comparable. In the third figure two independent processes are shown. In APPENDIX II it is explained how these figures are modeled.

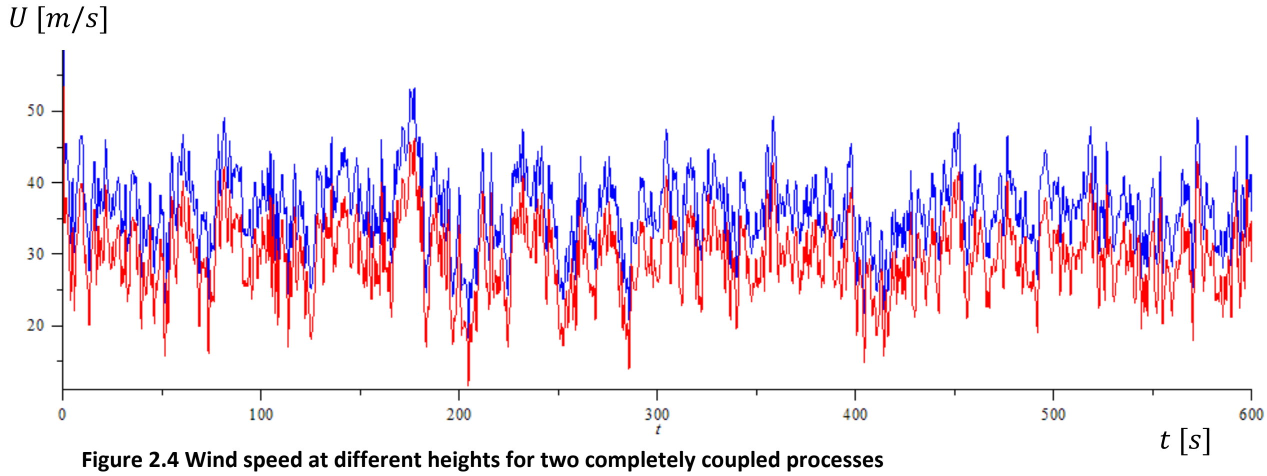

Figure 2.4 Wind speed at different heights for two completely coupled processes

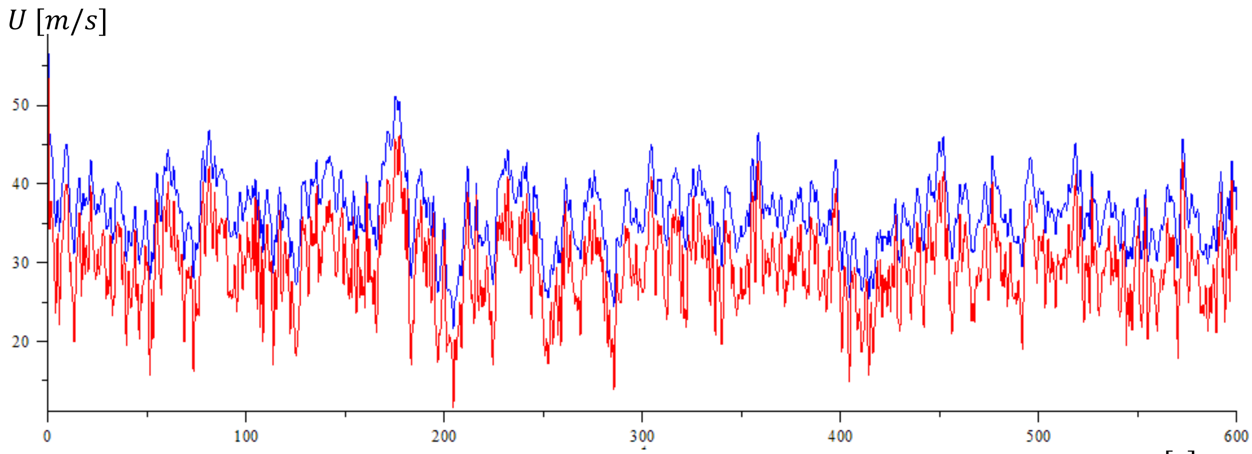

Figure 2.5 Wind speed at different heights for two processes when the coherence is taken into account

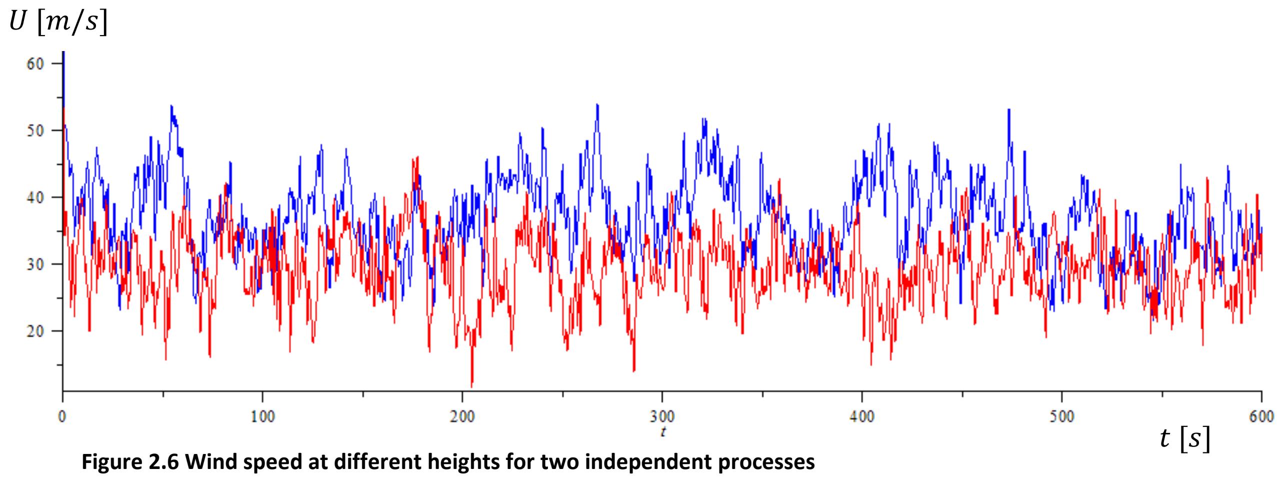

Figure 2.6 Wind speed at different heights for two independent processes

2.3 Wind Flow near a Structure

It is important to understand the behavior of the wind flow near a structure. The flow around a structure will eventually determine the response of the structure. In order to understand this, is it necessary to investigate the different aspects that determine the wind flow around structures. In this chapter the basic equations of the forces for a body in a laminar constant flow are described. This is done to show the background of these forces and the pressure on a structure can be explained based on simplified theoretical examples.

Probably the most important equation in fluid mechanics is Bernoulli's equation. For a fluid that is incompressible and inviscid the following equation holds.

$$p_1 + \frac{1}{2}\rho {u_1}^2 + g\rho z_1 = p_2 + \frac{1}{2}\rho {u_2}^2 + g\rho z_2 \qquad \textbf{(2.3.1)}$$

For air the gravity forces can be neglected. When the air around a structure is analyzed, and it is assumed that the velocity of the air flow against the structure is zero, the dynamic pressure can be calculated. The density of the air remains the same when the flow is considered to be incompressible. The freestream dynamic pressure can be given with the following equation.

$$q = C_p \frac{1}{2}\rho u^2 \qquad \textbf{(2.3.2)}$$

Where ρ is the density and u is the velocity of the flow. C_p is a non-dimensional pressure coefficient. The wind velocity can be divided into a mean wind velocity and a turbulent part. This is also described in the previous chapter. For the freestream dynamic pressure this means that

$$q = C_p \frac{1}{2}\rho (U_m + U(t))^2 = C_p \frac{1}{2}\rho {U_m}^2 + C_p \rho U_m U(t) + C_p \frac{1}{2}\rho U(t)^2 \qquad \textbf{(2.3.3)}$$

The last term is the square of the time dependent wind velocity. This term can be neglected for small turbulence intensities in the design calculations, because of the small influence.

From aerodynamics it can be noted that there are three different loadings on a structure that can be dedicated to the wind flow. These three loadings are the lift forces, the drag forces and aerodynamic moments. Lift is the component perpendicular to the direction of the freestream velocity of the wind. (The freestream velocity is the velocity of the wind there where it is not influences by the structure.) The drag forces act parallel to the direction of the freestream. The forces are a combination of dynamic pressure and viscous friction. Most of the civil structures are blunt bodies, and therefore is most of the force built up from the dynamic pressure. The values or ratios of the drag and lift forces on a structure are dependent of different aspects. Most important influence factors are the Reynolds number, the Mach number and the angle of attack on the structure. Of course are also the shape of the structure and the dimensions very important. The Reynolds number is a measure of ratio of inertia forces to viscous forces in a flow. The Reynolds number determines whether viscous friction or dynamic pressure dominates. The viscous force can be given by;

$$F_v = \mu v L \qquad \textbf{(2.3.4)}$$

Where μ is the dynamic viscosity, v is the velocity of the flow and L is the characteristic length of the object. For the inertia force or the drag force the following expression can be given:

$$F_i = \rho v^2 L^2 \quad \textbf{(2.3.5)}$$

When the ratio between these two forces is calculated the Reynolds number is obtained. Note that ν is the kinematic viscosity and can be expressed as $\nu = \mu/\rho$.

$$Re = \frac{F_i}{F_v} = \frac{\rho v^2 L^2}{\mu v L} = \frac{\rho v L}{\mu} = \frac{vL}{\nu} \quad \textbf{(2.3.6)}$$

The Mach number is the ratio between the flow velocity and the velocity of the speed of sound. For the wind speed it can be said that the Mach number is always lower than 0.3. This means that the flow can be considered as incompressible and inviscid and the Bernoulli's equation can be used to model this flow.

Near the surface of the object the velocity of the flow is affected by the friction with the surface. This boundary layer is comparable with the boundary layer that is presented for the wind near the surface of the earth. Of course is the thickness of the boundary layer of the object much smaller.

If the flow is assumed to be laminar, the behavior can be analyzed for different Reynolds numbers. For a very low Reynolds number, the flow will follow the surface of the body even at sharp corners. When the Reynolds number is increased, symmetric vortexes can occur behind the object. When the Reynolds number is increased even further the symmetry of the vortexes breaks. A Von Karman vortex trail can be observed downstream of the object. At even higher Reynolds numbers the inertia forces predominate, and a turbulent wake is formed behind the object.

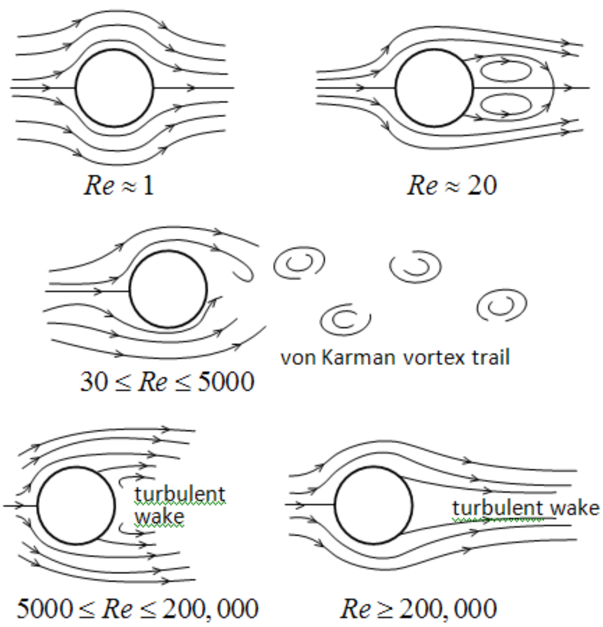

Figure 2.7 Behavior of the flow for different Reynolds numbers

When a flow around an object is observed it can be stated that flow separation can occur, especially at sharp corners. At the location where flow separation occurs, the flow decelerates and friction at the boundary layer slows the flow down. If the length of the object along with the direction of the wind flow is long enough, reattachment can occur. Whether or not this reattachment of the wind flow occurs is also dependent of the Reynolds number. If reattachment occurs the area between the boundary layer and the surface of the structure experience reverse flow of air and turbulence.

Aerodynamic forces and moments

There are only two basic sources that entirely determine the aerodynamic forces and moments, the pressure distribution over the body surface and the shear stress distribution over the body surface. These aerodynamic forces are explained by Anderson very clearly (Anderson, 2011). The shear stress acts tangential to the surface of the body and the pressure acts normal to the surface of the body. The total sum of the shear stress and the pressure integrated over the surface of the body result in a resultant aerodynamic force and moment. The aerodynamic force can be divided into two components. One of the components acts perpendicular to the freestream and one acts parallel to the freestream, respectively the lift and drag force. These forces can be seen as components of the normal force and axial force that work on the object. If the angle of attack is defined as α, the geometrical relation can be defined for the lift and drag.

$$L = N\cos(\alpha) - A\sin(\alpha) \quad \textbf{(2.3.7)}$$
$$D = N\sin(\alpha) + A\cos(\alpha) \quad \textbf{(2.3.8)}$$

The normal and axial forces can be obtained by considering a small part of the upper and lower part of the body. For a small part with length ds, the contribution to the axial and normal force can be calculated. When θ is the angle of the surface of the body it holds for the upper part of the body that

$$dN_u = -p_u ds_u cos(\theta) - \tau_u ds_u sin(\theta) \quad \textbf{(2.3.9)}$$
$$dA_u = -p_u ds_u sin(\theta) + \tau_u ds_u cos(\theta) \quad \textbf{(2.3.10)}$$

For the lower body the equations become

$$dN_l = p_l ds_l cos(\theta) - \tau_l ds_l sin(\theta) \quad \textbf{(2.3.11)}$$
$$dA_l = p_l ds_l sin(\theta) + \tau_l ds_l cos(\theta) \quad \textbf{(2.3.12)}$$

The total normal and axial forces can be obtained by integrating over the total surface of the body form the leading edge (LE) to the trailing edge (TE).

$$N = -\int_{LE}^{TE} (p_u cos(\theta) + \tau_u sin(\theta))\, ds_u + \int_{LE}^{TE} (p_l cos(\theta) - \tau_l sin(\theta))\, ds_l \quad \textbf{(2.3.13)}$$
$$A = \int_{LE}^{TE} (-p_u sin(\theta) + \tau_u cos(\theta))\, ds_u + \int_{LE}^{TE} (p_l sin(\theta) + \tau_l cos(\theta))\, ds_l \quad \textbf{(2.3.14)}$$

These equations can be substituted in the geometrical relations for the drag and lift forces.

$$\begin{aligned} L = \int_{LE}^{TE} &[-\cos(\alpha)\,(p_u cos(\theta) + \tau_u sin(\theta)) + \sin(\alpha)\,(p_u sin(\theta) - \tau_u cos(\theta))] ds_u \\ &+ \int_{LE}^{TE} [\cos(\alpha)\,(p_l cos(\theta) - \tau_l sin(\theta)) - \sin(\alpha)(p_l sin(\theta) + \tau_l cos(\theta))] ds_l \end{aligned} \quad \textbf{(2.3.15)}$$

$$\begin{aligned} D = \int_{LE}^{TE} &[\sin(\alpha)\,(-p_u cos(\theta) + \tau_u sin(\theta)) + \cos(\alpha)\,(-p_u sin(\theta) + \tau_u cos(\theta))] ds_u \\ &+ \int_{LE}^{TE} [\sin(\alpha)\,(p_l cos(\theta) - \tau_l sin(\theta)) + \cos(\alpha)(p_l sin(\theta) + \tau_l cos(\theta))] ds_l \end{aligned} \quad \textbf{(2.3.16)}$$

The value of the aerodynamic moments depends on the location of where the moment equilibrium is taken. The moment can also be obtained from the shear stress and pressure. When moment equilibrium is taken around the leading edge, and a positive moment is assumed clockwise, the following equation can be formulated for the upper and lower part of the body.

$$dM_u = (p_u cos(\theta) + \tau_u sin(\theta))x ds_u + (-p_u sin(\theta) + \tau_u cos(\theta))y ds_u \quad \textbf{(2.3.17)}$$
$$dM_l = (-p_l cos(\theta) + \tau_l sin(\theta))x ds_l + (p_l sin(\theta) + \tau_l cos(\theta))y ds_l \quad \textbf{(2.3.18)}$$

The total moment can be given by integrating over the surface:

$$M = \int_{LE}^{TE} [(p_u cos(\theta) + \tau_u \sin(\theta))x - (p_u sin(\theta) - \tau_u \cos(\theta))y] ds_u + \int_{LE}^{TE} [(-p_l cos(\theta) + \tau_l \sin(\theta))x + (p_l sin(\theta) + \tau_l \cos(\theta))y] ds_l \quad \textbf{(2.3.19)}$$

The shear stress and pressure are dependent of the velocity of the flow. The equations are only valid for bodies in a laminar flow. To simplify the equations, the drag force, lift force and aerodynamic moment can be taken into account by using coefficients.

$$F_D = \frac{1}{2} C_D \rho u^2 A_{ref} \quad \textbf{(2.3.20)}$$
$$F_L = \frac{1}{2} C_L \rho u^2 A_{ref} \quad \textbf{(2.3.21)}$$
$$M = \frac{1}{2} C_M \rho u^2 A_{ref} l_{ref} \quad \textbf{(2.3.22)}$$

Where C_D, C_L and C_M are respectively the coefficients for the drag, lift and aerodynamic moment. A_{ref} is the reference area and l_{ref} is the reference length. The coefficients have no constant values. However in most cases a constant value is taken into account for the calculation because of simplicity. For example the dynamic wind pressure against a building can be given in the following way

$$q_w = C_D \frac{1}{2} \rho u^2 \quad \textbf{(2.3.23)}$$

In most design calculation for buildings a constant value of 1.2 is taken into account for the drag coefficient (C_D). This value can be split up, for the pressure at the front of the structure a value of 0.8 is taken into account and for the suction behind the structure the coefficient has a value of 0.4.

It is however not correct to give the drag coefficient the same value for all structures or objects. Using a constant values might result in substantial deviation of the empirical result.

Vortex shedding
An important phenomenon that can occur near an object in a flow is vortex shedding. Vortex shedding is mostly of importance for relatively short bodies (see also figure 2.9). Because when reattachment can occur this will in most cases stabilize the body, and therefore minimize the effect of vortex shedding. Especially for flexible structures it is important to take the phenomenon of vortex shedding into account. In *Vibrations of Structures* by *J.W. Smith* it is clearly described why this is of importance (Smith, 1988):

"A further feature of vortex shedding is that at resonance the motion of the structure tends to result in the aerodynamic forces becoming better correlated over the length or the height of the structure. This leads to the conditions of 'lock in' in which the vortex shedding remains in resonance over a relatively wide band of wind speed"

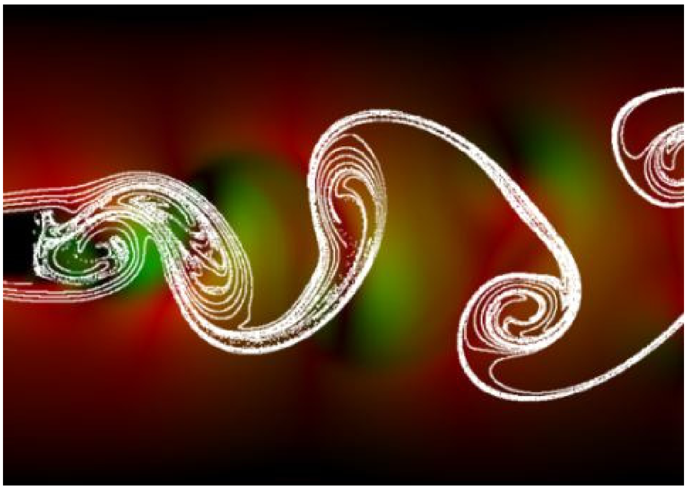

Figure 2.8 Von Karman vortex trail

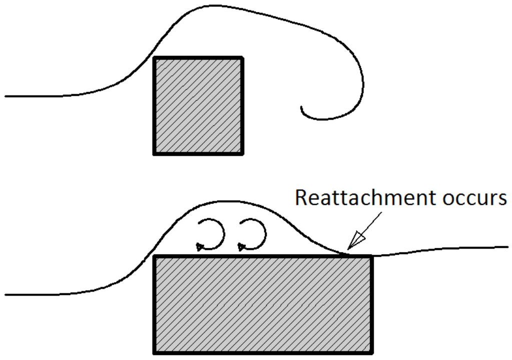

Figure 2.9 Reattachment of the flow dependent on the width of the structure

Aerodynamic Admittance

The aerodynamic admittance function is an adjustment for the dynamic pressure coefficient for the actual body in a wind flow. It relates the fluctuations in the velocity to the cross-wind force fluctuations, for a structure that is subjected to a wind flow. The aerodynamic admittance function gives the effectiveness of a frequency when the turbulent wind velocity is transformed to an aerodynamic force. The aerodynamic admittance function can be represented by the function of Sears when the turbulence is sufficiently high. Experimental data show that the function describes the aerodynamic admittance very accurate for a thin airfoil for which the function was designed. For lower turbulence, the function of Sears underestimates the aerodynamic admittance (Jancauskas, et al., 1983). The function of Sears is defined as following.

$$\chi^2(\omega) = \frac{\left[J_0\left(\frac{\omega l\pi}{U}\right)K_1\left(i\frac{\omega l\pi}{U}\right) + iJ_1\left(\frac{\omega l\pi}{U}\right)K_0\left(i\frac{\omega l\pi}{U}\right)\right]}{K_1\left(i\frac{\omega l\pi}{U}\right) + K_0\left(i\frac{\omega l\pi}{U}\right)} \quad \textbf{(2.3.24)}$$

In this formula the frequency is given by ω, l is the cord length of the structure and U is the mean velocity. The functions J_0 and J_1 are Bessel functions of the first kind, K_0 and K_1 are Bessel functions of the second kind. This function of Sears is developed for a thin symmetrical airfoil. Davenport suggested that for slender bridge decks it might be reasonable to use Sears function for determining the forces. Therefore in some cases the Sears function is used for all cross sections and all turbulences. The function is however not designed and not applicable for all these cases. Large deviations with wind tunnel testing or experiments and the theoretical model were measured. The reason why the Sears function is only applicable for high turbulences is explained by Jancauskas and Melbourne (Jancauskas, et al., 1983) and according to them it can be devoted to the reattachment of the shear layer:

"For an aerofoil section (operated well below its stall angle) all of the lift force results from the integrated of the pressures exerted on the aerofoil by a fully attached flow. For a bluff structure (such as the bridge section), however, a proportion of the lift force results from the net effect of low

pressure regions formed under the reattachment shear layers at the leading edges of the structure. As the turbulence intensity of the flow increases, so does the rate of entrainment of fluid into the two shear layers."

This means that the influence of the low pressure regions on the total lift force relatively decreases when the turbulence is increased. For low turbulence intensities the aerodynamic admittance for bluff object has a value between the Sears functions and the quasi-steady value. By Vickery (1965) the following function for the aerodynamic admittance was proposed.

$$\chi(\omega) = \frac{1}{1 + \left(\frac{2\omega\sqrt{A}}{U}\right)^{4/3}} \tag{2.3.25}$$

This formula was also recommended by Bearman (1980). In this formula A is the frontal area of the structure. For calculations for the vertical buffeting behavior of bridges, both the vertical and the longitudinal wind spectrum is taken into account. Different aerodynamic admittance functions can be used for the longitudinal and the vertical wind turbulence. In most analysis the aerodynamic admittance function is assumed to be equal for both directions. (Le, 2007)

2.4 Wind Induced Vibrations

In this chapter the mechanism buffeting is described. The other phenomena that can occur due to the wind flow are described in APPENDIX 0. In this appendix the phenomena vortex shedding, divergence, galloping and flutter are described and the mathematical representation of these phenomena is given. These four aeroelastic phenomena mentioned in the appendix are not taken into account in the analysis of the bridges.

Buffeting

The turbulence of the wind causes buffeting forces on a structure. These buffeting forces can cause heaving of the structure. The turbulence of the wind can occur in all directions. Buffeting is a different mechanism than the other four mechanisms described in APPENDIX 0. The buffeting forces are not self-exciting, because the structure has no influence on the fluctuations of the wind flow. It can be true that other mechanisms are activated due to the buffeting forces. Because of fluctuations in the wind flow there is no constant wind pressure against the structure. When these pressure fluctuations have a frequency near the natural frequency of the structure, resonance can occur.

For the modeling of buffeting forces quasi-static forces can be used (Costa, et al., 2007). The aerodynamic coefficients, which are used to determine the drag force, lift force and aerodynamic moment, are dependent on the angle of attack and the shape. These coefficients are determined by static wind tunnel testing. The drag force, lift force and aerodynamic moment are given by the equations 2.4.1, 2.4.2 and 2.4.3.

$$F_D = \frac{1}{2} C_D(\alpha)\rho U^2 A_{ref} \quad \textbf{(2.4.1)}$$

$$F_L = \frac{1}{2} C_L(\alpha)\rho U^2 A_{ref} \quad \textbf{(2.4.2)}$$

$$M = \frac{1}{2} C_M(\alpha)\rho U^2 A_{ref} l_{ref} \quad \textbf{(2.4.3)}$$

In these equations the wind speed is built up from the mean wind speed and the fluctuating wind velocity.

$$U = U_m + U(t) \quad \textbf{(2.4.4)}$$

Classification of bridge decks

It is difficult to predict whether or not a certain bridge is susceptible for dynamic effects due to the wind. It is possible to make a global classification of bridges which are susceptible for the different phenomena based on literature. Cable stayed bridges and suspension bridges are most prone for wind induced vibrations. There are basically three types of bridge deck cross sections for these bridges; truss girder bridges, plate girder bridges and box girder bridges. Truss girders are used, and are still the most popular bridge deck system, for suspension bridges. Plate girders are not used for suspension bridges after the collapse of the Tacoma Narrows Bridge in 1940. But this system is used for cable stayed bridges, mostly because of relatively cheap structure. Box girders are used for both suspension bridges and cable stayed bridges.

Truss girders are mainly used to stiffen the deck of suspension bridges. The girders do influence the geometry of the bridge deck. The large height of the truss girders gives rise to higher drag forces. These bridge decks are therefore more sensitive for buffeting forces in the horizontal direction of the wind. In order to design shallower bridge decks plate girders where developed. These plate girders have a reduced height in comparison with the truss girders. As a consequence are the drag forces lower. The plate girders made it possible to design lighter structures. This had consequence for the supporting cables and the towers as well. Too light and slender structures led to aeroelastic problems. This could clearly be observed in the case of the Tacoma Narrows Bridge. For this reason the plate girders are no longer used for suspension bridge decks. For economic reasons plate girders are still used for cable stayed bridges (Matsumoto, et al., 2000).

In 1959 a new type of bridge deck was introduced by Gilbert Roberts of Freeman Fox and Partners (Ricciardelli, 2003): the box girder. The box girder has a more aerodynamic designed shape and is less prone to wind drag. Because of the box shape it has a high torsional stiffness.

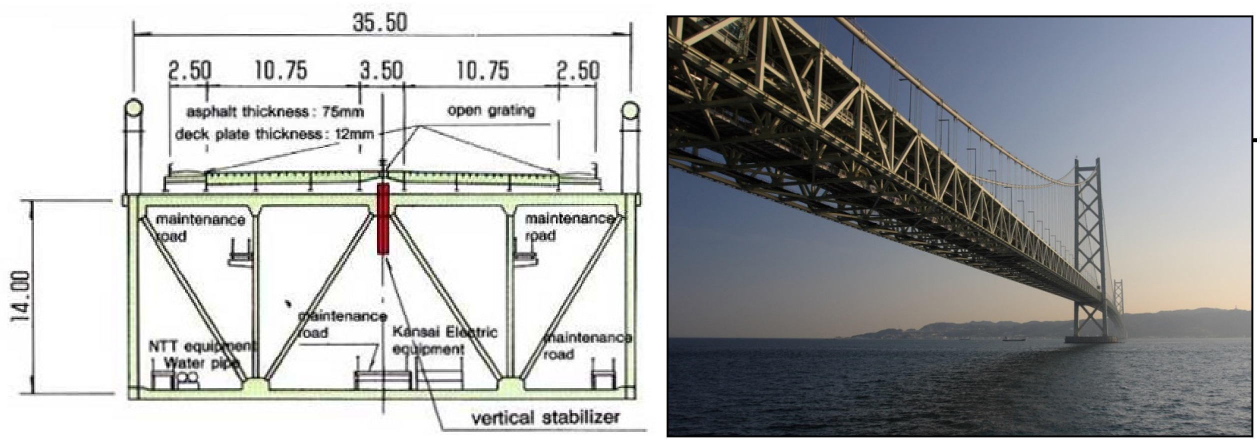

Figure 2.10 Akashi Kaikyo Bridge, example of a truss girder suspension bridge
Source: http://gme.udc.es/en/initiatives/era-2000/recently-constructed-bridges/akashi-kaikyo-bridge

Table 2.1 Overview of the longest suspension and cable stayed bridges (Ge, et al., 2011)

Bridge name	Bridge type	Country	Year built	Length main span	Girder type	Wind induced problem
Akashi Kaikyo	Suspension	Japan	1998	1991 m	Truss	Flutter
Zhejiang Xihoumen	Suspension	China	2008	1650 m	Box	Flutter
Great Belt	Suspension	Denmark	1998	1625 m	Box	Vortex
Jiangsu Runyang S.	Suspension	China	2005	1490 m	Box	Flutter
Humber	Suspension	United Kingdom	1981	1410 m	Box	None
Jiangsu Jiangyin	Suspension	China	1999	1385 m	Box	None
Hong Kong Tsing Ma	Suspension	China	1997	1377 m	Box	Flutter
Verrazano	Suspension	United States	1964	1298 m	Truss	None
Golden Gate	Suspension	United States	1937	1280 m	Truss	None
Hubei Yangluo	Suspension	China	2007	1280 m	Box	None
Jiangsu Sutong	Cable stayed	China	2008	1088 m	Steel box	Stay cables
Tatara	Cable stayed	Japan	1999	890 m	Steel box	Stay cables
Normandy	Cable stayed	France	1995	856 m	Steel box	Stay cables
3rd Jiangsu Nanjing	Cable stayed	China	2005	648 m	Steel box	Stay cables
2nd Jiangsu Nanjing	Cable stayed	China	2001	628 m	Steel box	Stay cables
Zhejiang Jintang	Cable stayed	China	2008	620 m	Steel box	Stay cables
Hubei Baishazhou	Cable stayed	China	2000	618 m	Steel box	Stay cables
Fujian Qingzhou	Cable stayed	China	2003	605 m	Plate girder	Flutter
Shanghai Yangpu	Cable stayed	China	1993	602 m	Plate girder	Stay cables
Shanghai Xupu	Cable stayed	China	1997	590 m	Steel box	None

Ge and Xiang presented an overview of the longest cable stayed bridges and suspension bridges (Ge, et al., 2011). In table 2.1 this overview with the wind induced problem is given. From this table it can be seen that most wind induced problems for suspension bridges are due to flutter. For cable stayed bridges most of the problems arises with vibrations of the stay cables.

It cannot be said that one particular bridge deck or bridge design is always prone to wind induced problems. The dimensions of the bridge do play an important role for wind induced vibrations. At an increasing height buffeting in the wind direction will become more important because of the larger drag. Also vortex shedding can be of importance for bridges with a relative large height. The span of a bridge determines also the susceptibility for wind induced vibrations. For large span bridges almost always the wind load is the determining factor for design. The width of the bridge also influences the behavior of the bridge in a wind flow. A smaller width can be disadvantageous because the bridge may be more prone to vortex shedding. However a larger width can trigger other effects like flutter. The stiffness of the bridge influences the behavior as well. The Tacoma Narrows Bridge had a very flexible deck and in combination with the aerodynamics of the H-shaped cross section flutter occurred at a certain wind velocity.

In the Eurocode EN 1991-1-4 some design regulations are given in order to detect structures that are sensitive for flutter and/or divergence (see also APPENDIX III). This standard gives three design rules based on the dimensions and properties of the structure. The standard can be used as a guideline to detect structures that can be sensitive for wind induced torsion. Kirch stated that these criteria do not cover all the situations (Kirch, et al., 2010).

2.5 Process Description

In order to give an answer to the problem definition defined in the Plan of Action, the process of the project are described here. With this process description a guideline is given for the strategy of the project. The steps are divided into three main categories: the bridge design, the dynamic modeling and the analysis. In this master thesis the sensibility is tested for a bridge designed with normal strength concrete (NSC) and compared with a bridge design for fibre reinforced ultra-high strength concrete (frUHSC). In order to make this comparison both designs should be developed beforehand. The bridge designs are tested based on dynamic models for buffeting. The aeroelastic phenomena flutter, galloping, vortex shedding and divergence are not taken into account in this project. For the model first a single degree of freedom system is used. In order to make the model more reliable a multi degree of freedom system is modeled. In the analysis the results obtained from the models will be used to compare both bridge designs.

1A Bridge Design: Hand Calculations
First the dimensions of the cable stayed bridge should be determined. The comparison between the NSC bridge and the frUHSC bridge can be done by using the same basic design for both bridges. The main dimensions of a traditional cable stayed bridge are determined beforehand and are for both designs the same. This gives some starting points for the design. The dimensions will be determined globally. To accomplish this, some hand calculations are necessary. The dimensions of the main girders are based on the maximum occurring moment and normal force in the cross section.

1B Bridge Design: FE-model
After the global dimensions of the deck, cross beams, main girders and stay cables are determined, a FEM calculation is performed. Matrixframe will be used to calculate the FE-model. In this model the interaction between the stiffness of the main girders and the stiffness of the stay cables can be taken into account. The input of the FE-model is based on the hand calculations.

2A Dynamics: Analytical Approach
The bridge is modeled as a continuous Euler-Bernoulli beam. Based on this model the eigenfrequencies can be determined. The relation between the load and the motion of the system can be expressed in a transfer function. With the transfer functions the different eigenmodes of the system can be taken into account. The wind load is based on the spectrum for the vertical wind velocity and can be integrated over the length of the beam. The response spectrum of the middle of the main span of the bridge can be determined based on the transfer functions and the force spectrum. Because of the simplicity of the model, the analysis for this system can be done with Maplesoft (Technical computing software for engineers). The process of the calculation can be described as following.

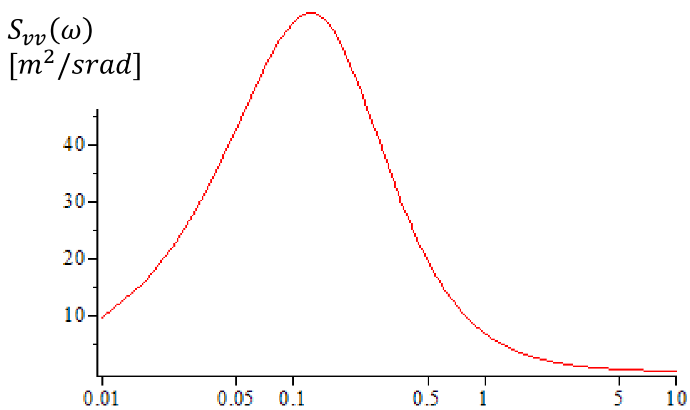

Figure 2.11 Wind spectrum (Davenport)

$\omega\ [rad/s]$

First the wind variance spectrum is modeled. This spectrum determines the effectiveness of the different frequencies. At the left side an example of such a wind spectrum is shown.

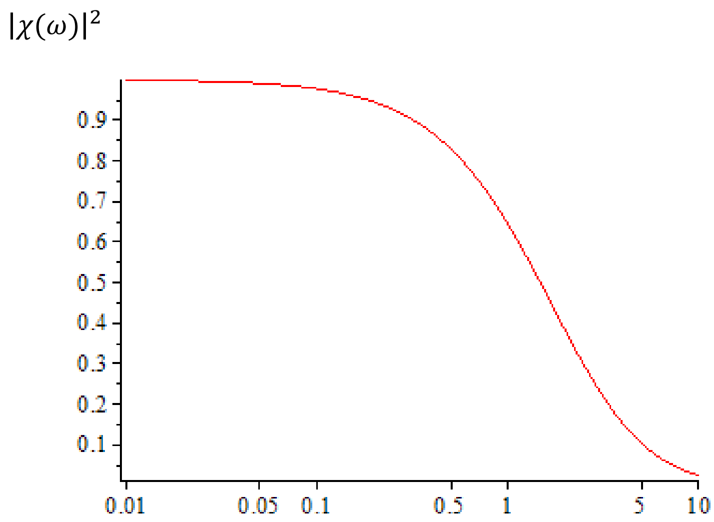

Figure 2.12 Aerodynamic admittance function
Formula 2.3.25 is used for this graph

In order to describe the force spectrum based on the given wind spectrum, it is necessary to use the aerodynamic admittance function.

$S_{FF} = |\alpha_a|^2 S_{vv}$

Where $|\alpha_a|^2$ describes the relation between the wind spectrum and the force spectrum and can be given by:

$|\alpha_a|^2 = (C_{w0}\rho U_m A)^2 \chi^2$

Where χ is the aerodynamic admittance. This gives the relation between the pressure coefficient for different frequencies and the static pressure coefficient.

$\chi = \frac{C_w(\omega)}{C_{w0}}$

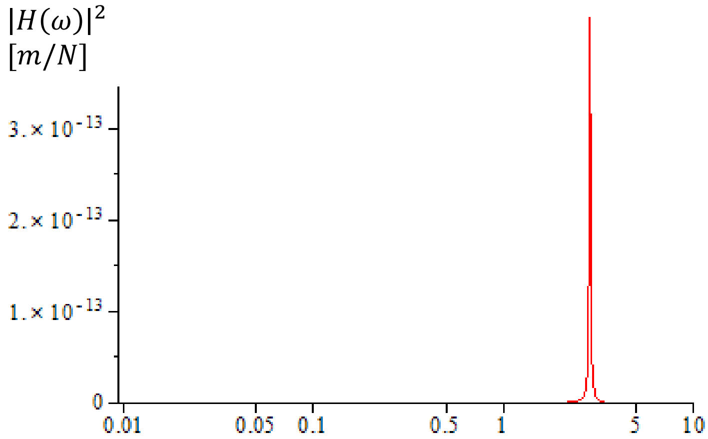

Figure 2.13 Transfer function for sDoF m-s-d-system

The transfer function is dependent of the structure and gives in this situation the relation between the force and the displacement for a single DoF mass spring damping system.

$$|H(\omega)|^2 = \frac{1}{m^2\omega_e^{\,4}\left(\left(1-\frac{\omega^2}{\omega_e^{\,2}}\right)^2 + \frac{4\zeta^2\omega^2}{\omega_e^{\,2}}\right)}$$

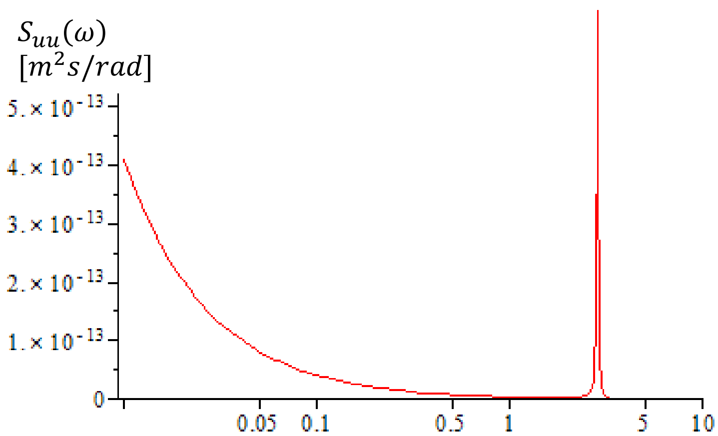

Figure 2.14 Response spectrum for sDoF m-s-d system

The response spectrum can be obtained from the force spectrum and the transfer function.

$S_{uu} = |H(\omega)|^2 S_{FF}$

This spectrum can also be written as:

$S_{uu} = |H(\omega)|^2 |\alpha_a|^2 S_{vv}$

Based on the response spectra for the system with NSC and UHSC it would be possible to compare the two systems.

2B Dynamics: Numerical Simulation

The natural frequencies of the bridge can also be determined by using a FE-model. This is done by assembling the stiffness matrix with the load-displacement method based on the FE-model. The number of nodes that will be used in the model can freely be chosen. By increasing the number of nodes accuracy of the calculation will probably increase as well. However the calculation time will increase also and therefore the calculation becomes more expensive. Therefore the main span of the bridge is divided into 26 bridge sections. The mass of these parts is lumped in a point that represents the section of the bridge. For the modal damping matrix it is assumed that the matrix is diagonal. The damping is proportional to the mass and stiffness matrix (proportional Rayleigh damping matrix). The distributed wind load is modeled as a point load at the different locations. The analysis is performed in Matlab.

The modal analysis of the nDoF-system can be described as following. First the equation of motion can be given in matrix-vector notation:

$$\boldsymbol{M}\underline{\ddot{z}} + \boldsymbol{C}\underline{\dot{z}} + \boldsymbol{K}\underline{z} = \underline{F}(t) \tag{2.5.1}$$

Using the modal analysis approach means that the forced motion is represented as a superposition of the normal modes of the free vibration of the structure multiplied with a unknown function of time. The general solution for the problem can be given by:

$$\underline{z}(t) = \sum_{i=1}^{N} \underline{\hat{z}_i}\, u_i(t) \tag{2.5.2}$$

Where $u_i(t)$ is the unknown function in time and $\sum_{i=1}^{N} \underline{\hat{z}_i}$ is the Eigenmatrix of the structure. This means that:

$$\underline{z}(t) = \boldsymbol{E}\,\underline{u}(t) \tag{2.5.3}$$

Substituting this in the EoM gives:

$$\boldsymbol{ME}\underline{\ddot{u}} + \boldsymbol{CE}\underline{\dot{u}} + \boldsymbol{KE}\underline{u} = \underline{F}(t) \tag{2.5.4}$$

Premultiplying this equation with the transposed Eigenmatrix gives:

$$\begin{gathered}\boldsymbol{E^T ME}\underline{\ddot{u}} + \boldsymbol{E^T CE}\underline{\dot{u}} + \boldsymbol{E^T KE}\underline{u} = \boldsymbol{E^T}\underline{F}(t) \\ \boldsymbol{M}^*\underline{\ddot{u}} + \boldsymbol{C}^*\underline{\dot{u}} + \boldsymbol{K}^*\underline{u} = \boldsymbol{E^T}\underline{F}(t)\end{gathered} \tag{2.5.5}$$

With the modal mass matrix, modal damping matrix and the modal stiffness matrix as:

$$\begin{gathered}\boldsymbol{M}^* = \boldsymbol{E^T ME} \\ \boldsymbol{C}^* = \boldsymbol{E^T CE} \\ \boldsymbol{K}^* = \boldsymbol{E^T KE}\end{gathered} \tag{2.5.6}$$

Orthogonality requires that all non-diagonal terms are zero. The modal damping matrix is generally not diagonal, but this is assumed in this modal analysis. Because the matrices are all diagonal the system can be uncoupled. This simplifies the problem considerably and the Eigen frequencies can be solved. Based on the Eigen frequencies the response spectrum of the system can be determined.

3 Analysis:

The bridge designs can be compared with each other based on the results of the dynamic models. The response spectra of the NSC bridge design and of the frUHSC bridge design can be analyzed and compared. The vertical displacements and the vertical accelerations of the midspan of the bridge will be used in this analysis for the comparison between both bridge designs. The standard deviation of the response of the bridge can be calculated based on the response spectra. With this standard deviation the peak values in a certain time period can be determined.

The parameters used in the models determine the outcome of the results. Because the values of the mass, damping and stiffness of the model possess some uncertainty, varying the parameters can show the influence of the parameters on the results. The influence of completely coupling the forces on the bridge and coupling the forces with cross spectra will be analyzed as well.

Eventually the results of the dynamic calculations will be tested on safety and comfort of the bridge. The static displacements according to the Eurocode can be determined and compared with the peak values from the dynamic analysis. Failure due to fatigue of the reinforcement bars can be checked as well. The comfort of the bridge can be based on the accelerations of the bridge.

3. Bridge Design

3.1 Starting points

In order to determine the buffeting performance of a fibre reinforced High Strength Concrete bridge, it will be necessary to make a comparison between a bridge of frUHSC and NSC. Most of the long span bridges in The Netherlands are cable stayed bridges. No suspension bridges are built in The Netherlands. The reason for this is simple; the soil cannot bear the high horizontal forces generated at the abutments.

There are different forms of cable stayed bridges. For this study a traditional cable stayed bridge is chosen. The basis of the structure is a cable stayed bridge with H-frame pylons. For the main span a length of 237.6 meters is taken into account. For The Netherlands this would be a long span bridge. The side spans are both 96.8 meter. The height of the deck above the mean water level is assumed to be 15 meter, a reasonable value for this type of bridge structure. The most optimum heights of the pylons above the bridge deck is determined based on a rule of thumb. The pylons have therefore a height of 62.5 meter above the deck. Each pylon has 10 stay cables at the side span and 12 stays for the midspan. Stay cables have a c.t.c distance of 8.8 meter at the anchorage point at the deck. The deck width is based on 2x2 lane system with the possibility to expand to a 2x3 lane system by using the emergency traffic lane as a third lane. The deck has a total width of 32.5 meter.

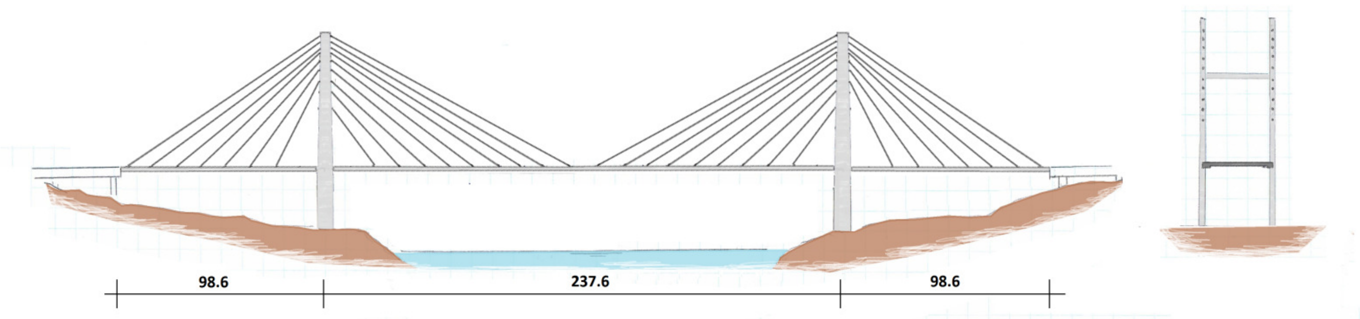

Figure 3.1 Schematic drawing of the cable stayed bridge design

The force transmission of the vehicle loads to the cable stays is realized with a concrete deck, cross beams and main girders. The main girders are carried by the stays. The consequence class is CC3. And it is assumed that the bridge is built in wind area I of the Netherlands.

A typical traditional building method will be used to build the bridge. The in situ casted deck sections will be built form the pylons. To balance the bridge pylon, the bridge deck at both sides of the pylon is built at the same building speed. The sections are built with the help of a temporary falsework structure. In figure 3.2 the building process is shown.

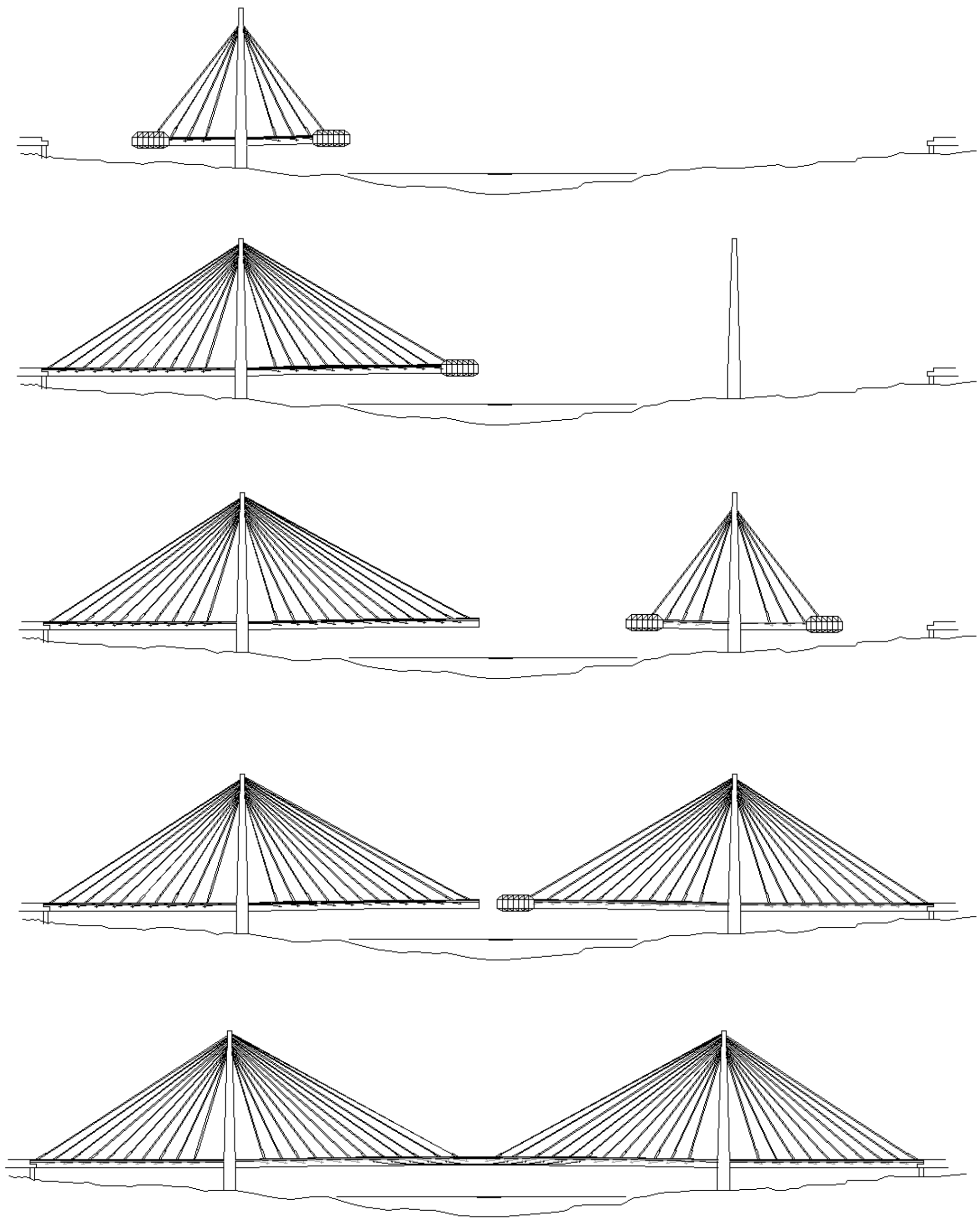

Figure 3.2 Construction process of the cable stayed bridge

Concrete class
To determine the difference between NSC and frUHSC it will be necessary to distinguish two different concrete classes. One class will represent the normal strength concrete while the other will represent the fibre reinforced ultra-high strength concrete. The design for the cable stayed bridge is based on these concrete classes. For the NSC the strength class C35/45 is selected. The strength class C170/200 is taken into account for the frUHSC. To gain strength the water-cement ratio is kept relatively low. A high amount of cement is added to the mixture. It is however not enough to lower the water-cement ratio in order to reach this high concrete class. Silica fume is added to fill up the pores between the cement grains. Silica fume has a large internal surface area and has the ability to form calcium-silicate-hydrates which cooperate to the strength. Because of the high internal surface area the amount of water that should be added to maintain the workability of the mixture would increase. This is not beneficial for the strength. A mixture of this type can therefore not without

superplasticizers. In order to achieve this high strength class it will be necessary to add steel fibers to the concrete mixture. These steel fibres will act as crack arresters and prevent brittle tensile behavior of the mixture. The adding of the fibres will not only influence the strength of the mixture but also the specific weight. The components of the concrete mixtures are given in the overview below.

	C35/45		*C170/200*	
Cement	360	kg/m^3	1075	kg/m^3
Water	145	kg/m^3	170	kg/m^3
Sand	790	kg/m^3	1030	kg/m^3
Gravel	1100	kg/m^3	-	kg/m^3
Silica fume	-	kg/m^3	165	kg/m^3
Superplasticizers	0.5	kg/m^3	39	kg/m^3
Steel fibers	-	kg/m^3	235	kg/m^3
Specific weight	2405	kg/m^3	2810	kg/m^3

Fibre Reinforced Ultra High Strength Concrete (frUHSC)

For the properties of frUHSC the information of www.uhsb.nl is used. The properties of frUHSC are not incorporated into the EC2. The properties of frUHSC can be determined based on the properties of NSC and HSC. Whether or not these properties can be extrapolated from the values that are known for NSC and HSC, is dependent on the results from tests. According to the theoretical approach that is used in the EC2 for HSC, the properties of frUHSC can be determined. When the properties are calculated according to EC2, this results in the following values for C170/200.

Characteristic value of the cube compressive strength:

$$f_{ck} = 200\ N/mm^2 \tag{3.1.1}$$

Characteristic value of the cylinder compressive strength:

$$f_{ck} = 170\ N/mm^2 \tag{3.1.2}$$

The average compressive strength is based on the standard deviation of test results. For all the concrete classes a value of $8\ N/mm^2$is taken into account for the standard deviation. For the average compressive strength this means:

$$f_{cm} = f_{ck} + 8 = 178\ N/mm^2 \tag{3.1.3}$$

The design value for the compressive strength is calculated based on the characteristic value of the cylinder compressive strength and the material factor of concrete.

$$f_{cd} = \frac{f_{ck}}{\gamma_c} = \frac{170}{1.5} = 113\ N/mm^2 \tag{3.1.4}$$

For the tensile strength mostly the correlation between the compressive strength and the tensile strength is taken into account. Another possibility is to determine the tensile strength empirically, with a tension test or a splitting test. The formula that is used to express the tensile strength based on the compressive strength in the EC2, is shown below:

$$f_{ctm} = 2.12 \ln\left(1 + \frac{f_{cm}}{10}\right) = 6.22\ N/mm^2 \tag{3.1.5}$$

This formula does not take the influence of the steel fibres into account. This means that the tensile strength for fibre reinforced concrete might be higher.

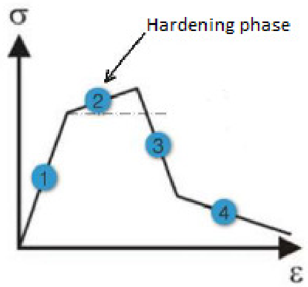

Figure 3.3 stress-strain figure for tension divided into four phases (Source: www.uhsb.nl)

From research it seems that the stress-strain relation of frUHSC deviates from the stress-strain relation of traditional concrete. The yield strain of frUHSC for a compressive stress increases and the ultimate limit strain decreases. Which means that the ratio between the ultimate limit strain and the yield strain decreases. The elastic strain is about 95% of the ultimate limit strain. The frUHSC will have a more brittle behavior than a traditional concrete mixture. The added steel fibres barely influences the compressive strength of the concrete. For the stress-strain relation of the tensile strength of the frUHSC, the steel fibres will influence the figure. The steel fibres will carry a part of the internal tensile strength when cracking of the concrete occurs. The stress-strain relation for tension can be divided into four parts. In the first phase, the concrete behaves elastic. This part of the graph has a linear elastic behavior. After this phase small cracks occur. The steel fibres that are added to the mixture will be tensioned at the locations of the cracks. An UHSC mixture without steel fibres will perform brittle. When sufficient steel fibres are added to the mixture, an increase of tensile stress can occur. This phase is called the hardening phase of the concrete. The angle of the graph will be lower than for the linear elastic part due to the cracks. When the strain is increased even further, the fibres will reach the yield stress. At this point the stress in the fibres cannot increase anymore (when the hardening curve of the steel is neglected.) This will result in an unstable decreasing curve. At an increasing strain, the ultimate strain of the steel fibres is reached or the fibres are pulled out of the concrete. The failure of the steel fibres results in a stable decreasing curve and eventually failure of the concrete.

The cracking of the frUHSC differs from the cracking of traditional concrete. The main difference is due to the strength relation between the cement and the aggregates. For traditional concrete mixtures, the strength of the aggregates is higher than the strength of the cement mixture. When cracks occur, these will be formed around the aggregates through the cement mixture. Especially at the interfacial zone (binding zone between the cement and the aggregate), microcracks will occur. The interfacial zone is the weakest link in the concrete mixture partly due to the higher water-cement ratio. For frUHSC the strength of the aggregates is lower than the cement mixture, this gives rise to cracks through the aggregates. The cracks will not go through the steel fibres.

For Young's modulus use is made of the correlation to the compressive strength in the EC2. Only the short term Young's modulus can be determined based on this correlation.

$$E_{cm} = 22000\left(\frac{f_{cm}}{10}\right)^{0.3} = 52185\ N/mm^2 \qquad \textbf{(3.1.6)}$$

The long term Young's modulus should be determined based on the stress-strain relation of the concrete mixture.

The French AFGC-Setra 2002 gives a guideline for dealing with frUHSC. When for the tensile part of the stress-strain relation this guideline is taken into account the figure 3.14 can be drawn. In this figure the elastic strain for the compressive strength is 2.3‰. The ultimate strain for the compressive zone is equal to 2.6‰.

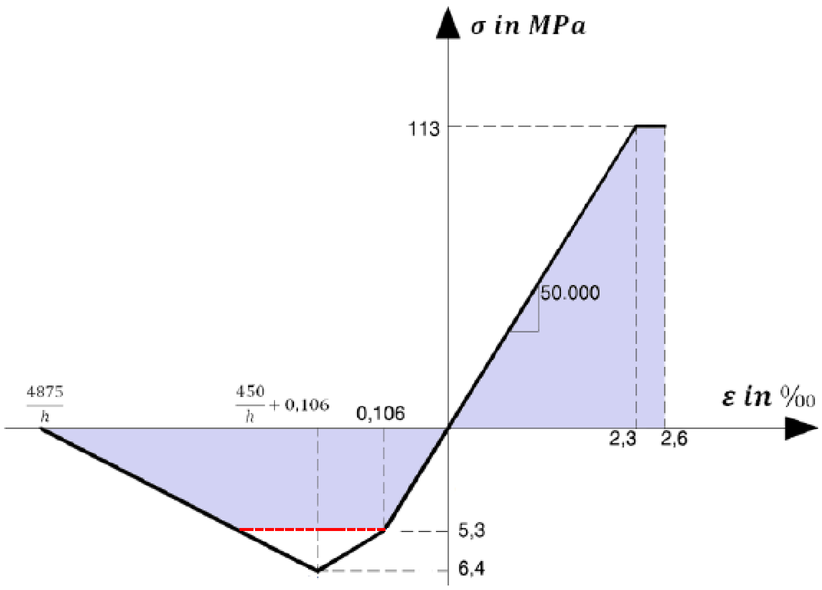

Figure 3.4 stress-strain relation with the tensile part according to AFGC-Setra 2002 (Source: www.uhsb.nl)

The correlation between the compressive strength and the creep coefficient for NSC and HSC shows a graph with a decreasing trend. When this trend is extrapolated for UHSC it can be seen that the creep coefficient goes to 0.8. The time when the load is applied and the relative humidity will have a negligible influence according to this trend line.

3.2 Determining Global Dimensions

In order to give a decent comparison between a cable stayed bridge deck of a normal concrete strength class and a fibre reinforced ultra-high concrete strength class, a design calculation is made for both strength classes. The load transmission is for both bridges realized in the same matter. The dimensions of the bridge deck, the cross girders, the main girders and the stays are determined based on global design calculations.

The design calculation for the determination of the dimensions of the superstructure of the bridge for NSC is made in APPENDIX IV. The calculation for the frUHSC can be found in APPENDIX V.

Two models are used to determine the dimensions of the main girders. The first model is in the building stage when the bridge decks from the two pylons are not connected. When the bridge deck is connected the total system changes. The pylons are clamped at the foot of the pylon. The bridge has one continuous deck, with only expansion joints at the connection with the approach bridges. To avoid problems with expansion and shrinkage of the bridge, all the supports are sliding supports except for one support at one of the pylons.

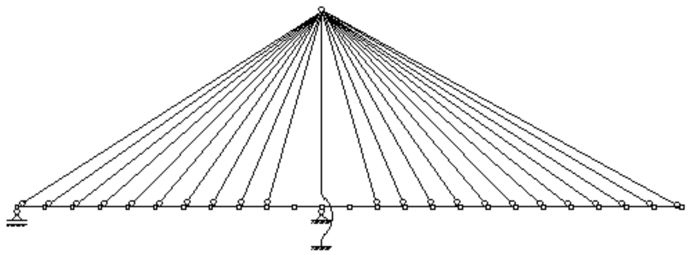

Figure 3.5 Static mechanical system of the bridge before closure of the gap at midspan (Building phase)

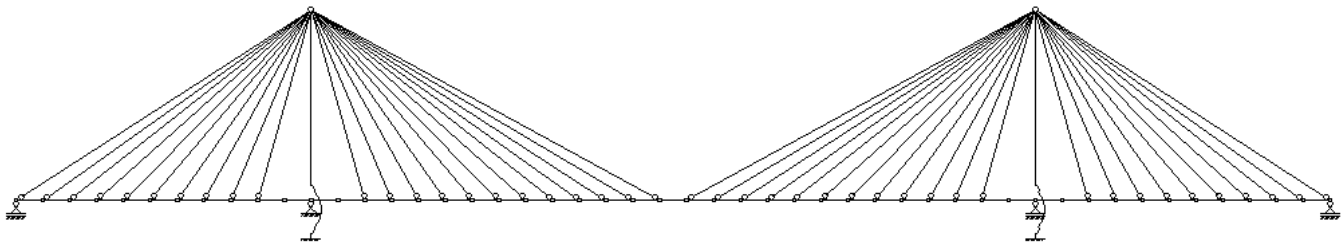

Figure 3.6 Static mechanical system of the bridge after closure of the gap at midspan (Final phase)

The bridge deck will be constructed from a ribbed system. The ribs have a center to center distance of 2.0 meter. The ribs work as small T-beams and gives the floor sufficient strength and stiffness, while reducing the weight of the floor. The ribs span in longitudinal direction over a distance of 4.4 meter. Cross beams will carry the load to the main girders. These cross beams are I-shaped sections, with the top flange integrated into the deck. I-shaped sections are used to reduce the weight of the bridge and to save material. The main girders are supported by a stay cable every 8.8 meter. These girders have a T-shaped or a I-shaped cross section. The dimensions of the bridge deck and the stay cables are partly dependent on the concrete class. Using a higher concrete class will reduce the necessary cross section. Because this will save weight, the dead load on the girders will also be reduced.

The difference in mechanical systems for the building phase and the final phase leads to large differences in internal forces. Especially the moments in the bridge deck deviate a lot when the two phases are compared. Where the final phase knows large positive moments at midspan, in the building phase these moments are not present. The building phase has mainly a large negative moment at the support. The moment at midspan can be reduced by changing the parameters of the stay cables. The stay cables near midspan should be relatively stiff in order to reduce the moment. The stay cables nearer to the pylon can be made less stiff. The stiffness of the stay cables can be increased or decreased by changing the cross sectional area. With other words, the number of strands that are applied in the stay cables can dependent on the required stiffness of the stay cable. By applying stiffer stay cables near the midspan the field moment is lifted and reduced in value.

3.3 Results NSC Calculation

In APPENDIX IV the design calculation is performed for a cable stayed bridge with concrete class C35/45. The dimensions determined in this design calculation are shown in the figures 3.7 and 3.8. In figure 3.7 the cross section of the bridge is given and in figure 3.8 the longitudinal cross section of the cable stayed bridge is shown. The cross sectional properties of the bridge deck can be found in APPENDIX IV and are also summed up below.

$$A_{c,tot} = 20.775\ m^2$$
$$I_{zz} = 6.753\ m^4$$
$$W_{c,top} = 8.647\ m^3$$
$$W_{c,bottom} = 4.597\ m^3$$
$$\rho_c = 2500\ kg/m^3$$
$$E_c = 34 \cdot 10^9\ N/m^2$$

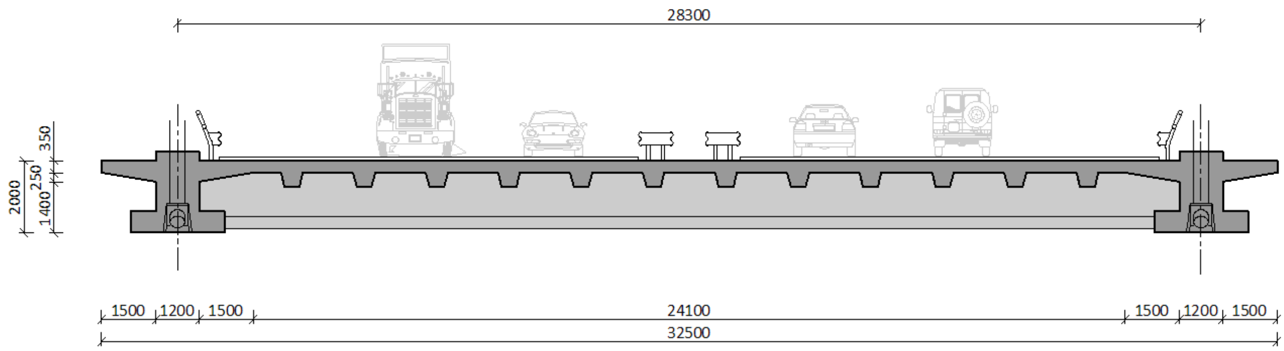

Figure 3.7 Cross section of the cable stayed bridge of NSC

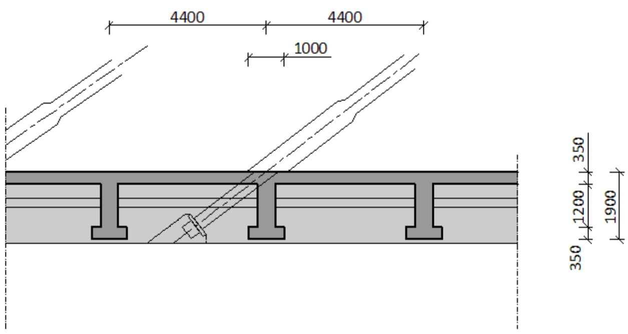

Figure 3.8 Part of the longitudinal cross section of the cable stayed bridge of NSC

The stays of a cable stayed bridge are also calculated in the design calculation. These stays play an important role in the total stiffness of the bridge deck. A FE-model is used to take the interaction between the stay cables and the bridge deck into account.

3.4 Results frUHSC Calculation

The design calculation for the cable stayed bridge with frUHSC (C170/200) is performed in APPENDIX V. In this design calculation the global dimensions are calculated and shown in the figures 3.9 and 3.10.

$$A_{c,tot} = 10.830\ m^2$$
$$I_{zz} = 0.7849\ m^4$$
$$W_{c,top} = 2.6598\ m^3$$
$$W_{c,bottom} = 0.7811\ m^3$$
$$\rho_c = 2900\ kg/m^3$$
$$E_c = 50 \cdot 10^9\ N/m^2$$

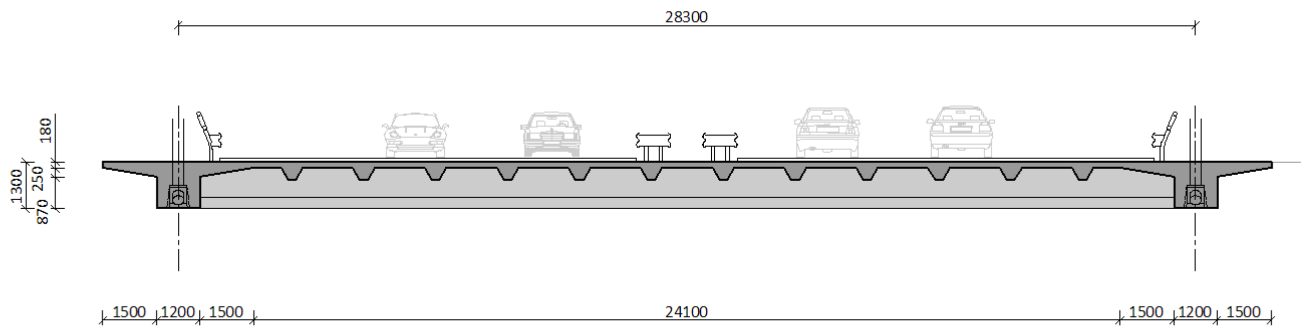

Figure 3.9 Cross section of the cable stayed bridge of frUHSC

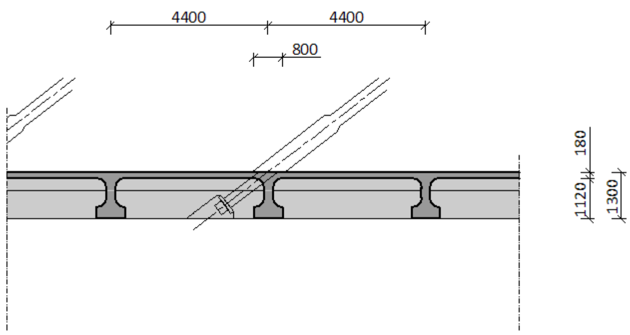

Figure 3.10 Part of the longitudinal cross section of the cable stayed bridge of frUHSC

In comparison with the design for the NSC bridge, the cross sectional area is reduced with about 50%. Also the bending stiffness is much lower. The bending stiffness of the frUHSC bridge deck is about 17% of the value of the bending stiffness of the NSC bridge deck.

4. Analytical Approach Dynamic System

In this chapter the response of the bridge is approached analytically. For the calculation the bridge is modeled as a Euler-Bernoulli beam on an elastic foundation with rotation springs at both ends of the beam. Only the vertical vibrations of the bridge are taken into account. It is assumed that the torsional natural frequencies do not coincide with the vertical natural frequencies of the bridge. The response of the bridge is calculated with Maplesoft 15.

4.1 Determining Natural Frequency

The vertical bending vibrations of the bridge can be estimated with an analytical solution for a continuum system with infinite degrees of freedom. A possible representation of the main span of the bridge, is shown in figure 4.1. The Euler-Bernoulli beam is elastically supported and at both ends the beam is supported by rotation springs.

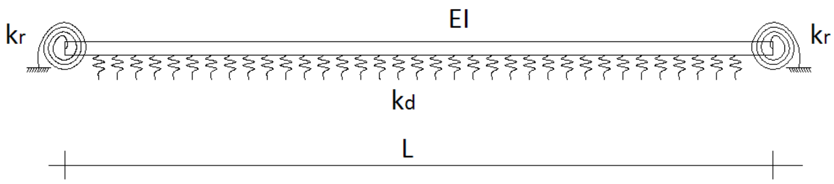

Figure 4.1 Schematic representation of the main bridge span

The Equation of Motion for this type of beam can be derived.

$$\rho_c A_c \frac{\partial^2 w}{\partial t^2} + \frac{\partial^2}{\partial x^2}\left(EI\frac{\partial^2 w}{\partial x^2}\right) + k_d w = 0 \tag{4.1.1}$$

In this equation the external force is disregarded. The time dependent part and the displacement dependent part of the equation can be separated with the harmonic form $w(x,t) = W(x)e^{i\omega t}$.

$$-\omega^2 \rho_c A_c e^{i\omega t} W(x) + EIe^{i\omega t}\frac{\partial^4 W(x)}{\partial x^4} + k_d W(x) e^{i\omega t} = 0 \tag{4.1.2}$$

The time dependent part of the equation can be taken out of the equation. This gives a fourth order differential equation:

$$\frac{\partial^4 W(x)}{\partial x^4} - \beta^4 W(x) = 0 \tag{4.1.3}$$

Where:

$$\beta^4 = \frac{\omega^2 \rho_c A_c - k_d}{EI} \tag{4.1.4}$$

The general solution of the equation can be written as:

$$W(x) = \sum_{k=1}^{4} C_k e^{\lambda_k x} \tag{4.1.5}$$

Substituting the general solution in equation 4.1.3, gives the characteristic equation:

$$\lambda_k = \beta^4 \tag{4.1.6}$$

And the eigenvalues can be obtained.

$$\begin{gathered}\lambda_1 = \beta \\ \lambda_2 = -\beta \\ \lambda_3 = \beta i \\ \lambda_4 = -\beta i\end{gathered} \tag{4.1.7}$$

By substituting the eigenvalues in the general solution it reads.

$$W(x) = C_1 e^{\beta x} + C_2 e^{-\beta x} + C_3 e^{\beta i x} + C_4 e^{-\beta i x} \tag{4.1.8}$$

This general solution can also be written as:

$$W(x) = A\cosh(\beta x) + B\sinh(\beta x) + C\cos(\beta x) + D\sin(\beta x) \tag{4.1.9}$$

The boundary conditions for this problem are given below. The displacement of the beam at both end sides is zero and the end moment is dependent of the rotational spring stiffness.

B.C.1 $W(0) = 0$

B.C.2 $EI\left.\frac{\partial^2 W}{\partial x^2}\right|_{x=0} = k_r \left.\frac{\partial W}{\partial x}\right|_{x=0}$

B.C.3 $W(L) = 0$

B.C.4 $EI\left.\frac{\partial^2 W}{\partial x^2}\right|_{x=L} = -k_r \left.\frac{\partial W}{\partial x}\right|_{x=L}$

Substituting the boundary conditions in the general solution and writing this in a matrix-vector equation the following can be obtained.

$$\begin{bmatrix} 1 & 0 & 1 & 0 \\ EI\beta^2 & -\beta k_r & EI\beta^2 & -\beta k_r \\ \cosh(\beta L) & \sinh(\beta L) & \cos(\beta L) & \sin(\beta L) \\ EI\beta^2\cosh(\beta L) + \beta k_r \sinh(\beta L) & EI\beta^2\sinh(\beta L) + \beta k_r\cosh(\beta L) & -EI\beta^2\cos(\beta L) - \beta k_r \sin(\beta L) & -EI\beta^2\sin(\beta L) + \beta k_r\cos(\beta L) \end{bmatrix} \begin{bmatrix} A \\ B \\ C \\ D \end{bmatrix} = \underline{\mathbf{0}} \tag{4.1.10}$$

A frequency equation can be obtained when the determinant of the matrix is set equal to zero. By doing this the frequency equation would be equal to:

$$\begin{gathered}\beta^2 {k_r}^2[\sinh^2(\beta L) + 2\cosh(\beta L)\cos(\beta L) - \cosh^2(\beta L) - 1] - 4EI^2\beta^4\sinh(\beta L)\sin(\beta L) \\ + 4k_r EI\beta^3[\sinh(\beta L)\cos(\beta L) - \cosh(\beta L)\sin(\beta L)] = 0\end{gathered} \tag{4.1.11}$$

The intersection with the neutral axis gives a value for β. This value can be substituted into equation 4.1.4. This gives the natural frequencies of the system.

$$\omega_n = \sqrt{\frac{EI{\beta_n}^4 + k_d}{\rho_c A_c}} \tag{4.1.12}$$

4.2 Transfer Function

For the analysis of the system it is necessary to describe the transfer function of the system. In a damped NDoF system the transfer function $H_{z_iF_p}$ relates the amplitude of the displacement of mode j to the force that is applied to degree of freedom p.

$$z_j = H_{z_jF_p}F_p \tag{4.2.1}$$

The equation of motion can be given by the following matrix equation:

$$\boldsymbol{M}\underline{\ddot{z}} + \boldsymbol{C}\underline{\dot{z}} + \boldsymbol{K}\underline{z} = \underline{F}(t) \tag{4.2.2}$$

When the theory form the modal analysis is applied, the system can be uncoupled. The i^{th} uncoupled equation can be written as:

$$m_{ii}{}^*\ddot{u}_i + c_{ii}{}^*\dot{u}_i + k_{ii}{}^*u_i = \sum \underline{\hat{z}}_{i,p}{}^T\hat{F}_p e^{i\omega t} \tag{4.2.3}$$

Where u_i is the i^{th} modal coordinate.
Substitution of $u_i = C_i e^{\omega ti}$ gives:

$$u_i = \frac{\sum \underline{\hat{z}}_{i,p}{}^T\hat{F}_p}{[-\omega^2 m_{ii}{}^* + \omega i c_{ii}{}^* + k_{ii}{}^*]} e^{\omega ti} \tag{4.2.4}$$

When only the j^{th} degree of freedom is considered the equation becomes.

$$z_j = \sum_i \underline{z}_{i,j}u_i = \sum_i \underline{z}_{i,j} \frac{\sum \underline{\hat{z}}_{i,p}{}^T\hat{F}_p}{[-\omega^2 m_{ii}{}^* + \omega i c_{ii}{}^* + k_{ii}{}^*]} e^{\omega ti} \tag{4.2.5}$$

This means that the transfer function can be written as:

$$H_{z_jF_p} = \sum_i \frac{\underline{z}_{i,j}\underline{\hat{z}}_{i,p}}{[-\omega^2 m_{ii}{}^* + \omega i c_{ii}{}^* + k_{ii}{}^*]} \tag{4.2.6}$$

4.3 Damping

The damping of a structure can basically be split up in a damping due to the geometry and material damping and aerodynamic damping. When the damping due to the material is considered, the kinetic energy is converted to heat. A part of the kinetic energy can dissipate through the supports. This type of damping is referred as the geometric damping. Another possibility for a structure to dissipate energy is through the air. The aerodynamic damping is proportional to the velocity of the structure in relation to the velocity of the air flow.

The damping is in many cases expressed as the damping ratio, and gives the ratio between the damping and the critical damping. The critical damping is dependent of the mass and the stiffness of the structure. This means that the critical damping varies for different structures. However the material damping will change for different structures as well. The damping ratio is therefore a relatively constant value for expressing the amount of damping in a system.

The material damping of different materials can be found in the *CUR 75 Demping van bouwconstructies* (CUR, 1977). In the CUR-report the material damping ratios for reinforced concrete, prestressed concrete and steel are given. The material damping of these three materials are given below.

	$\zeta_m = c_m/c_{cr}$
Reinforced Concrete	*0.9%*
Prestressed Concrete	*0.9%*
Steel	*0.4%*

Due to the normal force in the concrete the material will probably behave as prestressed concrete. The compressive stress-strain diagrams of the materials can be compared. Comparing these diagrams for the concrete classes C35/45 and C170/200 and steel S235 shows that the elastic part of the compressive stress of the frUHSC has values for the stiffness and strength between the NSC and the steel. In the CUR-report it is suggested that the material damping ratio can be expressed as following:

$$\zeta_m = \frac{R}{2\rho_c} \qquad \textbf{(4.3.1)}$$

Where R is the dampingsfactor per frequency and ρ is the mass density of the material. When the dampingsfactor would be equal for both concrete classes the density of the material would determine the damping ratio.

From these observations it seems that it would be logical that the material damping ratio for frUHSC would be lower than for NSC. The British design rules for aerodynamic effect of bridges gives that the material damping ratio for concrete is equal to $\zeta_m = 0.8\%$. And because the bridge is cable supported this value should be multiplied with a reduction factor of 0.75 (Highways-Agency, et al., 2001). This gives a damping ratio of $\zeta_m = 0.6\%$. For a steel cable supported bridge this would mean that the damping ratio would be equal to $\zeta_m = 0.36\%$. Based on this information the material damping ratio for frUHSC is estimated on 0.45%. But because of the uncertainty of this value other value are taken into account as well in the analysis (see chapter 4.6.4).
The geometric damping due to energy dissipation of the bearings is small in comparison with the material damping because of the length of the bridge and therefore not taken into account.

The value of the aerodynamic damping depends on the wind speed and the natural frequency. The CUR 75 report (CUR, 1977) gives the following expression for the aerodynamic damping ratio.

$$\zeta_{aero} = \frac{1/2 C_D \rho U A}{2m\omega_n} \qquad \textbf{(4.3.2)}$$

This formula shows that the aerodynamic damping becomes less important for higher eigenfrequencies.

The effect of the damping on peak of the dynamic amplification factor for a sDoF system can be seen in figures 4.2 and 4.3. In these figures four transfer functions with different damping ratios are plotted. The height of the peak reduces when the damping ratio increase.

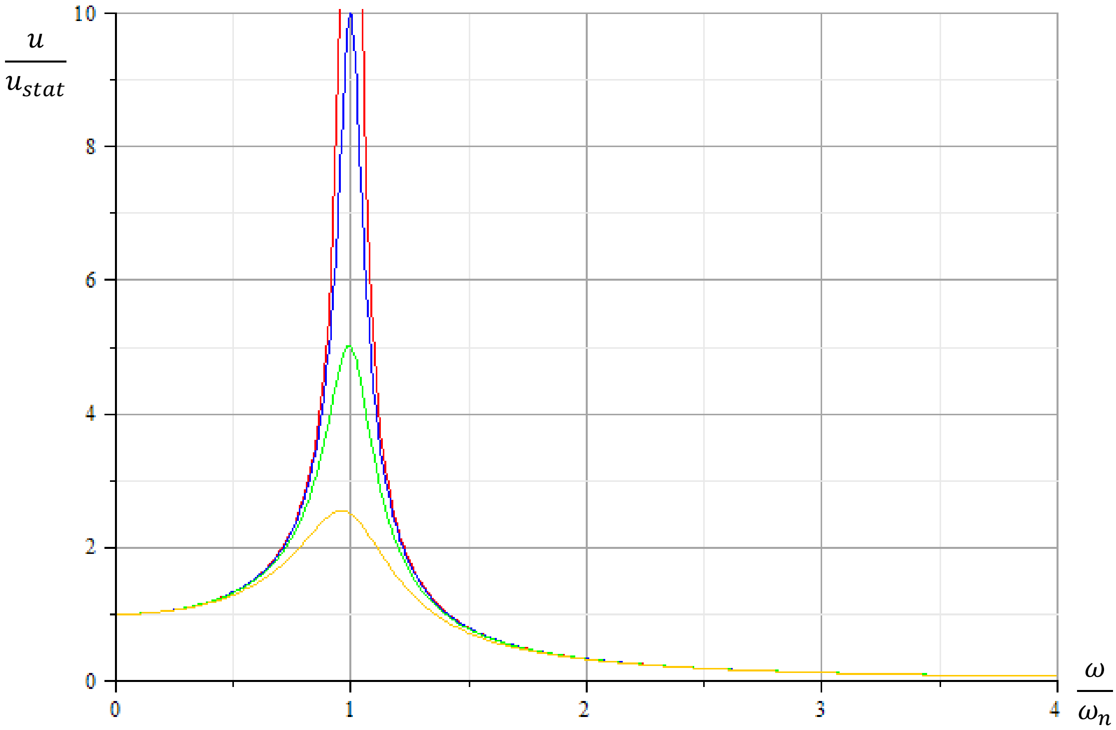

Figure 4.2 Dynamic amplification function for different damping ratios

In figure 4.3 the peaks of the dynamic amplification factor for the damping ratios 0.4%, 0.6% and 0.9% is shown. The height of the peak is proportional to the damping ratio. The height of the peak can be estimated with $1/(2\zeta)$.

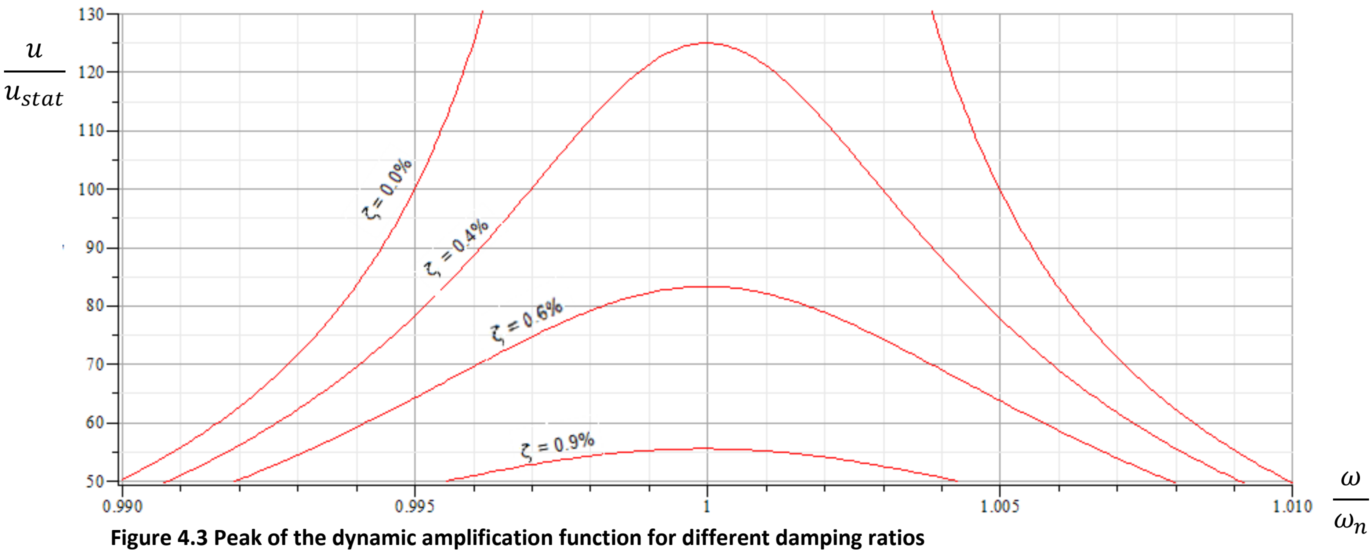

Figure 4.3 Peak of the dynamic amplification function for different damping ratios

4.4 Response Spectrum

The response spectrum of the displacement at mid span of the bridge due to the lift force can be determined with the following formula.

$$S_{uu}(\omega) = \int_0^L \int_0^L H_{u_{L_1}} H_{u_{L_2}}{}^* S_{L_1 L_2}(\omega) dy_1\, dy_2 \qquad \textbf{(4.4.1)}$$

The transfer functions, $H_{u_{L_1}}$ and $H_{u_{L_2}}{}^*$, and the cross-spectrum of the lift forces $L_1 = L(y_1, t)$ and $L_2 = L(y_2, t)$, $S_{L_1 L_2}(\omega)$, should be integrated over the length of the structure because of the distributed load.

The transfer functions can be expressed as following:

$$H_{u_{L_1}} = \sum_i \frac{u_i(y_{midspan}) u_i(y_1)}{k_i - \omega^2 m_i + c_i \omega i} \qquad \textbf{(4.4.2)}$$

$$H_{u_{L_2}}{}^* = \sum_j \frac{u_j(y_{midspan}) u_j(y_2)}{k_j - \omega^2 m_j - c_j \omega i}$$

In these transfer functions, $u_i(y)$ is the i^{th} eigenmode of the structure, k_i is the i^{th} generalized stiffness, m_i is the i^{th} generalized mass and c_i is the i^{th} generalized damping. It should be noted that $c_i \omega$ is a complex value.
Substituting these transfer functions in equation 4.4.1 gives:

$$S_{uu}(\omega) = \int_0^L \int_0^L \sum_i \frac{u_i(y_{midspan}) u_i(y_1)}{k_i - \omega^2 m_i + c_i \omega i} \cdot \sum_j \frac{u_j(y_{midspan}) u_j(y_2)}{k_j - \omega^2 m_j - c_j \omega i} \cdot S_{L_1 L_2}(\omega) dy_1\, dy_2 \qquad \textbf{(4.4.3)}$$

The part of the equation that is not dependent of y_1 or $y_2$can be taken out of the integral.

$$S_{uu}(\omega) = \sum_i \frac{u_i(y_{midspan})}{k_i - \omega^2 m_i + c_i \omega i} \cdot \sum_j \frac{u_j(y_{midspan})}{k_j - \omega^2 m_j - c_j \omega i} \cdot \int_0^L \int_0^L u_i(y_1) u_j(y_2) S_{L_1 L_2}(\omega) dy_1\, dy_2 \qquad \textbf{(4.4.4)}$$

When the damping is relatively small the response spectrum can be approximated with the following formula:

$$S_{uu}(\omega) \approx \sum \frac{u_i(y_{midspan})^2}{(\rho A)^2 \omega_i{}^4 \left[\left(1 - \frac{\omega^2}{\omega_i{}^2}\right)^2 + 4\zeta_i{}^2 \frac{\omega^2}{\omega_i{}^2} \right]} \cdot \int_0^L \int_0^L u_i(y_1) u_j(y_2) S_{L_1 L_2}(\omega) dy_1\, dy_2 \qquad \textbf{(4.4.5)}$$

Where ω_i is the i^{th} eigen frequency of the structure, ρA is the weight of the structure per unit length and ζ_i is the i^{th} damping ratio. The last part of the response spectrum can be calculated as following.

$$\int_0^L \int_0^L u_i(y_1) u_j(y_2) S_{L_1 L_2}(\omega) dy_1\, dy_2 = |J_i(\omega)|^2 S_{LL}(\omega) \qquad \textbf{(4.4.6)}$$

To take into account the correlation of the wind loading along the length of the bridge for the different modes of the bridge the function $|J_i(\omega)|^2$ is used. This function can be expressed as following:

$$|J_i(\omega)|^2 = \frac{1}{\left[\int_0^L u_i(y)^2 dy\right]^2} \int_0^L \int_0^L coh_{y_1 y_2}(y_1, y_2, \omega) u_i(y_1) u_i(y_2) dy_1 dy_2 \tag{4.4.7}$$

Where the coherence is a frequency dependent function for the mutual distance of y_1 and y_2.

$$coh_{y_1 y_2}(y_1, y_2, \omega) = \exp\left(-\frac{\omega\sqrt{C_y{}^2 (y_1 - y_2)^2}}{2\pi U_m}\right) \tag{4.4.8}$$

The analysis of the spectrum $S_{LL}(\omega)$ can be obtained by considering the time dependent lift force on the structure per unit length.

$$\tilde{L} = \frac{1}{2}\rho U_m{}^2 B \left[C_L \frac{2U(t)}{U_m} + \left(\frac{\partial C_L}{\partial \alpha} + \frac{h}{B} C_D\right)\frac{W(t)}{U_m}\right] \tag{4.4.9}$$

When h is the height of the bridge and B the width, the ratio h/B will be small. Therefore this term can be neglected. This gives:

$$\tilde{L} = \rho C_L B U_m U(t) + \frac{1}{2}\rho \frac{\partial C_L}{\partial \alpha} B U_m W(t) \tag{4.4.10}$$

When the cross-spectrum of the longitudinal and vertical turbulence is neglected, the spectrum of $\tilde{L}$ can be given by:

$$S_{\tilde{L}\tilde{L}}(\omega) = \rho^2 U_m{}^2 B^2 \left(C_L{}^2 S_{UU}(\omega) + \frac{1}{4}\frac{\partial C_L}{\partial \alpha}\bigg]_{\alpha=0}^2 S_{WW}(\omega)\right) \tag{4.4.11}$$

When the aerodynamic admittance function is taken into account the spectrum for L can be given by:

$$S_{LL}(\omega) = \rho^2 U_m{}^2 B^2 \left(C_L{}^2 S_{UU}(\omega) + \frac{1}{4}\frac{\partial C_L}{\partial \alpha}\bigg]_{\alpha=0}^2 S_{WW}(\omega)\right) |\chi(\omega)|^2 \tag{4.4.12}$$

Where the reduced spectrum for the longitudinal wind velocity can be given by the Von Karman-Harris reduced spectrum:

$$\frac{\omega S_{UU}(\omega)}{2\pi \sigma_U{}^2} = \frac{4\left(\frac{\omega L_U}{2\pi U_m}\right)}{\left(1 + 70.8\left(\frac{\omega L_U}{2\pi U_m}\right)^2\right)^{5/6}} \tag{4.4.13}$$

And for the reduced spectrum for the vertical wind velocity can be given by the equation of Bush and Panofsky:

$$\frac{\omega S_{WW}(\omega)}{2\pi\sigma_W{}^2} = \frac{2.15\left(\frac{\omega L_W}{2\pi U_m}\right)}{\left(1 + 11.16\left(\frac{\omega L_W}{2\pi U_m}\right)^{5/3}\right)} \qquad \textbf{(4.4.14)}$$

From the data of the Engineering Science Data Unit (ESDU) the following values are given for the turbulence lengths: $L_U = 200m$ and $L_W = 18m$. For the determination of the standard deviation of the wind speed ($\sigma_U = I_U U_m$), the information of the ESDU was used as well: $I_U = 11\%$ and $I_W = 6\%$. (ESDU85020, 2001)

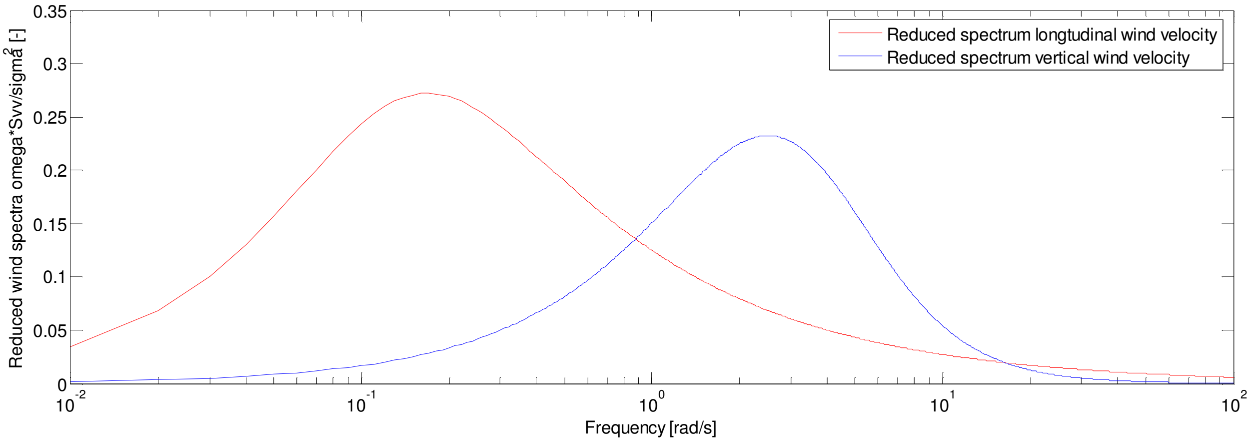

Figure 4.4 Reduced wind spectra for longitudinal and vertical direction

4.5 Numerical Values

In this chapter the numerical values used for the calculations are given. The numerical values for stiffness and the natural frequencies of the system are determined in this chapter.

4.5.1 Stiffness

For the determination of the stiffness value for both of the cable stayed bridges, the FE-model is used. In the model the super dead load and 40% of the distributed life load is applied as contribution for the mass. The displacement at midspan is determined for these loads. Subsequently the bridge is loaded with an additional uniform distributed unit load of 100kN/m. The additional displacement of the mid span of the bridge can be used for the calculation of the stiffness value. In table 4.1 the displacements obtained from the FE-models are given.

Table 4.1 Displacement of midspan according to the FE-model

	Displacement at midspan due to Super dead load + 0.4Life load	Displacement at midspan due to Super dead load + 0.4Life load + Unit load	Additional displacement due to Unit load
NSC	0.1047m	0.2718m	0.1671m
frUHSC	0.1579m	0.4211m	0.2632m

The stiffness value is determined based on:

$$k_s = \frac{L \cdot q_{unit}}{u_{unit}} \tag{4.5.1}$$

NSC bridge spring stiffness:

$k_s = 142.2 \cdot 10^6 N/m$

frUHSC bridge spring stiffness:

$k_s = 90.27 \cdot 10^6 N/m$

4.5.2 Natural Frequencies of Vertical Vibrations

The natural frequencies for vertical vibrations of the cable stayed bridge design can be calculated based on the formula found in equation 4.1.12. Before this formula can be used some parameters should be determined first. The Young's modules, moment of inertia and the cross sectional area are determined in APPENDIX IV and APPENDIX V.

For the rotational spring stiffness the value can be determined based on the values found in the FE-model. Due to the additional unit load, that was also used for determining the displacements at midspan (table 4.1), an additional moment at the support and an additional rotation at the support can be found as well. Based on these values, an estimation of the rotational spring stiffness can be given.

The elastic stiffness that supports the beam is based on the cable stay supports. A possible solution to find a value for this spring stiffness is by modeling the spring supported beam in Matrixframe. The unit load should give rise to an analogous displacement as was found in the FE-model. By varying the elastic spring stiffness the same displacement can be found. With some iterations the spring stiffness can be found.

	NSC (C35/45)		*frUHSC (C170/200)*	
$E_c =$	$34 \cdot 10^9$	N/m^2	$52 \cdot 10^9$	N/m^2
$I_c =$	6.753	m^4	0.7849	m^4
$A_c =$	20.775	m^2	10.830	m^2
$\rho_c =$	2500	kg/m^3	2900	kg/m^3
$k_r =$	$7.6 \cdot 10^9$	Nm/rad	$3.4 \cdot 10^9$	Nm/rad
$k_d =$	$640 \cdot 10^3$	N/m^2	$395 \cdot 10^3$	N/m^2

For the mass of the super dead load a value of 4245 kg/m is taken into account. And for the mass due to the life load 40 % is taken into account (5606 kg/m).

With these values the characteristic length can be solved from equation 4.1.11. This gives a value of:

	NSC (C35/45)		*frUHSC (C170/200)*	
$\beta_1 =$	0.01712329	m^{-1}	0.01828603	m^{-1}
$\beta_2 =$	0.02935524	m^{-1}	0.03083187	m^{-1}
$\beta_3 =$	0.04198603	m^{-1}	0.04349618	m^{-1}
$\beta_4 =$	0.05480717	m^{-1}	0.05627393	m^{-1}
$\beta_5 =$	0.06774291	m^{-1}	0.06913794	m^{-1}

The values can be substituted into equation 4.1.12 in order to obtain the natural frequencies.

	NSC (C35/45)	frUHSC (C170/200)
$\omega_1 =$	$3.268 \quad rad/s$	$3.116 \quad rad/s$
$\omega_2 =$	$3.622 \quad rad/s$	$3.235 \quad rad/s$
$\omega_3 =$	$4.680 \quad rad/s$	$3.621 \quad rad/s$
$\omega_4 =$	$6.625 \quad rad/s$	$4.415 \quad rad/s$
$\omega_5 =$	$9.414 \quad rad/s$	$5.673 \quad rad/s$

It can be seen that especially the first natural frequency is for a large part determined by the stiffness of the stays. For the higher natural frequencies the bending stiffness of the bridge becomes of more importance. This also explains why the values of the frUHSC bridge are much closer to each other than the values of the NSC bridge.

Intermezzo: Verification Natural frequency Rayleigh-Ritz Method

For the verification of the formula found for the natural frequencies for the vertical vibration of the beam, the Rayleigh-Ritz method is used. The Rayleigh-Ritz method makes use of the energy of the system. A certain shape for the deflection curve is necessary in order to solve the system. In *Vibration Problems in Engineering* (p.461-466) by Weaver, Timoshenko and Young (Weaver, et al., 1990), the Rayleigh-Ritz method is used to determine an estimation of the first natural frequency of the stretched wire. In the calculation below the same approach is used. In order to model the elastic supporting springs and the rotation spring at the support, the information of the article *Dynamics of Nonlinear Beams on Elastic Foundation* by Akour is used (Akour, 2010).

First the potential and kinetic energy in the system should be determined. For the kinetic energy it is assumed that the entire cross section displaces without a rotation. The kinetic energy can be represented with the following formula:

$$T(w) = \int_0^l \frac{1}{2}\rho_c A_c \left(\frac{\partial w}{\partial t}\right)^2 dx \tag{4.5.2}$$

In this formula the following equation of kinetic energy can be recognized $T = 1/2mv^2$.
For the potential energy the following equation is presented:

$$U(w) = \frac{1}{2}\int_0^l \left[EI\left(\frac{\partial^2 w}{\partial x^2}\right)^2 + k_d w^2\right] dx + \frac{1}{2}k_r\left(\frac{\partial w}{\partial x}\right)^2_{x=L} \tag{4.5.3}$$

The bending stiffness of the beam and the spring stiffness of the elastic 'foundation' can be found in the integral. The potential energy of rotation spring stiffness of the support can be found in the last term. The maximum potential energy can be obtained when the beam is in the extreme position.

$$w_{max} = X \tag{4.5.4}$$

The maximum kinetic energy occurs when :

$$\frac{\partial w}{\partial t}_{max} = \omega X \tag{4.5.5}$$

Substituting this into the equations of kinetic and potential energy gives:

$$T_{max} = \int_0^l \frac{1}{2}\rho_c A_c \omega^2 \left(\frac{\partial X}{\partial t}\right)^2 dx \tag{4.5.6}$$

$$U_{max} = \frac{1}{2}\int_0^l \left[EI\left(\frac{\partial^2 X}{\partial x^2}\right)^2 + k_d X^2\right] dx + \frac{1}{2}k_r\left(\frac{\partial X}{\partial x}\right)^2_{x=l} \tag{4.5.7}$$

This gives:

$$\frac{1}{2}\rho_c A_c \omega^2 \int_0^l \left(\frac{\partial X}{\partial t}\right)^2 dx = \frac{1}{2}EI\left\{\int_0^l \left[\left(\frac{\partial^2 X}{\partial x^2}\right)^2 + \frac{k_d}{EI}X^2\right] dx + \frac{k_r}{EI}\left(\frac{\partial X}{\partial x}\right)^2_{x=l}\right\} \tag{4.5.8}$$

Where X can be represented by a summation of functions.

$$X(x,t) = a_1\varphi_1(x) + a_2\varphi_2(x) + \ldots \tag{4.5.9}$$

It is important that the boundary conditions hold in this equation ($w_{(x=\pm l)} = 0$). This can be accomplished by using symmetric curves.

$$X(x,t) = a_1(l^2 - x^2) + a_2(l^2 - x^2)x^2 \tag{4.5.10}$$

The coefficients a_1 and a_2 should be selected in such a way that the ratio of U_{max}/T_{max} is minimalized. This can be accomplished with:

$$\frac{\partial}{\partial a_j} \cdot \frac{\int_0^l \left[\left(\frac{\partial^2 X}{\partial x^2}\right) + \frac{k_d}{EI}X^2\right] dx + \frac{k_r}{EI}\left(\frac{\partial X}{\partial x}\right)^2_{x=l}}{\int_0^l X^2 dx} \tag{4.5.11}$$

Elaborate this differentiation gives:

$$\int_0^l X^2 dx \cdot \frac{\partial}{\partial a_j}\left\{\int_0^l \left[\left(\frac{\partial^2 X}{\partial x^2}\right) + \frac{k_d}{EI}X^2\right] dx + \frac{k_r}{EI}\left(\frac{\partial X}{\partial x}\right)^2_{x=l}\right\} - \left\{\int_0^l \left[\left(\frac{\partial^2 X}{\partial x^2}\right) + \frac{k_d}{EI}X^2\right] dx + \frac{k_r}{EI}\left(\frac{\partial X}{\partial x}\right)^2_{x=l}\right\} \cdot \frac{\partial}{\partial a_j}\int_0^l X^2 dx = 0 \tag{4.5.12}$$

From equation 4.5.8 it can be seen that:

$$\int_0^l \left[\left(\frac{\partial^2 X}{\partial x^2}\right)^2 + \frac{k_d}{EI}X^2\right] dx + \frac{k_r}{EI}\left(\frac{\partial X}{\partial x}\right)^2_{x=l} = \frac{\rho_c A_c \omega^2}{EI}\int_0^l \left(\frac{\partial X}{\partial t}\right)^2 dx \tag{4.5.13}$$

Substituting this into the second part of equation 4.5.12 gives:

$$\frac{\partial}{\partial a_j}\left\{\int_0^l \left[\left(\frac{\partial^2 X}{\partial x^2}\right) + \frac{k_d}{EI}X^2 - \frac{\rho_c A_c \omega^2}{EI}X^2\right] dx + \frac{k_r}{EI}\left(\frac{\partial X}{\partial x}\right)^2_{x=l}\right\} = 0 \tag{4.5.14}$$

When the derivative is taken with respect to a_1 and a_2 the two equation that can be found can written in matrix form:

$$\begin{bmatrix} A_{11} & A_{12} \\ A_{21} & A_{22} \end{bmatrix} \begin{bmatrix} a_1 \\ a_2 \end{bmatrix} = \underline{\mathbf{0}} \quad \textbf{(4.5.15)}$$

Where:

$$A_{11} = 8l + \frac{16}{15}\frac{k_d}{EI} l^5 - \frac{16}{15}\frac{\rho_c A_c \omega^2}{EI} l^5 + 1.1290752 \cdot 10^5 \frac{k_r}{EI} \quad \textbf{(4.5.16)}$$
$$A_{12} = A_{21} = 8l + \frac{16}{105}\frac{k_d}{EI} l^7 - \frac{16}{105}\frac{\rho_c A_c \omega^2}{EI} l^7 + 1.5935135 \cdot 10^9 \frac{k_r}{EI}$$
$$A_{11} = 33.6l + \frac{16}{315}\frac{k_d}{EI} l^9 - \frac{16}{315}\frac{\rho_c A_c \omega^2}{EI} l^9 + 2.2489957 \cdot 10^{13} \frac{k_r}{EI}$$

When the determinant of the matrix is equal to zero, the frequencies can be solved. Two values can be found. Where the lowest value can be used for the first natural frequency. It should be noted that only half of the beam is considered $(l = L/2)$. With this method the natural frequency is approached from above. The Rayleigh-Ritz method gives an estimation of the first natural for the NSC bridge of: $\omega_1 = 3.292\ rad/s$ and for the frUHSC bridge of $\omega_1 = 3.123\ rad/s$. The error of these estimations with the actual natural frequency is respectively $\varepsilon = 0.75\%$ and $\varepsilon = 0.22\%$ for the NSC bridge and the frUHSC bridge. This verification shows that the expression found in 4.1.12 is correct.

The bridges do not only have vertical frequencies, but horizontal and torsional frequencies as well. The horizontal frequencies are high due to the high bending stiffness in horizontal direction. The horizontal motion of the bridge due to buffeting is therefore not taken into account. The torsional frequencies of the bridge can influence the motion of the bridge. Especially when the frequencies coincide with the vertical frequencies. In this report the torsional motions are disregarded. In order to determine whether or not the torsional frequencies are in the same range as the vertical frequencies a estimation of these frequencies is made.

Intermezzo: Torsional frequencies

The vertical frequencies of the bridge can be influenced by the torsional frequencies. In order to obtain the magnitude of these frequencies, it is necessary to determine the torsional frequencies with a simple method. Some 3D-FEM computer programs can determine the torsional frequencies of such a structure. However, when such a program is not used, the torsional frequencies can be estimated with some hand calculations.

The Equation of Motion can be written as:

$$\rho_c J \frac{\partial^2 \varphi}{\partial t^2} - \frac{\partial}{\partial x}\left(GJ_t \frac{\partial \varphi}{\partial x}\right) + c\varphi = m \quad \textbf{(4.5.17)}$$

Where ρ_c is the mass density, J is the polar moment of inertia, G is the shear modulus, J_t is the torque constant and c is the rotational stiffness per unit length. When the external force is not taken into account and the harmonic form of the rotation is substituted into the EoM it can be seen that:

$$\varphi(x,t) = \Phi(x) e^{i\omega t} \quad \textbf{(4.5.18)}$$

And thus:

$$\frac{\partial^2 \Phi(x)}{\partial x^2} + \alpha^2 \Phi(x) = 0 \tag{4.5.19}$$

Where:

$$\alpha^2 = \frac{\omega^2 \rho_c J - c}{G J_t} \tag{4.5.20}$$

The general solution for this second order differential equation can be written as:

$$\Phi(x) = \sum_{k=1}^{2} C_k e^{\lambda_k x} \tag{4.5.21}$$

This gives a general solution for this problem of:

$$\Phi(x) = A\cos(\alpha x) + B\sin(\alpha x) \tag{4.5.22}$$

For the values of α_n the rotational stiffness at the support should be known. When it is assumed that the bridge deck does not undergo a torsional rotation at the supports, the frequency can be expressed as:

$$\omega_n = \frac{n\pi}{L}\sqrt{\frac{GJ_t + c\left(\frac{L}{n\pi}\right)^2}{\rho_c J}} \tag{4.5.24}$$

The polar moment of inertia and the torque constant can be calculated based on the cross sections. The polar moment of inertia can be given by:

$$J = \int_A r^2 dA = I_{zz} + I_{yy} \tag{4.5.25}$$

This gives the following numerical values for the bridge designs:

$$J_{NSC} = 2139 m^4$$
$$J_{frUHSC} = 1054 m^4$$

For thin walled open section the torque constant can be given by the following formula:

$$J_t = \sum_i c_i w_i {t_i}^3 \tag{4.5.26}$$

Where c_i is a coefficient based on the ratio between the width and the thickness of each element. Based on this formula the torque constant can be calculated for both bridge designs. The cross girders in the bridge will have a certain influence on the torque constant as well.

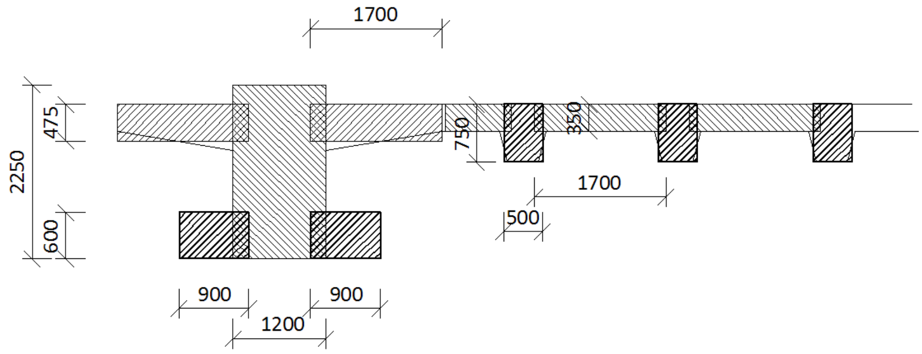

Figure 4.5 Deviation of cross section to determine the torque constant

In the tables 4.2 and 4.3 the torque constant is calculated for the NSC bridge design and the frUHSC bridge design.

Table 4.2 Determination of the torque constant for the NSC bridge

	Torque constant J_t	Length	Contribution
Main girders	$1.2715m^4 \quad x2$	$237.6m$	0.73%
Bridge deck	$0.0419m^4 \quad x12$	$237.6m$	0.14%
Cross girders	$0.0695m^4 \quad x53$	$28.3m$	0.13%
Total	$2.543 + 0.503 + 3.686 \cdot \frac{28.3}{237.6} = 3.485m^4$		

Table 4.3 Determination of the torque constant for the frUHSC bridge

	Torque constant J_t	Length	Contribution
Main girders	$0.6440m^4 \quad x2$	$237.6m$	0.77%
Bridge deck	$0.0086m^4 \quad x12$	$237.6m$	0.06%
Cross girders	$0.0457m^4 \quad x53$	$28.3m$	0.17%
Total	$1.288 + 0.103 + 2.420 \cdot \frac{28.3}{237.6} = 1.679m^4$		

Based on the stiffness of the stays the torsional stiffness per unit length can be determined.

$$c_{NSC} \approx 428 \cdot 10^6 Nm/m \cdot rad$$
$$c_{frUHSC} \approx 267 \cdot 10^6 Nm/m \cdot rad$$

This results into the following first four natural frequencies:

	NSC (C35/45)	*frUHSC (C170/200)*
$\omega_1 =$	$9.04 \quad rad/s$	$9.46 \quad rad/s$
$\omega_2 =$	$9.30 \quad rad/s$	$9.78 \quad rad/s$
$\omega_3 =$	$9.72 \quad rad/s$	$10.30 \quad rad/s$
$\omega_4 =$	$10.29 \quad rad/s$	$10.98 \quad rad/s$

From this calculation it seems that the torsional frequencies are in a higher range than the vertical bending frequencies. It is possible that with a more advanced calculation method the frequencies have some different values. But it seems that the first torsional frequency is larger than 1.5 times the first bending frequency. From basic design rules this means that the torsional oscillations does not affect the vertical vibrations. In this report the torsional behavior is not taken into account any further.

In order to check whether or not the natural frequencies that were found are reasonable values for this type of bridges some values of reference bridges are given. The first natural vertical frequency of the bridges and the sources are given in table 4.2. Numerical values for the natural frequencies found in this chapter should be in the same order as the reference projects.

Table 4.2 Several reference bridges with first natural frequency

Name	*Type*	*Main span*	*Natural frequency*	*Reference*
Second Severn Crossing	Cable stayed composite plate girder	456m	0.34 Hz	(Macdonald, et al., 2005)
Wye Bridge	Cable stayed Steel box girder	408m	0.46 Hz	(Holmes, 2003)
Third Nanjing Bridge	Cable stayed steel box girder	648m	0.31 Hz	(Zhu, et al., 2007)
Melak bridge	Cable stayed concrete plate girder	340m	0.23 Hz	(Supartono, 2008)
Gi-Lu bridge	Cable stayed Concrete plate girder	240m	0.61 Hz	(Lu, et al.)

Comparing these values with the first natural frequency found, it can be seen that the fundamental frequency seems reasonable for this type of bridge. Especially the Gi-Lu bridge is very comparable with the design bridges used in this case study. The natural frequency of this bridge is close to the frequencies found in this analysis.

4.5.3 Response

For the determination of the response of the systems the following numerical values are taken into account.

Properties of the wind

Mean wind speed	$U_m = 36.62\ m/s$	
Turbulence intensity along wind	$I_U = 11\%$	
Turbulence intensity vertical wind	$I_W = 6\%$	
Standard deviation along wind	$\sigma_U = 4.028\ m/s$	
Standard deviation vertical wind	$\sigma_W = 2.197\ m/s$	
Air density	$\rho = 1.25\ kg/m^3$	
Lift coefficient	$C_L = 0.9$	
	$\left.\frac{\partial C_L}{\partial \alpha}\right\|_{\alpha=0} = 1.0$	(according to information of (Ruscheweyh, 1982) p.116)

Properties NSC bridge design

Width of the bridge	$B = 32.5\ m$
Length of the bridge	$L = 237.6\ m$
Cross sectional area	$A_c = 20.775\ m^2$
Mass density	$\rho_c = 2500\ kg/m^3$
Natural frequency	$\omega_1 = 3.268\ rad/s$
	$\omega_3 = 4.680\ rad/s$
	$\omega_5 = 9.414\ rad/s$
Material damping ratio	$\zeta_m = 0.6\%$
Aerodynamic damping ratio	$\zeta_{aero,1} = 0.12\%$
	$\zeta_{aero,3} = 0.08\%$

	$\zeta_{aero,5} = 0.04\%$
Total Damping ratio	$\zeta_1 = 0.72\%$
	$\zeta_3 = 0.68\%$
	$\zeta_5 = 0.64\%$

Properties frUHSC bridge design

Width of the bridge	$B = 32.5\ m$
Length of the bridge	$L = 237.6\ m$
Cross sectional area	$A_c = 10.83\ m^2$
Mass density	$\rho_c = 2900\ kg/m^3$
Natural frequency	$\omega_1 = 3.116\ rad/s$
	$\omega_3 = 3.621\ rad/s$
	$\omega_5 = 5.673\ rad/s$
Material damping ratio	$\zeta_m = 0.45\%$
Aerodynamic damping ratio	$\zeta_{aero,1} = 0.10\%$
	$\zeta_{aero,3} = 0.09\%$
	$\zeta_{aero,5} = 0.05\%$
Total Damping ratio	$\zeta_1 = 0.55\%$
	$\zeta_3 = 0.54\%$
	$\zeta_5 = 0.50\%$

For the calculation the procedure is followed as is described in paragraph 4.4. The midspan of the bridge is considered in this calculation. The eigenmodes of the system are assumed to be sinusoide functions. Because the even eigenmodes have no displacement at midspan, these modes are not taken into account.

In the figure 4.6 the response spectra of the vertical displacement for the bridges in the wind are shown. It can be seen that in the response spectrum of the NSC bridge that only the first and the third natural frequency have influence on the response of the system. For the frUHSC bridge the fifth eigenfrequency has still influence on the response.

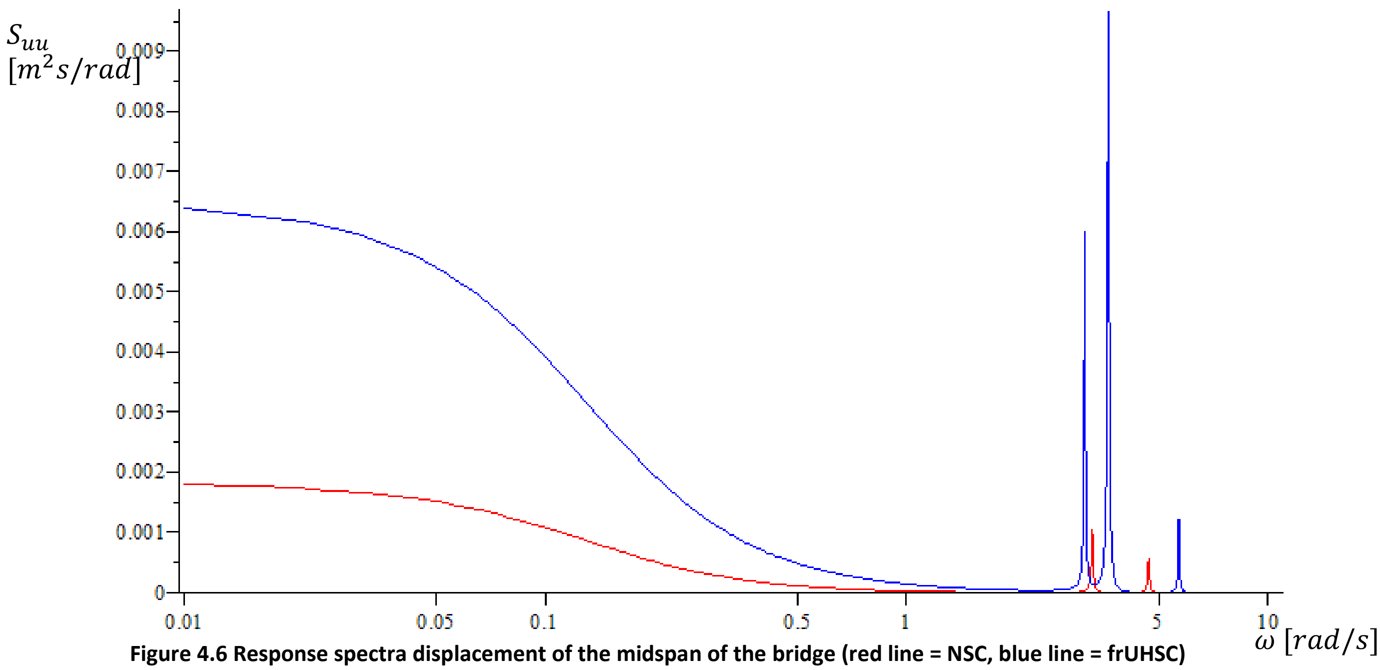

Figure 4.6 Response spectra displacement of the midspan of the bridge (red line = NSC, blue line = frUHSC)

According to figure 4.6 the third natural frequency of the frUHSC bridge design has more influence of the response than the first natural frequency. The standard deviation can be calculated for both spectra. This gives $\sigma_u = 0.02154m$ for the standard deviation of the response spectrum of the NSC bridge and $\sigma_u = 0.05164m$ for the frUHSC bridge. This would mean that the peak value during a 6 hour storm is 0.0930m and 0.2225m for respectively the NSC bridge design and the frUHSC bridge design. The last value is almost 2.4 times larger than the peak value of the displacement at midspan for the NSC bridge design.

When the time dependent domain is considered, the displacement of the midspan of the bridge due to the turbulence can be shown. In figure 4.7 the displacement of the midspan of the bridge of NSC and frUHSC is shown. It can be seen that the displacement at midspan of the frUHSC bridge reaches higher values than for the NSC bridge.

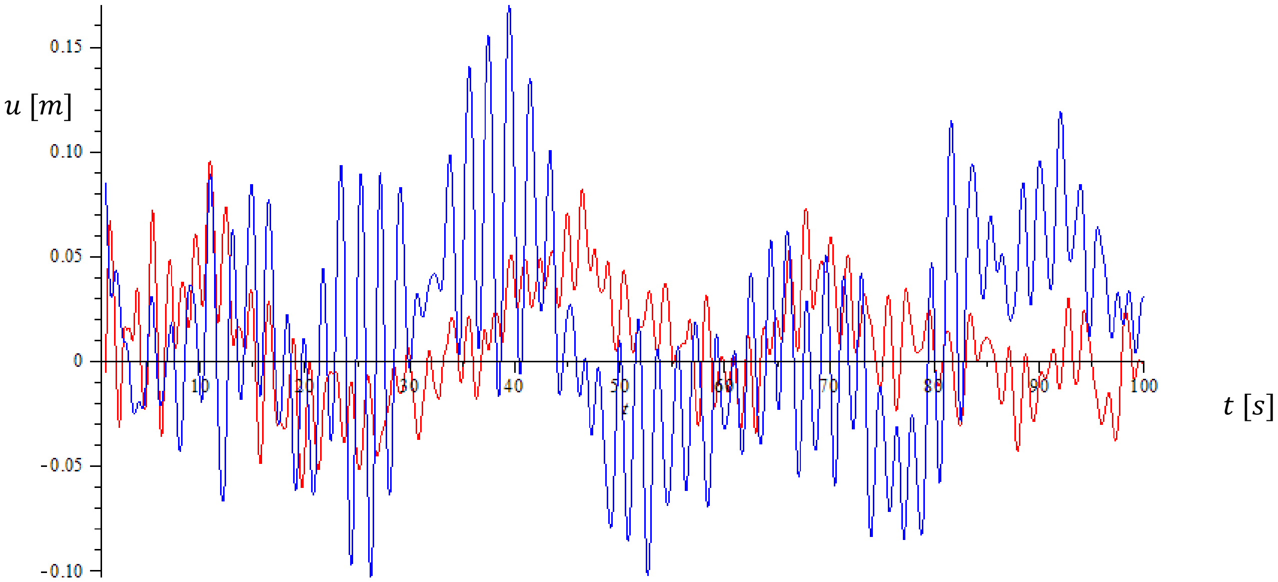

Figure 4.7 Vertical displacement of the midspan in time domain (red line = NSC, blue line = frUHSC)

4.6 Parameter Study

Because of the uncertainties in the calculations, the sensitivity of the result due to the values of the input parameters is tested. In this parameter study the response is tested by changing the values for the damping, the stiffness of the stays, the mass and the rotation springs.

4.6.1 Varying the Stiffness of the Stays

When the stiffness of the stays is reduced the natural frequencies of the bridge will become lower. This will result that the natural frequencies become closer to the frequency where the peak occurs in the wind spectrum. In this study the value for stiffness of the stays is changed with +10% and -10% of the original value. For the stiffness of the stays of the NSC bridge this gives 576 N/m^2 and 704 N/m^2 and for the frUHSC bridge this gives 355.5 N/m^2 and 434.5 N/m^2. A possibility of expressing the influence of changing these parameters is by calculating the standard deviation of the response spectrum.

$$\sigma_u{}^2 = \int_0^\infty S_{uu}(\omega)d\omega \tag{4.6.1}$$

When for the upper boundary of the integral the value of 10 rad/s is taken into account, the following values can be found;

	NSC (C35/45)			frUHSC (C170/200)		
$\sigma_{u,95\%} =$	0.02265	m	+5.2%	0.05450	m	+5.7%
$\sigma_u =$	0.02154	m		0.05154	m	
$\sigma_{u,105\%} =$	0.02054	m	-4.6%	0.04998	m	-3.0%

The influence of the stiffness of the stays on the standard deviations is about inversely proportional. In figure 4.8 the influence on the peak displacement for a period of 10 minutes due to the deviation of the stiffness of the stays is shown. For both bridges the relation is almost linear.

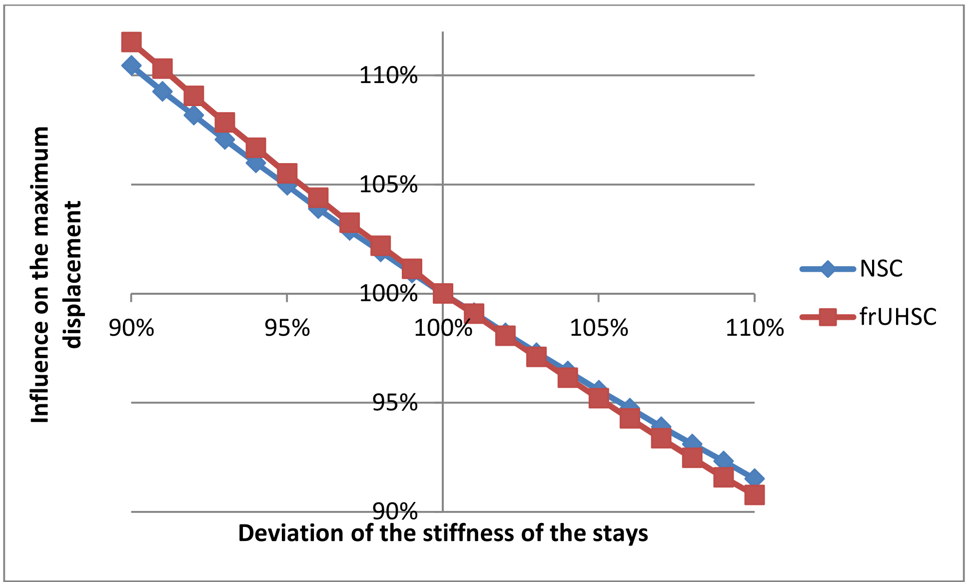

Figure 4.8 Influence of the stiffness of the stays on the displacement

4.6.2 Varying the Mass

In the calculation of the natural frequencies of the bridge, the self-weight, the super dead load and 40% of the life load taken into account. In order to analyze the effect of the life load on the response of the bridge two additional situations are considered. In the first situation there is no life load present on the structure and in the second situation the bridge is fully loaded.

	NSC (C35/45)		frUHSC (C170/200)	
$\omega_{1,LL0\%} =$	3.427	rad/s	3.348	rad/s
$\omega_{3,LL0\%} =$	4.908	rad/s	3.896	rad/s
$\omega_{5,LL0\%} =$	9.872	rad/s	6.102	rad/s
$\omega_{1,LL100\%} =$	3.066	rad/s	2.836	rad/s
$\omega_{3,LL100\%} =$	4.391	rad/s	3.301	rad/s
$\omega_{5,LL100\%} =$	8.832	rad/s	5.170	rad/s

The higher the mass of the structure the lower the natural frequencies of the bridge are. So when the bridge is fully loaded the structure becomes more sensitive for vibrations.

	NSC (C35/45)			frUHSC (C170/200)		
$\sigma_{u,LL0\%} =$	0.02120	m	-1.6%	0.04897	m	-5.0%
$\sigma_{u,LL100\%} =$	0.02219	m	+3.0%	0.05539	m	+7.5%

The varying of the mass has more influence of the response of the frUHSC bridge than on the NSC bridge. This can be devoted to the relative increase/decrease of the mass. Because the weight of the frUHSC bridge is much lower than the weight of the NSC bridge.

4.6.3 Varying the Rotation Spring Value

When the value of the rotation spring is changes the characteristic length of the system changes as well. This will result in different eigenfrequencies. For this parameter study the influence of changing the original value of the rotation springs with +10% and – 10% is investigated. The natural frequencies do not deviate a lot from the original values for the natural frequencies. This can be explained because, especially the lower natural frequencies, are largely determined by the stiffness of the stays.

	NSC (C35/45)		frUHSC (C170/200)	
$\omega_{1,90\%} =$	3.268	rad/s	3.116	rad/s
$\omega_{3,90\%} =$	4.666	rad/s	3.618	rad/s
$\omega_{5,90\%} =$	9.390	rad/s	5.659	rad/s
$\omega_{1,110\%} =$	3.272	rad/s	3.117	rad/s
$\omega_{3,110\%} =$	4.701	rad/s	3.633	rad/s
$\omega_{5,110\%} =$	9.451	rad/s	5.698	rad/s

	NSC (C35/45)			frUHSC (C170/200)		
$\sigma_{u,90\%} =$	0.02159	m	+0.2%	0.05164	m	+0.2%
$\sigma_{u,110\%} =$	0.02141	m	-0.6%	0.05120	m	-0.7%

From the standard deviations it can be seen that the rotation spring stiffness has relatively small influence on the displacements of the bridge. For values -10% and +10% the standard deviation changes 0.2% to 0.7%.

4.6.4 Varying the Damping Ratio

The influence of the damping on the response spectrum can be tested by changing the damping ratio. When the damping ratio is lowered with 0.05% the standard deviation becomes 1.1% and 2.6% higher for respectively the NSC bridge design and the frUHSC bridge design.

	NSC (C35/45)			frUHSC (C170/200)		
$\sigma_{u,-0.05\%} =$	0.02178	m	+1.1%	0.05289	m	+2.6%
$\sigma_{u,+0.05\%} =$	0.02132	m	-1.0%	0.05039	m	-2.2%

In figure 4.9 the influence of deviations in the damping ratios on the peak displacement is shown for both bridge designs. Adapting the damping ratio has more effect on the frUHSC bridge than it has on the NSC bridge. This can be explained, because the peaks that occur at the natural frequencies are influenced the most. The displacement response of the frUHSC bridge is more influenced by these peaks than the response of the NSC bridge (See also figure 4.6) .

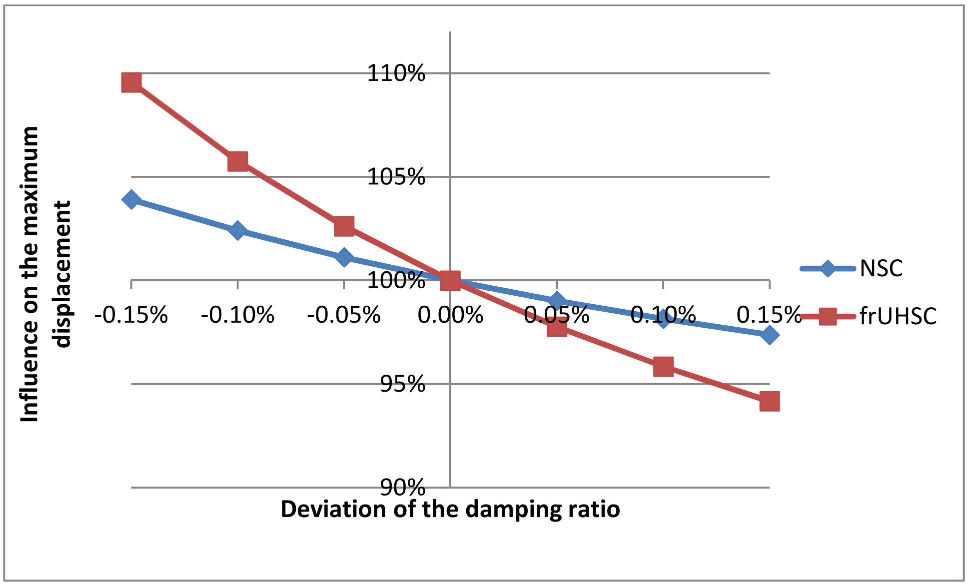

Figure 4.9 Influence of the damping ratio on the displacement

5. Numerical Simulation Matlab

In this chapter the response of both bridge designs is determined with a numerical simulation in the program Matlab. For the model of the bridge design a FE-model is used. This approach deviates from the analytical approach discussed in chapter 4. By using two different type of methods to calculate the response of the bridge increases the reliability of the calculations. The Matlab codes that where designed for this analysis are added in the appendices.

5.1 Wind

In order to model the wind in Matlab it is necessary to use the Fourier series and use certain spectra for the vertical wind velocity and longitudinal wind velocity. In APPENDIX VI the Matlab code that is used to model the wind is shown. In figure 5.1 the turbulent wind velocity is shown for the vertical and horizontal direction for a certain time period of 300 seconds.

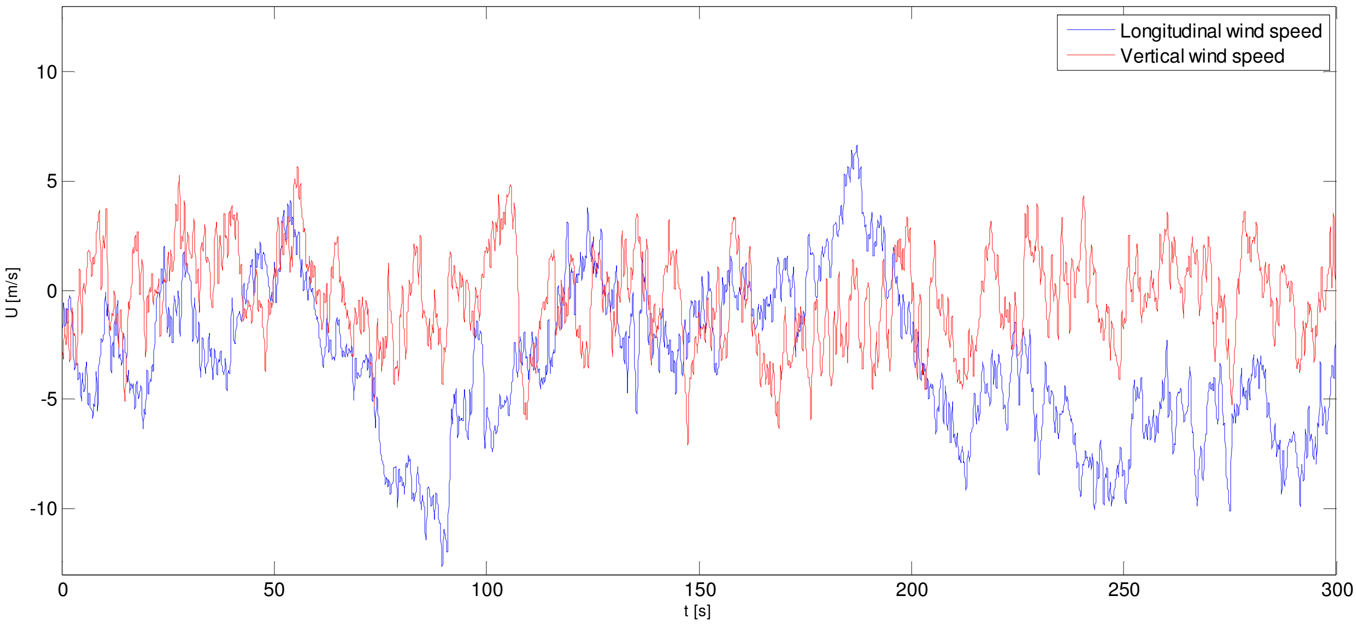

Figure 5.1 Wind velocity in vertical and longitudinal direction over a certain time period Longitudinal wind spectrum=VonKarman-Harris, vertical wind spectrum=Bush&Panofsky

5.2 Stiffness, mass, damping

In order to obtain the stiffness matrix for the bridge a FE-model is used. In the FE-model every main span node is loaded with a unit point load in a different load case. The displacements of each of these load cases can be obtained and this will give the inverse stiffness matrix of the system. The following equations show the procedure. The force vector is equal to the stiffness matrix times the displacement vector.

$$\boldsymbol{F} = \boldsymbol{K}\underline{z} \qquad \textbf{(5.2.1)}$$

The displacement vector is therefore also equal to the inverse stiffness matrix times the force vector.

$$\boldsymbol{K}^{-1}\boldsymbol{F} = \underline{z} \quad \textbf{(5.2.2)}$$

When the force vector consist of all zeros and one unit force and the displacement vector is known one column of the inverse stiffness matrix can be obtained.

$$\begin{bmatrix} \underline{p}_1 & \cdots & \underline{p}_{i-1} & \underline{p}_i & \underline{p}_{i+1} & \cdots & \underline{p}_n \end{bmatrix} \begin{bmatrix} 0 \\ \vdots \\ 0 \\ F_i \\ 0 \\ \vdots \\ 0 \end{bmatrix} = \begin{bmatrix} z_{1,i} \\ \vdots \\ z_{k,i} \end{bmatrix} \quad \textbf{(5.2.3)}$$

The i^{th} column of the inverse stiffness matrix can now be calculated with $\underline{p_i} = \underline{z_i}/F_i$. When all the load cases with unit loads at the nodes are considered the total inverse stiffness matrix can be obtained. The FE-model is designed with Matlab. The Matlab code that is designed for this model is shown in APPENDIX VII. For the elements Euler-Bernoulli beam elements are used. These elements have two nodes and three degrees of freedom per node. The properties of the elements are based on the values that were found in APPENDIX IV and APPENDIX V. For the cable stays the bending stiffness properties are set equal to zero. As a consequence the elements are reduced to two dimensional bar elements. In figure 5.2 a deformed plot is shown of the model when loaded with a unit point load at midspan.

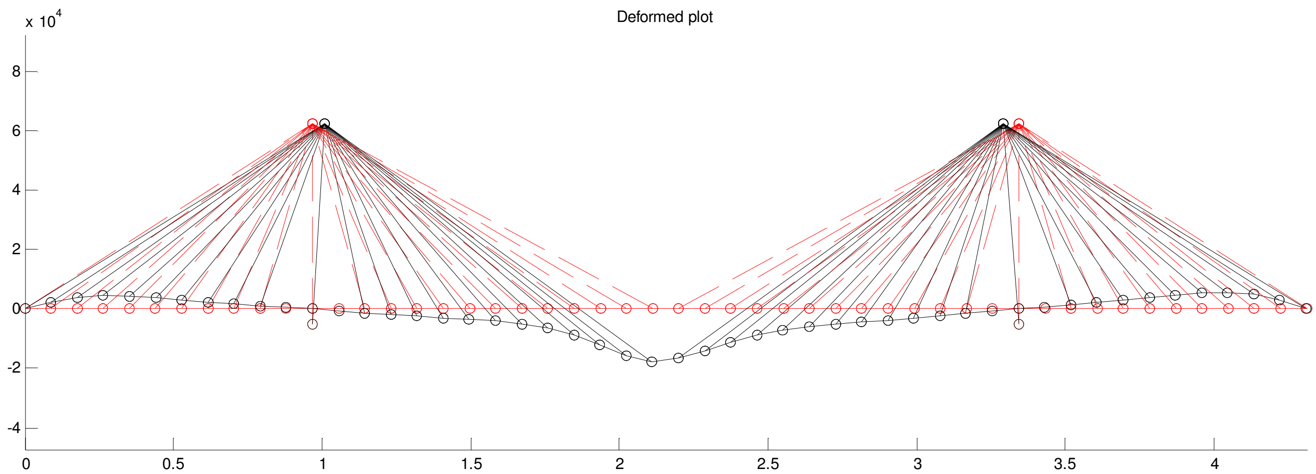

Figure 5.2 Deformed plot of the Matlab model

The mass matrix can be assembled as a diagonal matrix with lumped masses at the nodes. For the modal analysis it is necessary to calculate the eigenfrequencies. Matlab can calculate the generalized eigenvalues and the eigenvectors using the following function:

$$[E, \Omega] = eig(K, M) \quad \textbf{(5.2.4)}$$

Where Ω is a diagonal matrix of generalized eigenvalues and E is the matrix with eigenvectors.

$$\boldsymbol{KE} = \boldsymbol{ME\Omega} \quad \textbf{(5.2.5)}$$

The first column of the matrix E gives the first eigenmode of the system. The second column gives the second eigenmode. The first three eigenmodes are shown in figure 5.3.

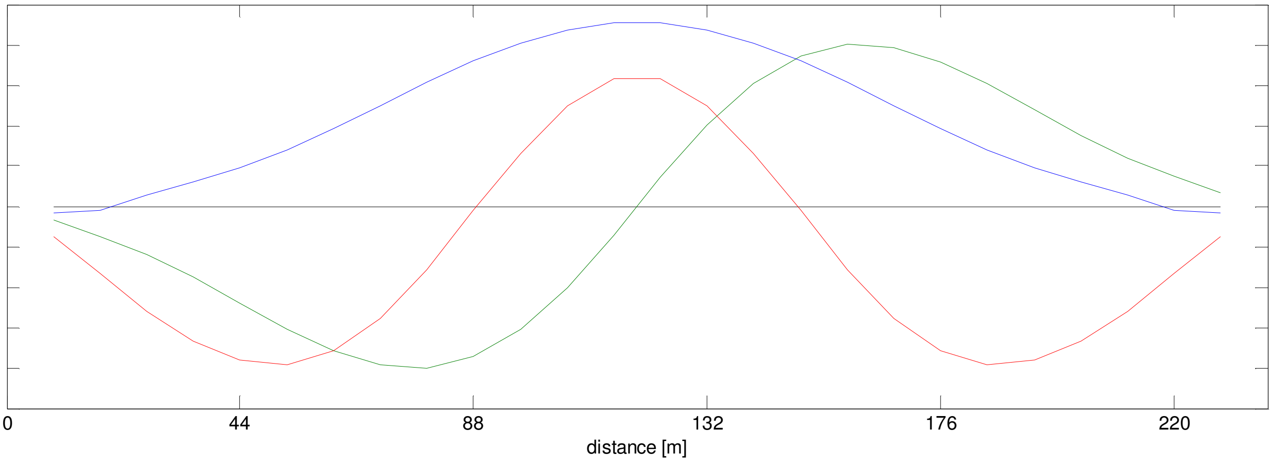

Figure 5.3 First three eigenmodes of the main span of the bridge

The generalized damping matrix is assumed to be diagonal. The Rayleigh damping matrix is used to describe the damping. The generalized damping matrix can be given by:

$$\boldsymbol{C} = 2\omega_1\omega_2\frac{\zeta_1\omega_2 - \zeta_2\omega_1}{{\omega_2}^2 - {\omega_1}^2}\boldsymbol{M} + 2\frac{\zeta_2\omega_2 - \zeta_1\omega_1}{{\omega_2}^2 - {\omega_1}^2}\boldsymbol{K} \tag{5.2.6}$$

For both bridge designs the following equation holds:

$$\frac{\omega_1}{\omega_2} < \frac{\zeta_2}{\zeta_1} < \frac{\omega_2}{\omega_1} \tag{5.2.7}$$

This means that the proportional damping can be visualized as is shown in figure 5.4. The program can find a positive value for all the frequencies, which means that the system does not become unstable after a certain frequency.

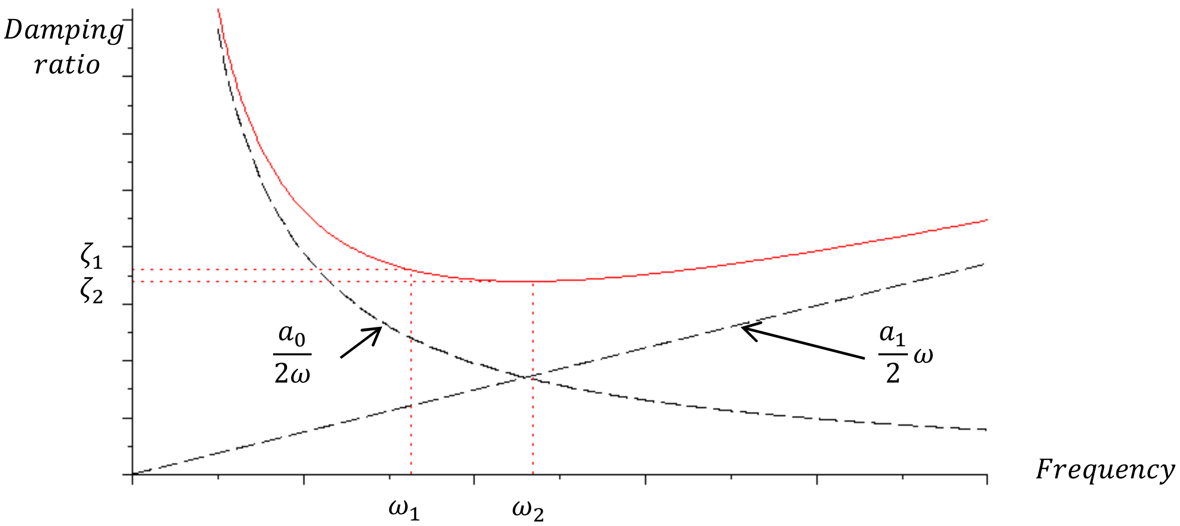

Figure 5.4 Proportional damping ratio for different frequencies

5.3 Transfer functions

The transfer functions of the midspan of the bridge that are obtained from the analysis are shown in figure 5.5. Some of the eigenfrequencies of the system can be seen as peaks in the figure. The transfer function of the NSC bridge shows a small peak for the second eigenfrequency of the system. This can be due to numerical imperfections of the calculation. The most important frequency is the first eigenfrequency of the system. For the NSC bridge system a value of 3.34 rad/s was found. The Matlab calculation gives a value of 3.30 rad/s for the frUHSC bridge system. Comparing these values with the values found with the analysis based on the analytical model shows that there is some deviation. However this deviation is relatively small: 2.2% for the NSC bridge and 5.9% for the frUHSC bridge. Especially when it is considered that two different models are used for the analysis. When the results of both methods are compared for the higher eigenfrequencies of the systems, it can be seen that the deviation is much larger.

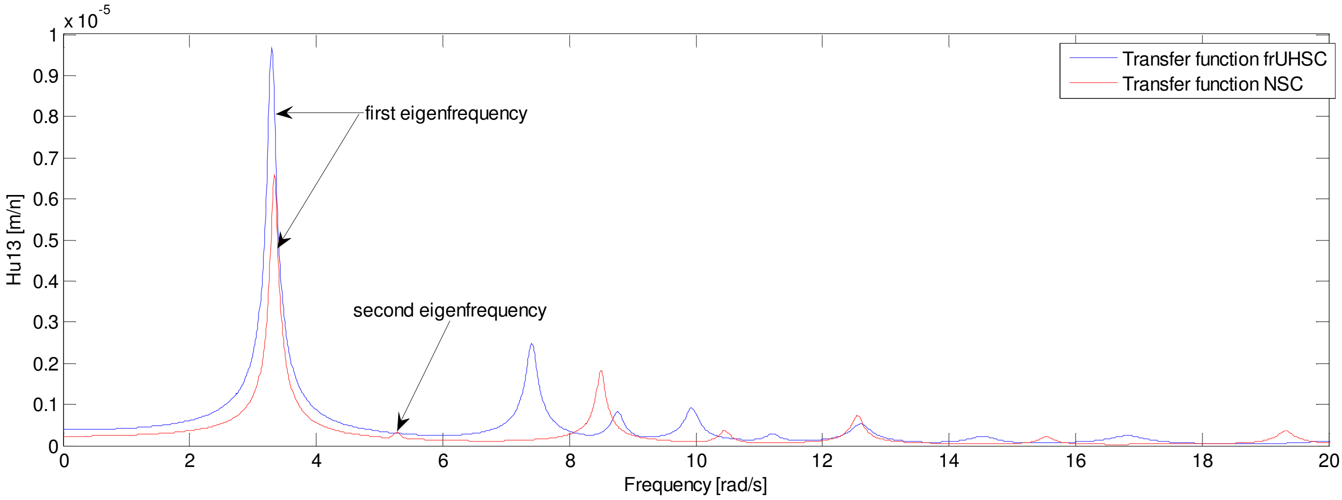

Figure 5.5 Transfer functions for the displacement at midspan

5.4 Force spectrum

The force spectrum is a combination of the wind spectra in horizontal and vertical direction. This is also explained in chapter 4.4. The function described in function 5.4.1 is shown in figure 5.6.

$$S_{LL}(\omega) = \rho^2 {U_m}^2 B^2 {L_{part}}^2 \left({C_L}^2 S_{UU}(\omega) + \frac{1}{4} \frac{\partial C_L}{\partial \alpha}\bigg]_{\alpha=0}^2 S_{WW}(\omega) \right) |\chi(\omega)|^2 \tag{5.4.1}$$

The forces acting on the nodes can be described with the force spectrum. The relation between the forces on the different nodes can be with cross spectra because the forces are not completely coupled. In the Matlab code the coherence function is taken into account as a matrix that is frequency dependent.

$$coh_{F_j F_k}(\omega) = \exp\left(-\frac{C_y \omega}{2\pi U_m} |\Delta y_{j,k}|\right) \tag{5.4.2}$$

Where $|\Delta y_{m,n}|$ is a matrix with all the individual absolute distances.

$$S_{F_jF_k}(\omega) = S_{LL}(\omega)coh_{F_jF_k}(\omega) \quad \textbf{(5.4.3)}$$

Where $S_{F_jF_k}(\omega)$ is a full 26x26 matrix that changes for every frequency.

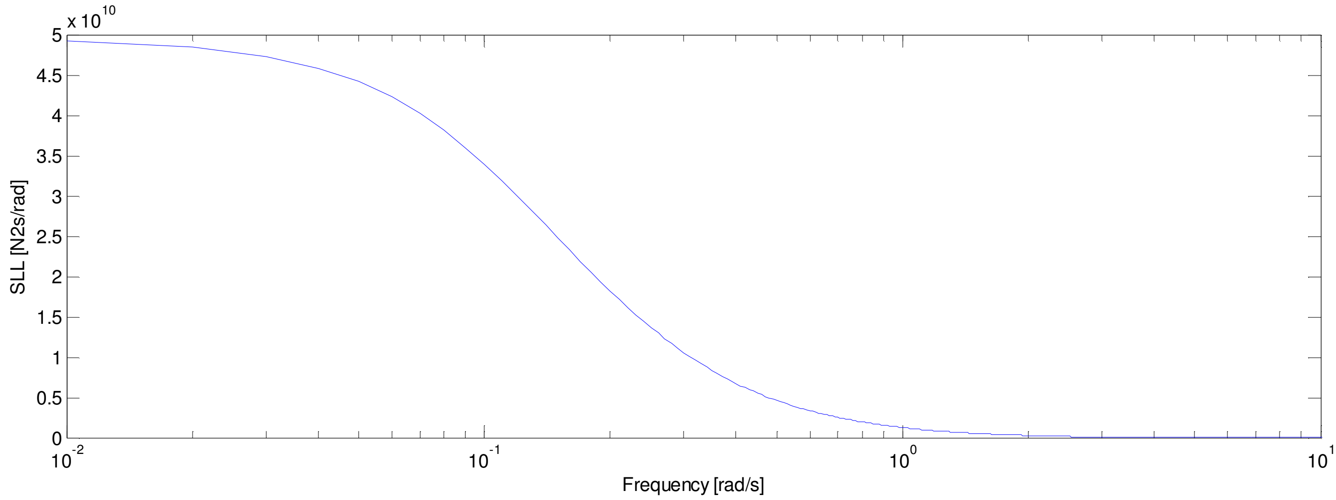

Figure 5.6 Spectrum for the vertical force on a section of the bridge

5.5 Response spectrum

The response spectrum can be obtained from the transfer function and the force spectra.

$$S_{z_{13}z_{13}}(\omega) = \sum_j \sum_k H_{z_{13}F_j} H_{z_{13}F_k}{}^{*} S_{F_jF_k} \quad \textbf{(5.5.1)}$$

In the Matlab code this gives that $H_{z_{13}F} = H_{z_{13}F_j} H_{z_{13}F_k}{}^{*}$ is a 26x26 matrix that changes for every given frequency. Therefore the matrix of force spectra can be multiplied with this matrix. When all rows and columns are summed up, the response spectrum of the displacement of node 13 is found.

$$S_{z_{13}z_{13}}(\omega) = \sum_{j=1}^{26}\sum_{k=1}^{26} \begin{bmatrix} H_{z_{13}F_1}(\omega) \\ \vdots \\ H_{z_{13}F_{26}}(\omega) \end{bmatrix} \begin{bmatrix} H_{z_{13}F_1}{}^{*}(\omega) & \dots & H_{z_{13}F_{26}}{}^{*}(\omega) \end{bmatrix} \begin{bmatrix} S_{F_1F_1}(\omega) & \dots & S_{F_1F_{26}}(\omega) \\ \vdots & \ddots & \vdots \\ S_{F_{26}F_1}(\omega) & \dots & S_{F_{26}F_{26}}(\omega) \end{bmatrix} \quad \textbf{(5.5.2)}$$

In figure 5.7 the response spectra are shown when all the forces are completely coupled. Figure 5.8 shows the response spectra when the force spectra for all the nodes are related with cross spectra. The difference between the two plots can clearly been seen at the first natural frequency. When the forces are not completely coupled, the influence of the natural frequency on the response is reduced significantly. This means that for both bridge designs the lower frequencies of the wind have the most influence on the displacement of the midspan of the bridge. And the displacements are hardly influenced by the resonance peak at the natural frequency. In figure 5.9 and 5.10 the response spectra of the vertical acceleration of the midspan are shown. It can be seen that the shape of the graphs shown in both figures is almost the same, but when the forces are completely coupled, the values are about eight times higher. From the figures it becomes clear that the accelerations are completely determined by the peaks at the natural frequencies. Simplifying the model by assuming that the forces are completely coupled will give results for the accelerations that deviate a lot from the results that would be found when the cross spectra are taken into account.

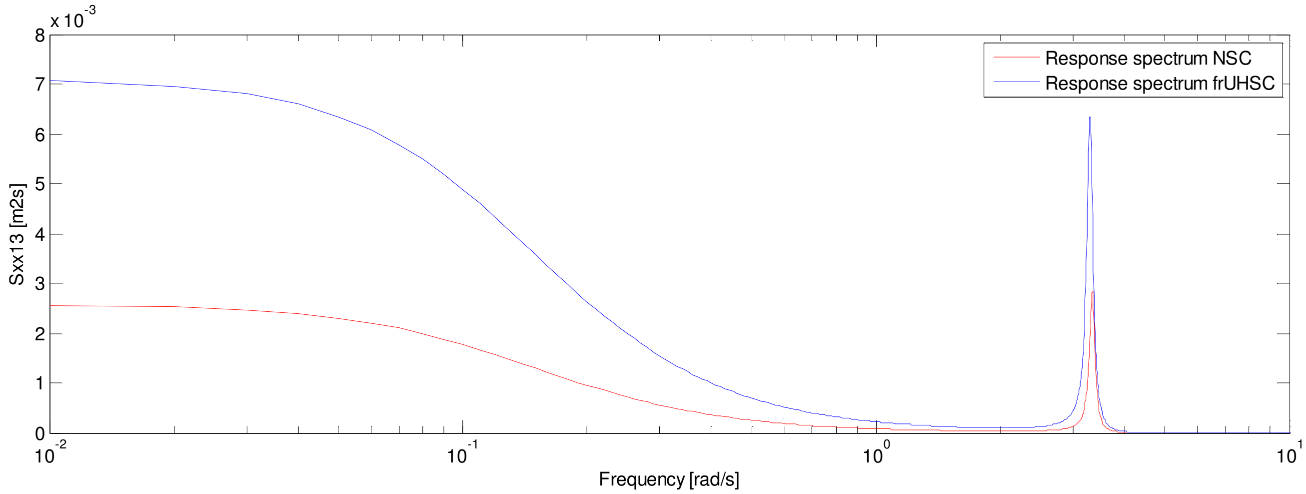

Figure 5.7 Response spectra for both bridge designs when the coherence is not taken into account

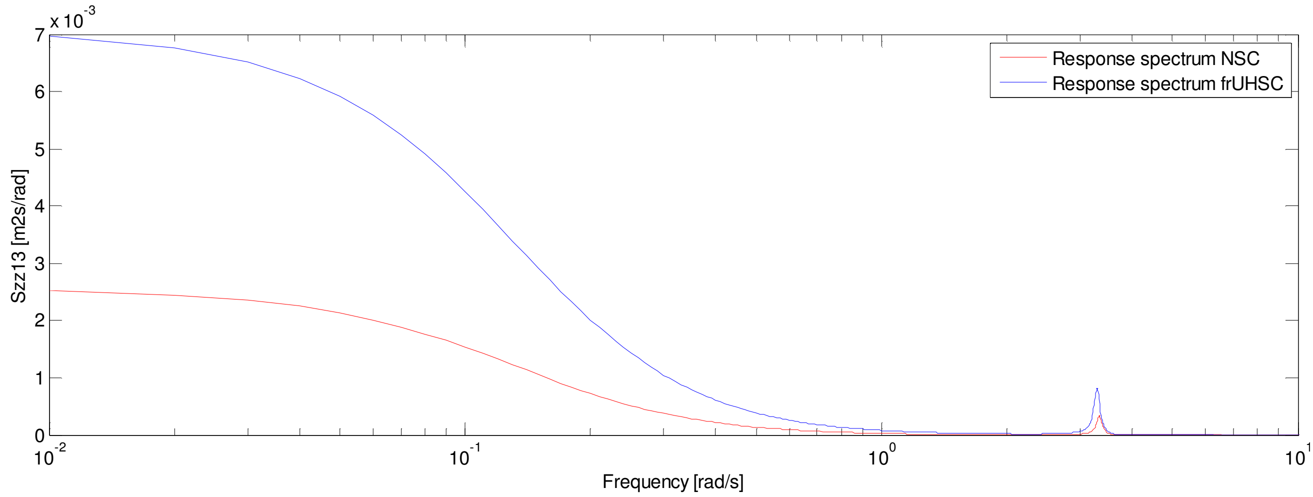

Figure 5.8 Response spectra for both bridge designs when the coherence is taken into account

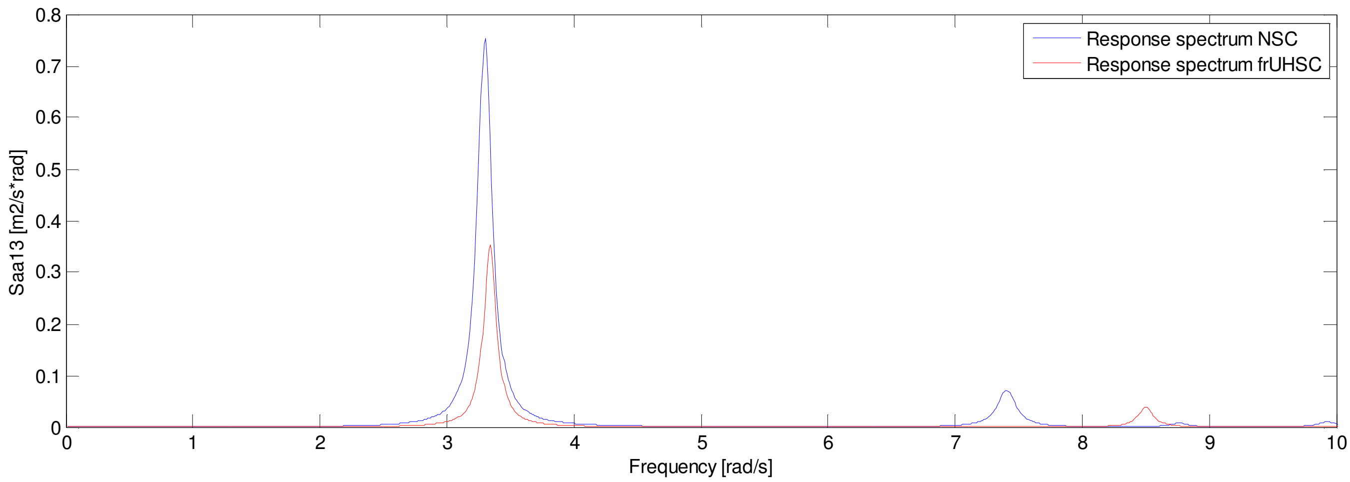

Figure 5.9 Response spectra of the acceleration of the midspan of the bridge when all the forces on the nodes are fully correlated

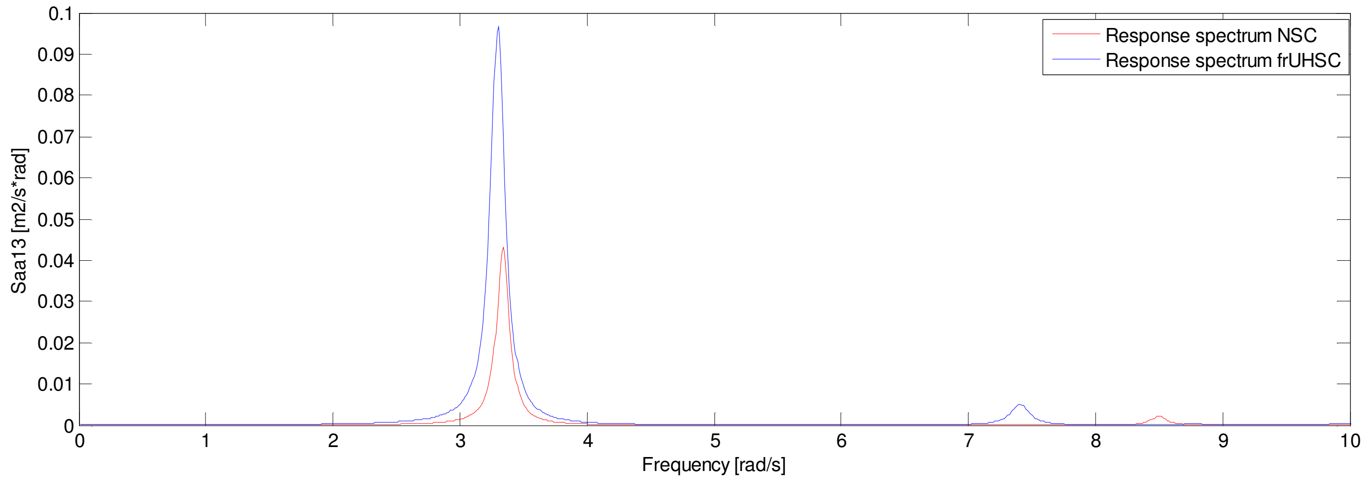

Figure 5.10 Response spectra of the acceleration of the midspan of the bridge when the forces on the nodes are related to each other with cross spectra

The displacements and accelerations can also been shown in a time domain. The response of the displacement of the midspan for a time period of 300 seconds is shown in figure 5.11.

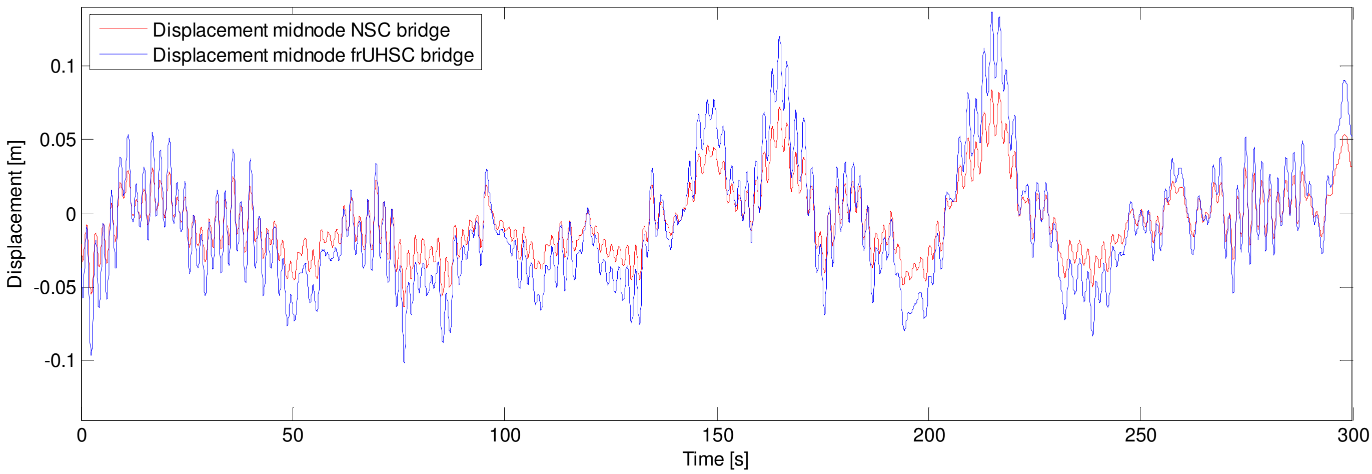

Figure 5.11 Time domain for the displacement of the midspan of the bridge

The peak values for a 10 minutes (600 second) and a 6 hour storm (21600 second) period can be can be determined. In table 5.1 the peak values are shown for the displacements and the accelerations of the NSC bridge design and the frUHSC bridge design when it is assumed that the displacements and accelerations have a normally distributed signal. The influence of the damping (±0.05%), the stiffness (±10%) and the mass is shown in the table.

Table 5.1 Peak values of the displacement and acceleration of the bridge and influence of parameters

	$z_{NSC,peak}$	$z_{frUHSC,peak}$	$\ddot{z}_{NSC,peak}$	$\ddot{z}_{frUHSCpeak}$
10min storm Completely coupled	0.0909 m	0.1479 m	0.7405 m/s^2	1.1432 m/s^2
10min storm Not completely coupled	0.0774 m	0.1286 m	0.3172 m/s^2	0.5047 m/s^2
6h storm Completely coupled	0.1157 m	0.1884 m	0.9430 m/s^2	1.4564 m/s^2
6h storm Not completely coupled	0.0986 m	0.1638 m	0.4039 m/s^2	0.6430 m/s^2
Damping +0.05%	98.5%	98.2%	96.7%	95.7%
Damping -0.05%	101.1%	102.2%	103.7%	104.9%
Stiffness +10%	87.2%	87.5%	92.5%	92.8%
Stiffness -10%	113.4%	113.1%	107.2%	106.8%
Mass 0%life load	97.2%	95.1%	102.7%	101.9%
Mass 100%life load	104.2%	107.3%	96.3%	96.6%

From table 5.1 is can be seen that the peak values are higher for the frUHSC bridge design. The values for the frUHSC bridge are about 1.6 times higher. Adjustments of the damping ratio by 0.05% has 1.1%-2.2% on the peak displacement and 3.3%-4.9% on the acceleration. The assumed stiffness of the bridge appeared to have significant influence on the response of the system. The same results were found in the parameter study performed in paragraph 4.6. This also shows that additional stiffness reduces the displacements and accelerations of the bridge.

5.6 Comparison with the Results of the Analytical Model

The results obtained from this numerical simulation can be compared with the results from the method based on the analytical model. The peak values during a 10 minute storm are used for this comparison. In table 5.2 the peak displacements and the peak accelerations of both models are shown.

Table 5.2 Peak values during a 10-min storm for both models

	$z_{NSC,peak}$	$z_{frUHSC,peak}$	$\ddot{z}_{NSC,peak}$	$\ddot{z}_{frUHSCpeak}$
10min storm Analytical model	0.0730 m	0.174 m	0.830 m/s^2	1.86 m/s^2
10min storm FE-model	0.0774 m	0.129 m	0.317 m/s^2	0.505 m/s^2

From these results it can be seen that the peak displacement for the NSC bridge has around the same value for both the analytical model and the FE-model. For the frUHSC bridge the peak displacements show a larger deviation. And when the accelerations are compared for both models, it can be seen that the analytical model gives much higher values than the method based on the FE-model. This can be explained, because the higher order natural frequencies of the analytical model have lower values compared with the FE-model. So the third and the fifth natural frequency of the analytical model have still large influence on the response. When for example the third natural frequency is compared for both models, it can be seen that the FE-model gives values that are around 4 rad/s higher than the analytical model. And because the higher order natural frequencies of the analytical model are lower, these frequencies have more influence on the response. This can especially been seen in the response of the accelerations, because these accelerations are almost entirely determined by the response at the natural frequencies. When the third and the fifth natural frequency are not taken into account in the calculation of the response, the accelerations correspond much better with the accelerations of the FE-model. These accelerations are than 0.38m/s^2 and 0.62m/s^2 for respectively the NSC bridge and the frUHSC bridge.

6. Allowable Vibrations and Displacements

In this chapter the results found in the analysis are checked on safety and comfort. First a comparison is made between the dynamic displacements and the displacements that can be found according to the Eurocode. The fatigue failure of the reinforcement bars due to the varying stress is examined in paragraph 6.2. In the last part of this chapter the discomfort due to high vertical accelerations is checked.

6.1 Static displacement according to the EuroCode

The vertical wind pressure on the bridge deck can be calculated according to the EuroCode 1991-1-4. (See also APPENDIX III.) The mean wind velocity in horizontal direction at the height of the bridge deck is equal to:

$$U_m(15) = 0.19\left(\frac{0.01}{0.05}\right)^{0.07} \cdot \ln\left(\frac{15}{0.01}\right) \cdot 1.0 \cdot 29.5 = 36.62m/s \tag{6.1.1}$$

The turbulence intensity is the ratio between the standard deviation and the mean wind velocity.

$$I_v = \frac{k_r k_I v_b}{U_m} = 0.137 \tag{6.1.2}$$

The extreme wind pressure can be determined based on the following calculation:

$$q_p = (1 + 7I_v)\frac{1}{2}\rho {U_m}^2 = 1640\ N/m^2 \tag{6.1.3}$$

The pressure coefficient is for the vertical direction of the bridge according to the EC1 equal to 0.9. The maximum displacement in the serviceability limit state can be calculated with the following distributed line load:

$$q_w = 0.9 \cdot 1.64 \cdot 32.5 = 47.97\ kN/m \tag{6.1.4}$$

In the Matlab FE-model this load model results in a displacement of 57mm for the NSC bridge and 93mm for the frUHSC bridge. These values a less high than the displacements that were found in the dynamic analysis. When the peak value for the displacements during a 10 minutes storm are used as a reference than the displacements found in the static calculation deviate respectively 26.4% and 27.7% for the NSC bridge and the frUHSC bridge.

6.2 Failure due to Fatigue

The bridge structure is subjected to millions of load cycles during in its lifetime. The fatigue performance of reinforced/prestressed concrete structures is relatively good. Failure due to fatigue can occur when cracks in the concrete are formed and the tensile stress in the reinforcement bars has a fluctuating value. In the Eurocode 1990-A2 it is stated that it can be necessary to check the fatigue performance of the bridge. Whether or not fatigue due to wind is of importance for these bridges is checked in the following calculations. When the design load is taken into account the bridge does not crack. This means that the stress fluctuations in the reinforcement is very low and therefore is fatigue not governing. In the calculation below it is assumed that the concrete has cracked in the tensile zone due to an exceptional load. This means that the reinforcement bars have to carry the tensile force to make internal equilibrium. In this situation the stress in the reinforcement is much higher. For the determination of the applied reinforcement use is made of the ULS of the cross section. The applied reinforcement in the bottom flange of the main girders is 2x2x27Ø32 for the NSC bridge design and 2x2x15Ø32 for the frUHSC bridge design. For the determination of the stress in the reinforcement the bridge is assumed to be loaded with the dead load and the super dead load only. The additional moment due to the wind is calculated based on a Rayleigh distribution. The stress fluctuations for the most outer reinforcement bars can be determined for certain occurrence levels. The moments and related stress ranges for 60%, 24%, 10%, 5% and 1% of the peaks are given in table 6.1.

Table 6.1 Stress range for different occurrence levels

	ΔM [NSC]	ΔM [frUHSC]	$2\Delta\sigma$ [NSC]	$2\Delta\sigma$ [frUHSC]
60%	731 kNm	260 kNm	0-12 N/mm^2	0-9 N/mm^2
24%	1348 kNm	481 kNm	0-22 N/mm^2	0-17 N/mm^2
10%	2038 kNm	720 kNm	0-33 N/mm^2	0-25 N/mm^2
5%	2760 kNm	983 kNm	0-45 N/mm^2	0-34 N/mm^2
1%	3807 kNm	1357 kNm	0-62 N/mm^2	0-47 N/mm^2

When this is summarized in a stress range distribution graph, figure 6.1 can be obtained. The allowable cycles at the stress levels is given in a normalized S-N curve. The S-N curve is based on the NEN 6008 (2008) for reinforcement steel B500B and is shown in figure 6.2.

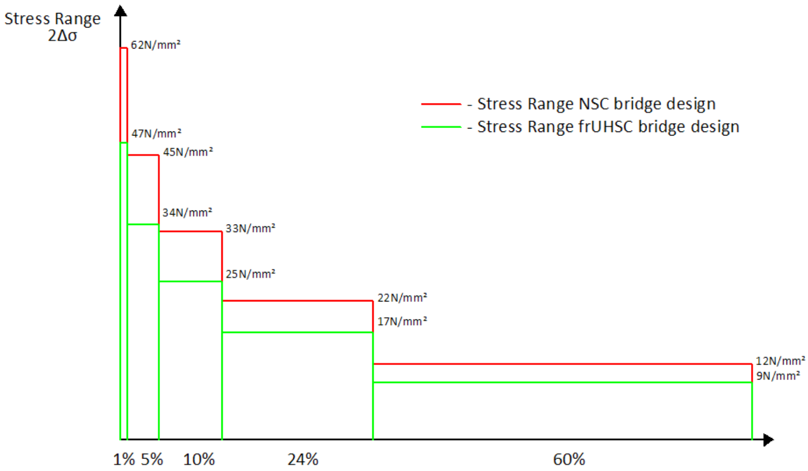

Figure 6.1 Stress range diagram

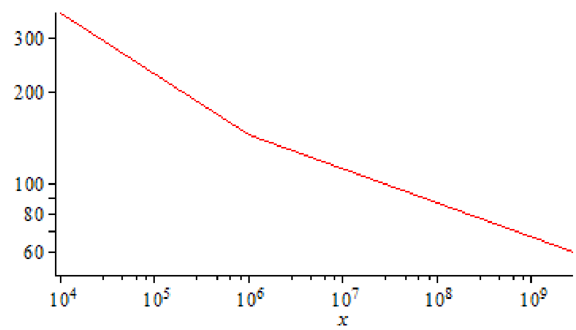

Figure 6.2 S-N curve

The number of peaks that occur in the lifetime of the bridge can be estimated by using the average time period of a cycle. The total life time of the bridge is in seconds:

$$T = 100 \cdot 365 \cdot 24 \cdot 3600 = 3.154 \cdot 10^9 s \tag{6.2.1}$$

The average time period of a cycle can be estimated with:

$$T_m = \frac{2\pi}{\omega_e} \tag{6.2.2}$$

This gives a total number of peaks in the lifetime of the bridge of:

$$n_{peaks} = T/T_m \tag{6.2.3}$$

Table 6.2 Number of occurring cycles and allowable cycles for different stress levels

$2\Delta\sigma$ [NSC]	Number of occurring cycles	Number of allowable cycles	$2\Delta\sigma$ [frUHSC]	Number of occurring cycles	Number of allowable cycles
12 N/mm^2	$1005\cdot10^6$	$5.5\cdot10^{15}$	9 N/mm^2	$994\cdot10^6$	$7.3\cdot10^{16}$
22 N/mm^2	$402\cdot10^6$	$2.3\cdot10^{13}$	17 N/mm^2	$398\cdot10^6$	$2.4\cdot10^{14}$
33 N/mm^2	$168\cdot10^6$	$6.1\cdot10^{11}$	25 N/mm^2	$166\cdot10^6$	$7.4\cdot10^{12}$
45 N/mm^2	$84\cdot10^6$	$3.7\cdot10^{10}$	34 N/mm^2	$83\cdot10^6$	$4.7\cdot10^{11}$
62 N/mm^2	$17\cdot10^6$	$2.0\cdot10^9$	47 N/mm^2	$17\cdot10^6$	$2.5\cdot10^{10}$

Using the Palmgren-Miner summation the following values can be obtained:

$$\sum_{i=1}^{k} \frac{n_i}{N_i} = D \qquad \textbf{(6.2.4)}$$

For the NSC bridge design D has a value of 0.0111, and for the frUHSC bridge a value of 0.0009 is found. Both value are much smaller than 1.0. This means that the bridges are not susceptible for fatigue problems caused by the wind, not even when a crack is formed. When a crack is formed the damping of the structure increases. This effect is not taken into account in this calculation.

6.3 Comfort for traffic

The guidelines for the design of structures by the Dutch government (Rijkswaterstaat) and the EuroCode gives no particular allowable value for the maximum acceleration of the bridge (in case the bridge is no pedestrian bridge). In the EuroCode 1990 A2 some serviceability criteria are given for vibrations of bridges. The code demands that no damage occurs at the bearings due to vibrations. For the allowable vibrations of the bridge deck itself, no particular criteria are given. Instead the discomfort for traffic is to be determined. For the allowable vertical acceleration of bridges Irwin (1978) suggested two curves (figure 6.3) (Irwin, 1978). One base curve for frequent events and one curve for storm conditions. When the fundamental frequency of the bridge is taken into account the for storm conditions the maximum allowable acceleration is according to Irwin's curve 0.42m/s^2. When a storm of 10 minutes is considered the peak value of the NSC bridge design is 0.32m/s^2 for the FE-model. For the frUHSC bridge design a value of 0.50m/s^2 is found. This would mean that the vertical acceleration of the frUHSC bridge is higher than the allowable acceleration.

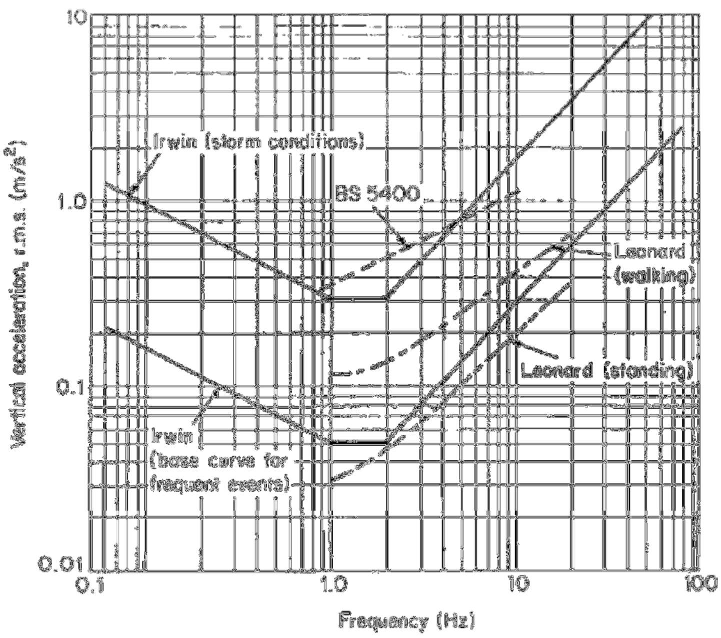

Figure 6.3 Allowable vertical acceleration of bridge according to Irwin (1978)
Source: (Dyrbye, et al., 1997)

7. Tuned Mass Damper

A possible solution for reducing the acceleration and displacements of the frUHSC bridge is by increasing the stiffness of the stays. But this would also mean that the costs of the bridge would increase. That a frUHSC bridge can be used as an alternative for the NSC bridge is because material and therefore costs can be saved due to the slender light weight structure. When this advantage is omitted the frUHSC bridge cannot compete with the NSC bridge. Another solution to reduce the acceleration of the bridge is by adding a Tuned Mass Damper (TMD). In figure 7.1 a schematic representation of a TMD is given.

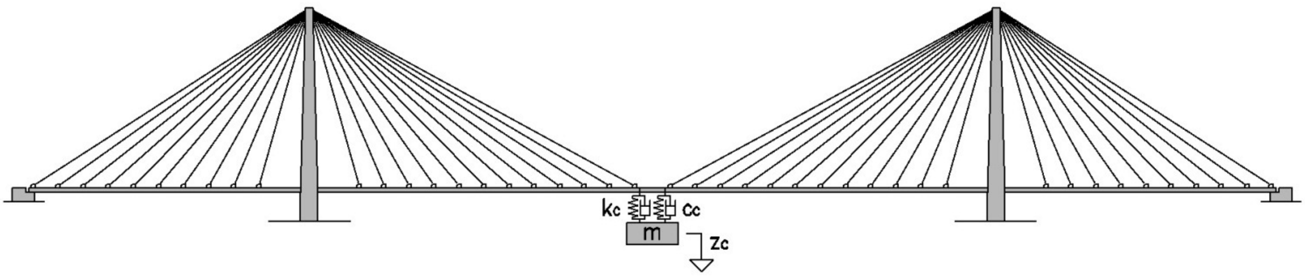

Figure 7.1 Schematic representation of the Tuned Mass Damper (TMD) at midspan of the bridge

When this TMD can be added to the midspan of the bridge in order to reduce the influence of the first eigenfrequency. The equations of motion for the bridge and the TMD can be given by:

$$\boldsymbol{M}\underline{\ddot{z}} + \boldsymbol{C}\underline{\dot{z}} + \boldsymbol{K}\underline{z} + \frac{1}{2}c_c(\dot{z}_{13} - \dot{z}_c) + \frac{1}{2}c_c(\dot{z}_{14} - \dot{z}_c) + \frac{1}{2}k_c(z_{13} - z_c) + \frac{1}{2}k_c(z_{14} - z_c) = \underline{F_w}(t) \quad \textbf{(7.1)}$$

$$m\ddot{z}_c + \frac{1}{2}c_c(\dot{z}_c - \dot{z}_{13}) + \frac{1}{2}c_c(\dot{z}_c - \dot{z}_{14}) + \frac{1}{2}k_c(z_c - z_{13}) + \frac{1}{2}k_c(z_c - z_{14}) = 0 \quad \textbf{(7.2)}$$

When these equations are combined the total equation of motion of the system can be written in Matrix form.

$$\begin{bmatrix} \boldsymbol{M}_{[26x26]} & \boldsymbol{0}_{[26x1]} \\ \boldsymbol{0}_{[1x26]} & m \end{bmatrix} \begin{bmatrix} \underline{\ddot{z}} \\ \ddot{z}_c \end{bmatrix} + \begin{bmatrix} c_{1,1} & \cdots & c_{13,1} & c_{14,1} & \cdots & c_{26,1} & 0 \\ \vdots & \ddots & \vdots & \vdots & \cdots & \cdots & \vdots \\ c_{1,13} & \cdots & c_{13,13} + 0.5c_c & c_{14,13} & \cdots & c_{26,13} & -0.5c_c \\ c_{1,14} & \cdots & c_{13,14} & c_{14,14} + 0.5c_c & \cdots & c_{26,14} & -0.5c_c \\ \vdots & \vdots & \vdots & \vdots & \ddots & \vdots & \vdots \\ c_{1,26} & \cdots & c_{13,26} & c_{14,26} & \cdots & c_{26,26} & 0 \\ 0 & \cdots & -0.5c_c & -0.5c_c & \cdots & 0 & c_c \end{bmatrix} \begin{bmatrix} \underline{\dot{z}} \\ \dot{z}_c \end{bmatrix} + \begin{bmatrix} k_{1,1} & \cdots & k_{13,1} & k_{14,1} & \cdots & k_{26,1} & 0 \\ \vdots & \ddots & \vdots & \vdots & \cdots & \cdots & \vdots \\ k_{1,13} & \cdots & k_{13,13} + 0.5k_c & k_{14,13} & \cdots & k_{26,13} & -0.5k_c \\ k_{1,14} & \cdots & k_{13,14} & k_{14,14} + 0.5k_c & \cdots & k_{26,14} & -0.5k_c \\ \vdots & \vdots & \vdots & \vdots & \ddots & \vdots & \vdots \\ k_{1,26} & \cdots & k_{13,26} & k_{14,26} & \cdots & k_{26,26} & 0 \\ 0 & \cdots & -0.5k_c & -0.5k_c & \cdots & 0 & k_c \end{bmatrix} \begin{bmatrix} \underline{z} \\ z_c \end{bmatrix} = \begin{bmatrix} \underline{F_w}(t) \\ 0 \end{bmatrix} \quad \textbf{(7.3)}$$

The values for the parameters of the TMD can be found with trial and error. The mass of the TMD is expressed as a part of the mass of one section (8.8 meter) of the bridge. The symbol γ is used to define the ratio between the mass of the TMD and one bridge section.

$$\gamma = \frac{m}{L_{part} A_c \rho_c} \tag{7.4}$$

The mass ratio is varied for four different damping ratios. It is known that the TMD should have the same eigenfrequency as the system in order to reduce the vibrations. When the mass and the damping ratio are known the spring stiffness of the TMD can be determined according to.

$$k_c = m\omega_e{}^2 + c_c{}^2/4m \tag{7.5}$$

In figure 7.2 the results are shown when the mass ratio is varies between $\alpha = 0.5\% - 10\%$ for the damping ratios 20%,10%,5% and 1%. For economic reasons the low mass ratio is most beneficial. Therefore it can be see that a damping ratio of 5% is the most efficient.

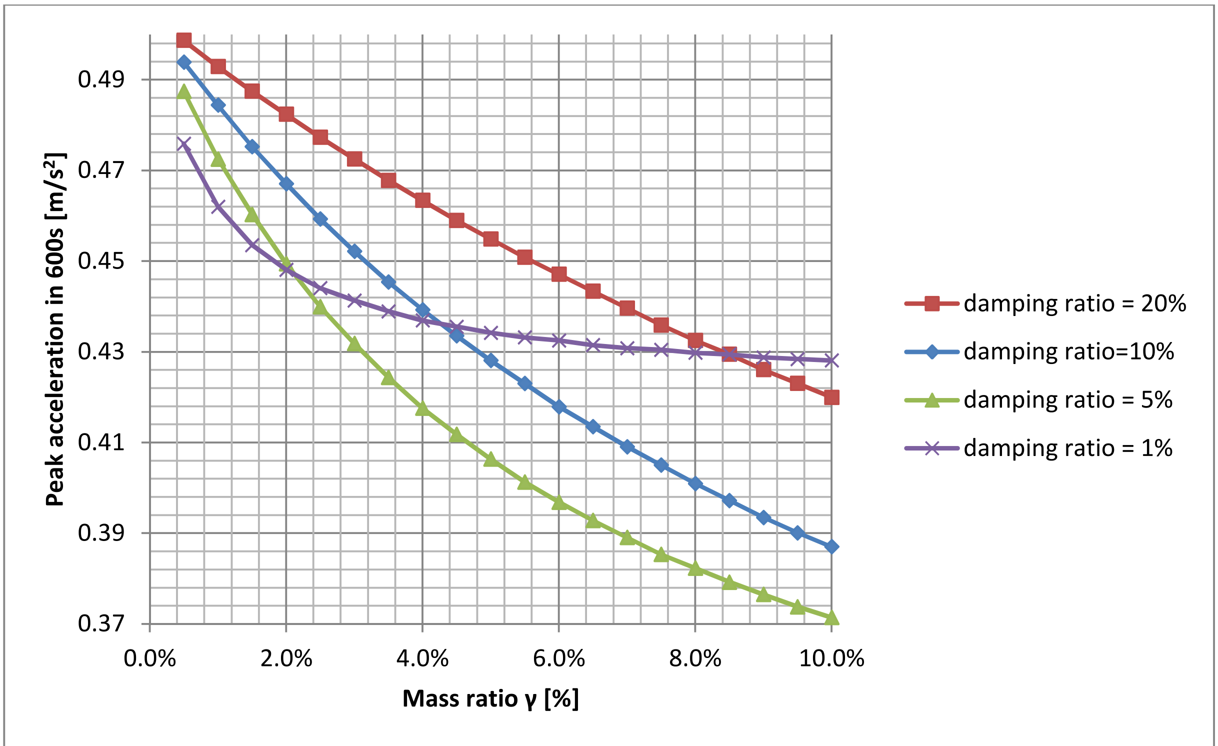

Figure 7.2 Peak acceleration during 600s storm for different mass ratios and damping ratios of the TMD

For a mass ratio of 4.0% and a damping ratio of 5% the maximum acceleration during a 10 minute storm is lower than the allowable acceleration of 0.42m/s^2. This results in a mass of the TMD of 11.055kg. It is possible that the other nodes still have a higher acceleration because it can be that the influence of the second mode becomes more important. When the acceleration of the other nodes is checked it can be seen that this is not the case. The first eigenmode is still dominant after adding the TMD. The accelerations are of the other nodes are therefore not higher than 0.42m/s^2

8. Concluding Remarks

In this report the buffeting performances of a typical cable stayed concrete bridge of Normal Strength Concrete (NSC) and fibre reinforced Ultra High Strength Concrete (frUHSC) were investigated. It is emphasized that only one bridge design for both the NSC and the frUHSC is considered in this report. The results found in this study are therefore only applicable for this particular bridge design and are not per definition applicable for other bridge designs as well. Nevertheless the results give some indication of the difference in sensitivity for wind induced vibrations between NSC bridges and frUHSC bridges. The following conclusions can be drawn from the results found in the analysis:

- By applying frUHSC the weight of the bridge deck can be reduced with 40% in this case study. This also results in a reduction of the cross section of the stays. Because both the mass of the bridge and the stiffness of the stays are reduced for the frUHSC bridge design, the first eigenfrequency does not deviate much from the first eigenfrequency of the NSC bridge design. Both eigenfrequencies have a value of around 0.5Hz when the bridge is represented with an analytical model of a Euler-Bernoulli beam on elastic supports. These values are also confirmed with the Rayleigh-Ritz method. The results of the numerical method based on the FE-model are consistent with the results based on the analytical model. The first eigenfrequency found with the numerical simulation deviates 2.2% and 5.9% from the approach based on the analytical model, respectively for the NSC bridge design and the frUHSC bridge design. It can be seen that the values found with the numerical simulation are therefore rather close to the values found in the analytical procedure, especially because both methods use different models. For the higher eigenfrequencies the deviation between both calculation method is much larger. Markedly is that the eigenfrequencies of the frUHSC bridge design are more closely spaced together than the eigenfrequencies of the NSC bridge design. This is due to the lower bending stiffness of the frUHSC bridge deck.

- When the force spectra on the nodes are not completely coupled but are related with cross spectra, the peak displacements are reduced with 13-15% in comparison with a system where the forces are completely coupled. The accelerations are more considerable reduced with 56-57%. In reality the forces along the length of the bridge are also not perfectly correlated. So the analysis where the cross spectra are taken into account will probably give results that are more corresponding with reality.

- Because the model is a simplified representation of the bridge and there is an uncertainty in the values of the parameters, some of the parameters are varied. The analysis shows that especially the stiffness of the stays have large influence on the outcome. Other parameters like the rotation spring stiffness and the damping are less dominant.

- In the EuroCode 1991-1-4 a method is given to determine the wind load on a structure. With this method the static displacements can be obtained. According to the dynamic analysis these static displacements should be multiplied with a DAF of 1.36-1.38 in order to obtain the displacements of the dynamic calculation. Because the traffic loads cause (in this case study) larger displacements the underestimation does not give per definition unwanted or unsafe situations.

- The chance that failure of the reinforcement bars occurs due to fatigue is for both bridge designs negligible small and is definitely not governing for the design.

- One of the most important observations in the analysis is that both bridge designs have approximately the same first eigenfrequency but the displacements and the accelerations of the frUHSC bridge are more than 59% higher in all the different analysis. The ratio of the peak displacements due to the varying wind load between the NSC bridge and the frUHSC bridge is in this analysis still proportional to the ratio of the static displacements of both bridge designs. It seems that no resonance occurs, the peaks in the response spectra of the FE-model at the fundamental frequency are small in comparison with the values of the response spectra for the lower frequencies. The influence of the resonance peak is about 10% on the displacement of the bridge. The response of the bridge is mainly determined by the lower frequencies because the wind spectra have the highest values for these frequencies. For the accelerations, the lower natural frequencies have large influence on the response of the bridge. When the comfort requirements are considered, the peak accelerations of the frUHSC bridge during storm conditions are higher than the allowable accelerations according to Irwins's curve. Because of the large influence of the stiffness of the stays on the final results, it is thinkable to strengthen the stays. But applying heavier stay cables will eliminate the use of frUHSC bridges due to the much higher costs. The material saving is the most important reason that frUHSC can compete with NSC. A possible solution to reduce the accelerations is by applying a Tuned Mass Damper (TMD).

9. Recommendations

Based on the research done in this report, some recommendations for further research can be given that is related to the subjects discussed in this report.

- Further research to the damping ratio of frUHSC. At the moment no tested data is available of the material damping for frUHSC and the relation to NSC.

- The torsional vibrations of the bridge can be of influence on the total motion of the bridge. Especially when the values of torsional frequencies and vertical bending frequencies are rather close together. In this report a first indication of the torsional frequencies is given. From these basic calculations it seems that the torsional frequencies are in a higher range than the bending frequencies. It is necessary to elaborate these calculations to give a more precise analysis.

- In this analysis use is made of a simplified analytical model and a two dimensional FE-model. Some software programs can be used to model the bridge design three-dimensional and calculate the response spectra. This can be done to increase the accuracy of the results.

- Only the buffeting performance is taken into account in this report. The difference between NSC bridges and frUHSC bridges needs further elaboration for the other mechanisms that can occur due to a wind flow as well.

- For this analysis only one bridge design of NSC and frUHSC is taken into account to determine the buffeting performance. In order to give a relation for the buffeting performance between NSC bridges and frUHSC bridges, it is necessary to compare many more designs.

Literature

Akour, S.N. 2010. *Dynamics of Nonlinear Beams on Elastic Foundation.* London : s.n., 2010.

Allen, D.W. 1987. *Numerical Simulation of Vortex-Induced Oscillation of an Elastically Mounted Circular Cylinder Using Body Fitted Coordinates.* Houston : Rice University, 1987.

Anderson, J.D. 2011. *Fundamentals of Aerodynamics.* New York : McGraw-Hill Companies, Inc., 2011.

Chen, Z.Q., et al. 2008. *Investigation on Influence Factors of Buffeting Response of Bridges and its Aeroelastic Model Verification for Xiaoguan Bridge.* Hunan : Hunan University, 2008.

Costa, C., et al. 2007. *Time-domain Buffeting Simulations for Wind-bridge Interaction.* Firenze : Elsevier Ltd., 2007.

CUR. 1977. *CUR 75 Demping van Bouwconstructies.* 1977.

Dyrbye, C. and Hansen, S. O. 1997. *Wind Loads on Structures.* Chichester : John Wiley & sons Ltd, 1997.

ESDU85020. 2001. *Characteristics of Atmospheric Turbulence near the Ground.* 2001.

Eurocode. *Eurocode 1991 Loads on Structures Part 1-4 General Loads - Wind Loads.* s.l. : Briswarenhuis.

Ge, Y.J. and Xiang, H.F. 2011. *Aerodynamic Challenges of Major Chinese Bridges.* s.l. : Tongji University, 2011.

Highways-Agency and et al. 2001. *Design Rules for Aerodynamic Effects on Bridges, Vol. 1 Sect. 3, BD 49/01.* 2001.

Holmes, J.D. 2003. *Wind loading of structures.* London : Spon Press, 2003.

Irwin, A.W. 1978. *Human Response to Dynamics Motion of Structures.* Londen : The Structural Engineer, 1978.

Jancauskas, E.D. and Melbourne, W.H. 1983. *The Aerodynamic Admittance of a Slender Box Girder Bridge Section.* Clayton : Monash University, 1983.

Kirch, A., Globes, M. and Peil, U. 2010. *Aeroelastic Divergence and Flutter: Critical Comments on the Regulations of EN 1991-1-4.* Braunschweig : Elsevier Ltd., 2010.

Kubo, Y., Hirata, K. and Mikawa, K. 1992. *Mechanism of Aerodynamic Vibrations of Shallow Bridge Girder Sections.* s.l. : Elsevier Ltd., 1992.

Le, T.H. 2007. *Unsteady Buffeting Forces and Gusts of Bridges with Proper Orthogonal Decomposition Applications.* Kyoto : Kyoto University Research Information Repository, 2007.

Lu, K.C., et al. *Ambient Vibration Study of the Gi-Lu Cable-Stay Bridge:Application of Wireless Sensing Units.* Tapei : s.n.

Macdonald, J.H.G. and Daniell, W.E. 2005. *Variation of modal parameters of a cable-stayed bridge identified from.* Bristol : Elsevier, 2005.

Manwell, J.F., McGowan, J.G. and Rogers, A.L. 2009. *Wind Energy Explained, Theory, Design and Application.* Chichester : John Wiley & Sons Ltd., 2009.

Matsumoto, M., Shirato, H. and Yagi, T. 2000. *Recent Topics on Bridge Aerodynamics, Wind struct.* 2000.

Ricciardelli, F. 2003. *On the Wind Loading Mechanism of Long-Span Bridge Deck Box Sections.* Reggio Calabria : Elsevier Ltd., 2003.

Ruscheweyh, H. 1982. *Dynamische Windwirkung an Bauwerken 2: Praktische Anwendungen.* Berlin : Konkordia GmbH, 1982.

Simiu, E. and Miyata, T. 2006. *Design of Buildings and Bridges for Wind, A Practical Guide for ASCE-7 Standard Users and Designers of Special Structures.* Hoboken : John Wiley & Sons, Inc., 2006.

Simiu, E. and Scanlan, R. H. 1996. *Wind Effects on Structures, Fundamentals and Applications to Design.* New York : John Wiley & Sons, Inc., 1996.

Smith, J.W. 1988. *Vibrations of Structures, Application in Civil Engineering Design.* London : Chapman and Hall Ltd., 1988.

Spijkers, J.M.J., Vrouwenvelder, A.W.C.M. and Klaver, E.C. 2006. *Dynamics of Structures, Part 1 Vibration of Structures.* Delft : Delft University of Technology, 2006.

Stathopoulos, T. and Baniotopoulos, C.C. 2007. *Wind Effects on Buildings and Design of Wind-Sensitive Structures.* Udine : SpringerWienNewYork, 2007.

Supartono, F.X. 2008. *Aerodynamic Response of Long Span Cable Stayed Concrete Bridge.* 2008.

Vrouwenvelder, A.W.C.M. *Random Vibrations.* Delft : Delft University of Technology.

Weaver, W., Timoshenko, S.P. and Young, D.H. 1990. *Vibration Problems in Engineering.* s.l. : John Wiley & Sons Inc., 1990.

Zhu, L.D., et al. 2007. *Flutter and buffeting performances of Third Nanjing.* Shanghai : Elsevier, 2007.